Monday, October 13, 2003
POSTER SESSION I
7:00 – 9:30 p.m.

Ansan V. Mangold N.
"Cold" or "Warm" Early Mars: New Analysis of Warrego Valles from THEMIS and MOLA Data **[#8072]**

Ansan V. Mangold N.
Identification of Past Polar Deposits Among Layered Terrains on Mars: Preliminary Results **[#8071]**

Azuma N. Takeda T. Funaki K.
Grain Growth of Ice Which Contains Microparticles **[#8041]**

Beaty D. W. Miller S. L. Bada J. L. Bearman G. H. Black P. B. Bruno R. J. Carsey F. D. Conrad P. G. Daly M. Fisher D. Hargreaves G. Henninger R. J. Huntsberger T. L. Lyons B. Mahaffy P. R. McNamara K. Mellon M. Papanastassiou D. A. Pollard W. Righter K. Rothschild L. Simmonds J. J. Spray J. G. Steele A. Zent A. P.
An Assessment of the Issues and Concerns Associated with the Analysis of Ice-bearing Samples by the 2009 Mars Science Laboratory **[#8076]**

Benson J. L. James P. B.
Yearly Comparisons of the Mars North Polar Cap: 1999, 2001, and 2003 MOC Observations **[#8097]**

Bonev B. P. James P. B. Bjorkman J. E. Hansen G. B. Wolff M. J.
Effects of Atmospheric and Surface Dust on the Sublimation Rates of CO_2 on Mars **[#8052]**

Byrne S. Ivanov A. B.
The Most Recent Section of the South Polar Layered Deposits **[#8108]**

Cockell C.
Challenges and Solutions for the Human Exploration of the Martian Poles **[#8126]**

Dassas K. Forget F.
Simulations of the Seasonal Variations of the Mars South Polar Cap: Preliminary Results **[#8054]**

Dohm J. M. Fairen A. G. Baker V. R. Ferris J. C. Anderson R. C. Uceda E. R.
Episodic Endogenetic-driven Atmospheric and Hydrologic Cycles and Their Influence on the Geologic Records of the Northern and Southern Hemispheres, Mars **[#8059]**

Eluszkiewicz J. Titus T. N.
A Microphysically-based Approach to Inferring Porosity, Grain Size, and Dust Abundance in the Seasonal Caps from Atmospherically-corrected TES Spectra **[#8068]**

Farrell W. M. Mahaffy P. R.
The Ability to Probe the Martian Polar Subsurface Via Ground-penetrating Radar **[#8014]**

Földi T. Bérczi Sz. Palásti E.
Experimental Instrument on Hunveyor for Collecting Bacteria by Their Electrostatic Coagulation with Dust Grains (FOELDIX): Observation of Electrostatical Precipitated Coagulated Units in a Nutrient Detector Pattern **[#8001]**

Forget F. Haberle R. M. Montmessin F. Cha S. Marcq E. Schaeffer J. Wanherdrick Y.
3D Simulations of the Early Mars Climate with a General Circulation Model **[#8070]**

"COLD" OR "WARM" EARLY MARS: NEW ANALYSIS OF WARREGO VALLES FROM THEMIS AND MOLA DATA . V. Ansan and N. Mangold, Orsay-Terre, FRE2566, CNRS et Université Paris-Sud, Bat. 509, 91405 ORSAY Cedex, France, ansan@geol.u-psud.fr.

Introduction: The debate about the Noachian climate is very dependent on the interpretation of geomorphic features like valley networks. Valley networks were first interpreted as surface runoff under warmer climate [1], but surface runoff has been criticized because of the low drainage density [2] and alternative hypothesis have been proposed in cold climate [e.g.3]. Flows sustained by regional hydrothermal activity have been involved especially for the Thaumasia region in which Warrego networks because of the association of runoff sources with old volcanoes and fault zone [4]. In this study we infirm this possibility and we show that fluvial activity due to precipitation is a likely process to form Warrego valleys. Evidences for such processes are taken from new MGS and Odyssey data.

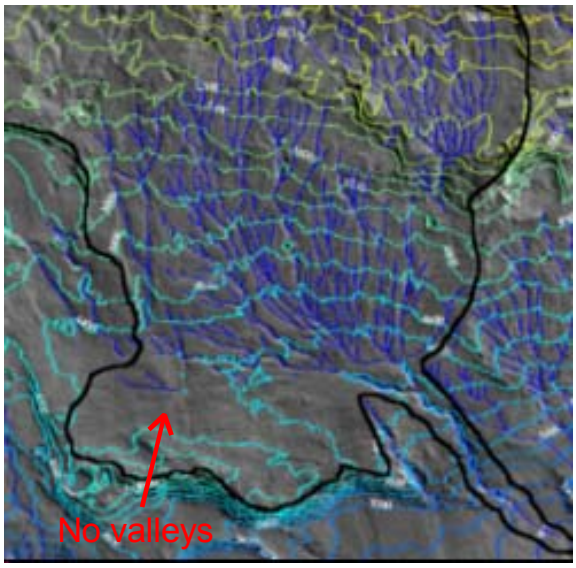

Fig. 1: Viking MDIM with MOLA elevation curves and warrego valles network in blue. Note the apparent absence of valleys on south flank whereas THEMIS data (Fig. 2) permit to identify valleys at this location.

MOC and THEMIS observations: Warrego Vallis is located on the southern part of the Thaumasia region, so the southern part of Tharsis bulge (Fig. 1). Other less developed networks similar in shape also exist on the flank east of Warrego. MOC high resolution images provide local information on the shape of valleys. Valleys are mantled by smooth material, likely dust eolian material. This filling of valleys makes the detection of small tributaries very difficult. New THEMIS IR images can be used to detect valleys that are not visible on Viking imagery. Indeed, THEMIS image south of the networks show several valleys not identified on the Viking images (Fig. 2). Their absence on Viking image (Fig. 1) is likely an effect of the sun incidence. THEMIS image permit to rebuilt a network geometry showing that the flank south of the main valley is involved in the network. The lack of volcanoes or large impact craters at the upper part of this south flank makes the hypothesis of hydrothermally controlled network unlikely. On the contrary, the smaller elevation difference of only 500 m on this flank may explain that valleys are less visible on Viking images.

Topography of the valley network: MOLA data shows that valley heads in the north part of the network occur at height of about 8 km. The average slope is of 0.03 with a total of 6000 m of elevation difference (Fig. 3). A usual criticism to runoff formed by precipitation is that networks are poorly dendritic, this means that intersection between rivers is low and not orthogonal like for dendritic pattern. However, the intersection angle depends strongly on the slope on which runoff forms. Terrestrial studies show that under about 0.026 of slopes (1.5°) the drainage is dendritic with nearly orthogonal intersections and up this value of 0.026 the drainage becomes parallel, with low angle intersections [5]. MOLA data shows that we are in the case of such parallel network, because slopes are of about 0.03 north of the main valley. The observed geometry is consistent with terrestrial parallel drainage due to the slope. On the contrary, the network is dendritic near the main valley where the slope is lower than 1.5°. In addition, we estimate a drainage density of 1.32 km^{-1}. This value is in the range of terrestrial environment by comparison to previous drainage densities usually less than 0.1 km^{-1} found from Viking data [2].

Origin of valley network: Finally, (1) MOC images show that valleys are strongly degraded and that small tributaries are possibly erased, (2) the regional slope measured by MOLA can explain the parallel geometry of the network and (3) THEMIS IR data shows that some valleys exist on the south flank showing that this network is not only controlled by sources on the northern part. Thus, evidences against runoff formed by precipitations are eliminated. On the contrary, it is unlikely that hydrothermal sources explain rivers in the south flank as they have their sources on a structural relief poorly related to any volcanic activity. Sapping is also difficult because it is controlled by layers and the geometry is different than typical sapping valley like Nirgal valleys. Moreover, the sources take place at elevations of up to 8 km which are the highest points

in the regions, making unlikely an underground system at such crest line without refilling by run off.

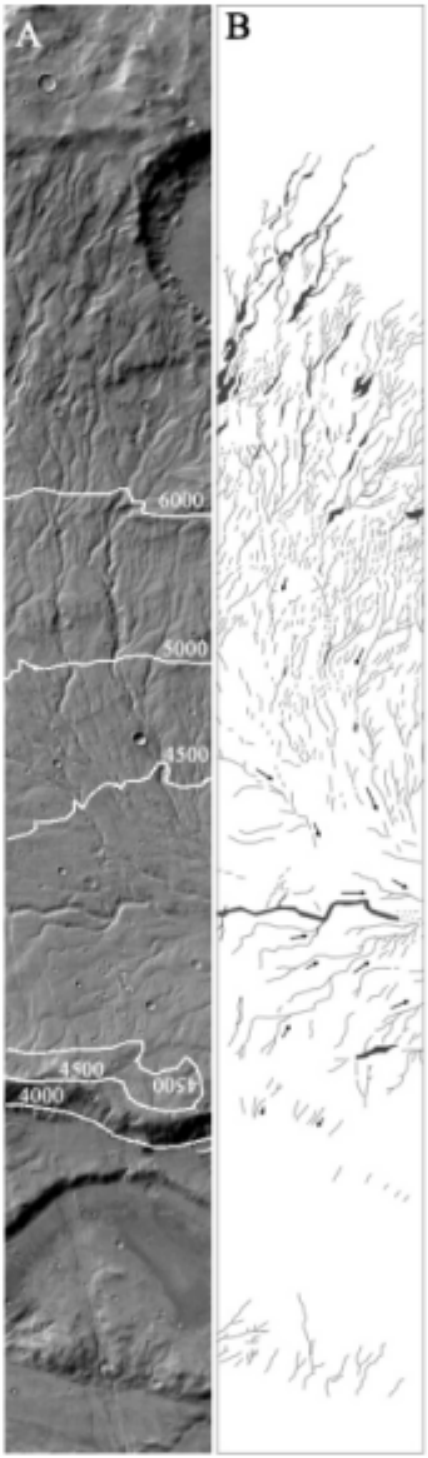

Fig. 2: A. Day-IR themis image I01714004 (100 m/pix) on which the MOLA altimetry is projected with a height interval of 500 m. B. In the lower part of the network, newly observed valleys connect to Warrego main valley with a North downstream. These valleys were not observed on Viking images.

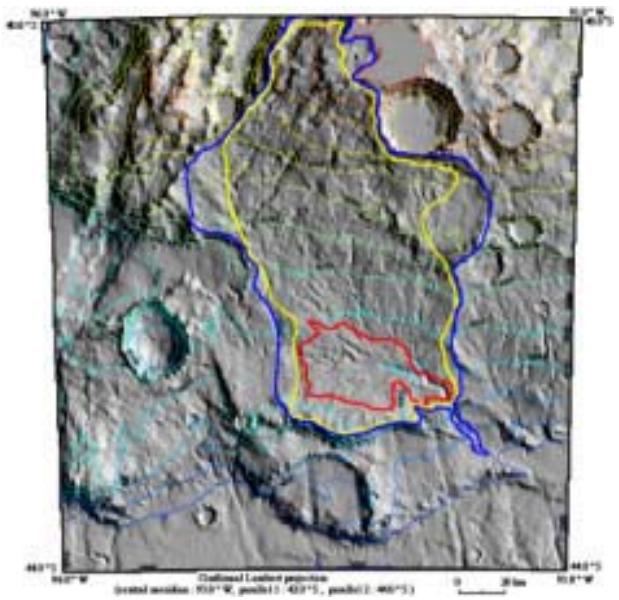

Fig. 3: Warrego Vallis from MOLA shaded relief. The yellow curve shows part of valley network where slopes are over 1.5°. The red curve limits the area where the slope is less than 1.5°. We see from the Themis data (Fig. 2) that the network is parallel in the yellow area and dendritic in the red area.

Conclusion: Using different sets of data, topography, visible and IR images at all possible scale, we show that Warrego valleys have characteristics in favour to surface runoff produced by precipitation. This conclusion favors observation such as those discussed by Craddock and Howard [7]. Warrego is a unique network in terms of density of drainage but the lack of other dense network can be explained because Warrego is one of the rare location with regional slope of more than 2°. Our conclusion, if confirmed by future works, would be useful to constrain climate models of Early Mars which often reject the possibility of warmer climate. It also shows the interest to use THEMIS data to identify valley networks on Mars.

References: [1] Craddock and Maxwell, *J.G.R.*, 102, E6, 13321-13340, 1997 [2] Carr, M. H., *J.G.R.*, 102 (E4), 9145-9152, 1997, [3] Carr, M. H., *Water on Mars*, 1996. [4] Dohm J. M. and K. L. Tanaka et al, *Planet. Spa. Sci.*, 47, 411-431, 1999. [5] Schumm, S.A., M. P. Mosley and W. E. Weaver, *Experimental flows*, WileyInterscience, 1987 [6] Tooth., *Earth Science Reviews*, 51, 67-107, 2000, [7] Craddock and Howard, *J.G.R.*, 107, E11, 5111, 2002.

IDENTIFICATION OF PAST POLAR DEPOSITS AMONG LAYERED TERRAINS ON MARS: PRELIMINARY RESULTS V. Ansan and N. Mangold, Orsay-Terre, FRE2566, CNRS et Université Paris-Sud, Bat. 509, 91405 ORSAY Cedex, France, ansan@geol.u-psud.fr.

Introduction: The origin of layered terrains interpreted to be of sedimentary origin on Mars is debated since their discovery from Viking observations [1,2,3]. Lacustrine, fluvial, volcanic ashes, eolian, ancient polar deposition are the usual hypothesis for their origin. Recently, using MOC images, light-toned deposits have been interpreted as old Noachian deposits formed under water [1]. In this study, we focus on the differences in geologic context, age and geomorphic between deposits on the floor of 4 craters (Fig. 1). We conclude that 2 crater deposits are likely due to past processes involving water at surface, but that the 2 others have more debatable origin.

Location and context of 4 crater interiors analyzed:
Holden crater: 27°S, 35°W. 100 km large crater at the mouth of Uzboi valles. Layered deposits are several hundreds of meters thick.
Terby crater: 28°S, 285°W. 100 km large crater north of Hellas. The crater floor is dissected by canyons where layered deposits are observed over 1 km.
Spallanzani crater: 58°S, 274°W. South-East of Hellas crater. The 50 km large crater is filled by deposits of about 1.5 km thick.
Galle crater (not to confound with Gale crater): 52°S, 30°W. Crater east of Argyre. Deposits are 500 m thick on the south of the crater floor.

Geomorphic characteristics: The erosion of these layered deposits is different from one crater to the other. Holden and Terby crater floors are dissected in canyons and cliffs where layers are observed. These layers are strong and homogeneous with no large debris aprons on the foot of scarps. On the contrary, Spallanzani and Galle layers are not so uniform, with numerous interlayers with strong erosion and low strength as visible by lot of small scarps. They do not show the typical light ton but they could be covered by thin layer of dust. Closed pits and large yardangs due to wind action confirm that the material is not very much consolidated. By comparison, light-toned deposits also display yardangs (Fig. 1B) but at a scale very different which implies a more consolidated material.

Age from stratigraphical relationships and crater counts: Holden deposits are overlain by dark material, both in the interior of valleys and on the top of cliffs. This material is probably a crust of eolian material accumulated after erosion of the deposits. These dark deposits are strongly craterized, sometimes nearly saturation, implying that the age of deposits are at least Hesperian, if not older. In Terby, same dark crust blanket the light-toned deposits which are only visible in some natural cross-section where this blanket was eroded. The large surface which is not dissected by canyons gives an age in the Noachian period from crater counts at MOC and Themis visible image scale. The blanket of dark material was probably removed recently explaining the low proportion of craters on the layered deposits. On the contrary, Galle and Spallanzani crater deposits are completely devoid of craters. They are also devoid of dark blanket, except some young dunes which fills pits and throughs. These deposits seem very young by comparison to Holden or Terby. Nevertheless both deposits are submitted to a strong and recent erosion, so it is not possible to know if the surface was exhumed from much older terrains than it appears.

Channels close to deposits: Both Holden and Terby have channels crossing the deposits. Uzboi vallis in the case of Holden, and different small channels going down from crater rims in the case of Terby. Galle is inside the region of Argyre which is supposed to have been dissected by channels in the Hesperian age but we do not see any fresh channels with potential age in agreement with the apparent youth of the layered terrains inside Galle. On the contrary, Spallanzani is apparently not connected with any channels.

Discussion: The 4 craters can be classed in two groups. On one hand, the deposits of Holden and Terby are probably both of Noachian age. They occur in connection with channels and valley networks. They correspond to the same light toned material than the layers of Terra Meridiani or Valles Meridiani analyzed by [1]. Both craters deposits are good candidates for sedimentary deposition under water as already proposed. On the other hand, Spallanzani and Galle deposits are much more desegregated by wind, the material is clearly different than for Holden and Terby. These craters are located at latitudes of 52° and 58° South, thus at latitudes where ice is stable close to the surface, or was stable in a recent past. Recent models show that deposits of ice and dust as polar layered deposits can occur much more equatorward than currently during period of high obliquity [e.g. 4]. They could thus be the result of past period of high obliquity. In such hypothesis, the deposits are quickly eroded by wind action and the closed pits and throughs could correspond to cryokarstic effects of the sublimation of ice which exists currently at these latitude. Alternatively, the deposits could be old and ice could be still present as ice is stable deep in the ground at these latitudes. Then the progressive erosion could have exhumed these terrains progressively and the sublimation would have created the pits and throughs. Finally,

if Spallanzani is a potential candidate for past polar deposits, Galle remains more uncertain because of the geological context in a region where water played a strong role in the past.

Conclusion: The identification of polar deposits on the whole planet may permit to give paleoclimatic informations. This study highlights the necessity to determine geomorphic criteria in order to discriminate between the different hypothesis for the origin of layered deposits. Among the 4 craters studied, Holden and Terby confirm past studies assuming that they are crater lakes, but the deposits of Spallanzani crater could correspond to potential polar deposits which are now eroded by wind.

References: [1] Malin and Edgett, Science, [2] Cabrol and Grin Global Planetary Changes 35, 199-219, 2002 [3] Carr, M. H., *Water on Mars*, 1996. [4] Michna et al., 6th Mars int. Conf. , Pasadena, 2003.

Fig. 1: A: MOC image of Holden crater. Note the cratered surface on the plateau. B MOC image of Terby crater. C. MOC close-up of Galle crater. Layers are freshly dissected. D. MOC image of Spallanzani crater. Closed pits and erosion of scarps imply large wind effects in the erosional process.

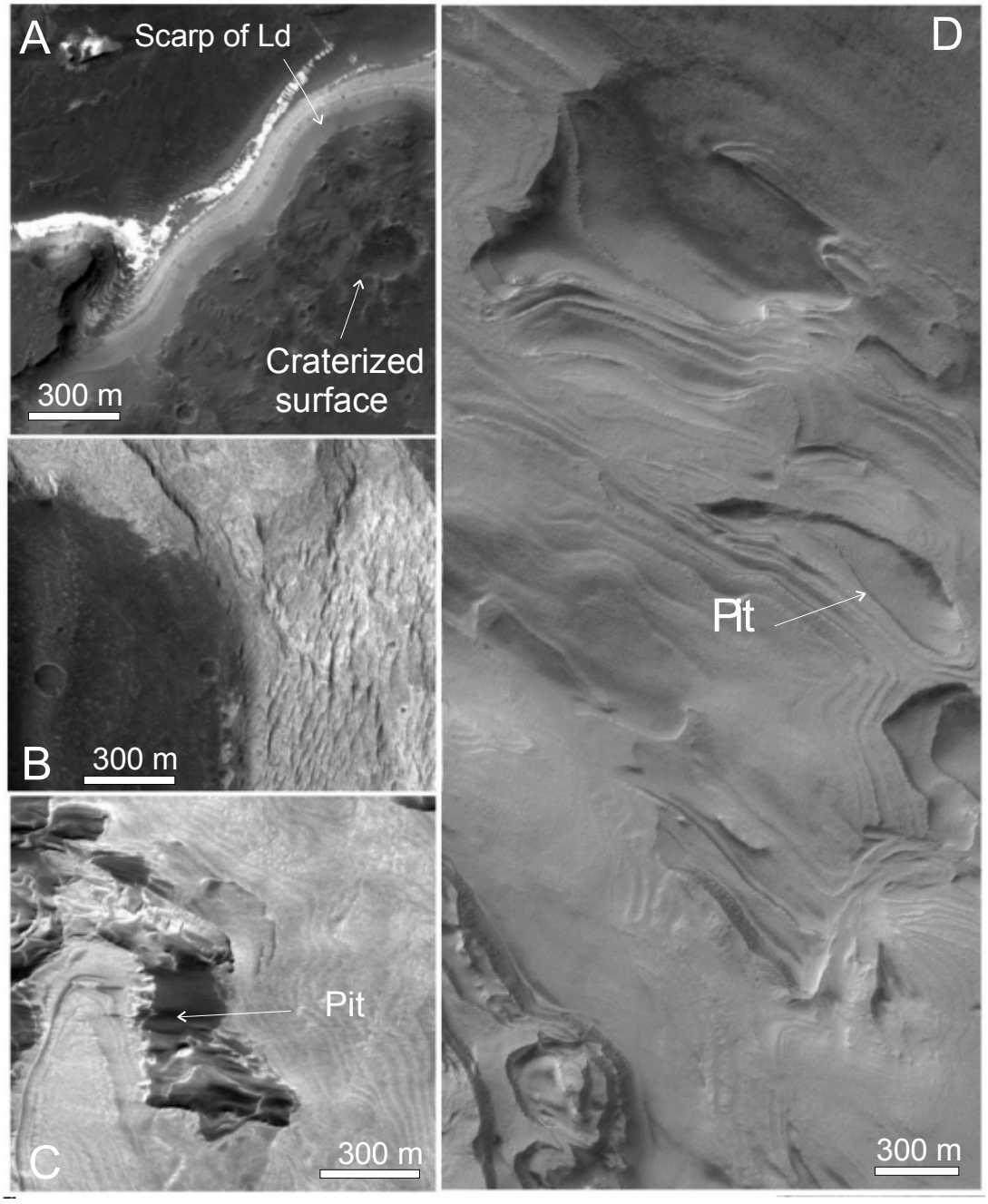

GRAIN GROWTH OF ICE WHICH CONTAINS MICROPARTICLES. N. Azuma, T. Takeda and K. Funaki, Department of Mechanical Engineering, Nagaoka University of Technology,Nagaoka, Niigata, 940-2188, Japan; azuma@mech.nagaokaut.ac.jp

Martian ice-cap ice contains a large number of microparticles (>1%vol.)[1] To estimate grain size in Martian polar ice caps is of vital importance to understand the deformation mechanisms in the ice caps. However, the estimate greatly depends on the microparticle content in ice because microparticles impede grain growth[2]. The dependence of grain growth rate on the concentration of microparticles have not been well investigated experimentally because of the difficulty in preparation of samples containing uniformly distributed microparticles.

We conducted grain growth experiments using artificial ice samples that have various concentrations (0.1-5%) of silica particles with a uniform size of 0.3 σm. Here we discuss the dependence of grain growth rate on concentration of microparticles (Fig 1 and Fig.2) . We also present the effect of the microparticles on the grain size evolution of ice during deformation.

References:
[1] Thomas P.et al. (1992) In Mars, ed. H.Kieffer et. al., Univ. Ariz.Press, 767-795
[2] Alley R.B. et al. (1986) J.Glaciol.,32 (112), 415-433

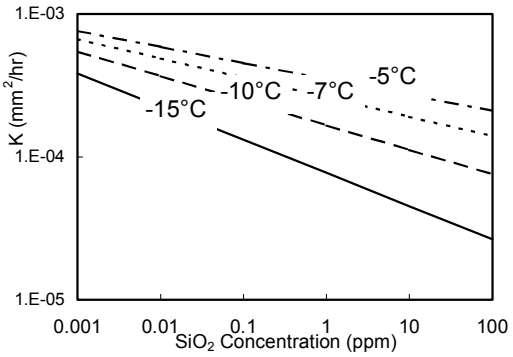

Figure 1 Results of grain growth experiments. K represents the grain growth rate.

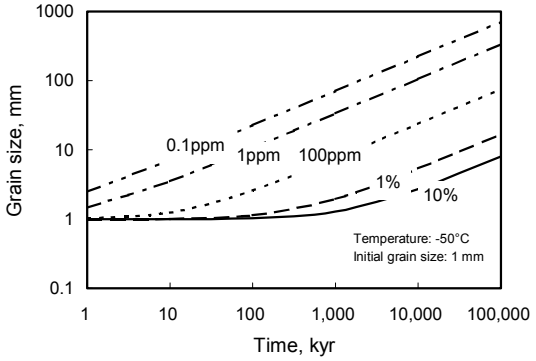

Figure 2 Grain size versus time curves estimated from present results.

AN ASSESSMENT OF THE ISSUES AND CONCERNS ASSOCIATED WITH THE ANALYSIS OF ICE-BEARING SAMPLES BY THE 2009 MARS SCIENCE LABORATORY. D.W. Beaty, (Mars Program Office, Jet Propulsion Laboratory, California Institute of Technology, dwbeaty@jpl.nasa.gov; 818-354-7968), S.L. Miller (JPL/Caltech), J.L. Bada (Univ. of Calif. San Diego), G.H. Bearman (JPL/Caltech), P.B. Black (CRREL, Picatinny Arsenal), R.J. Bruno (JPL/Caltech), F.D. Carsey (JPL/Caltech), P.G. Conrad (JPL/Caltech), M. Daly (MD Robotics), D. Fisher (Geological Survey of Canada), G. Hargreaves (USGS/National Ice Core Laboratory), R.J. Henninger (JPL/Caltech), T.L. Huntsberger (JPL/Caltech), B. Lyons (Byrd Polar Research Center), P.R. Mahaffy (NASA—GSFC), K. McNamara (NASA—JSC), M. Mellon (University of Colorado), D.A. Papanastassiou (JPL/Caltech), W. Pollard (McGill University), K. Righter (NASA—JSC), L. Rothschild (NASA—ARC), J.J. Simmonds (JPL/Caltech), J.G. Spray (University of New Brunswick), A. Steele (Carnegie Institute of Washington), A.P. Zent (NASA—ARC)

Introduction: In early 2003, the Mars Icy Sample Team (MIST) was formed to address several questions related to the acquisition and analysis of ice-bearing samples on the surface of Mars by a robotic mission. These questions were specifically framed in the context of planning for the 2009 Mars Science Laboratory (MSL) lander, but the answers will also also have value in planning other future landed investigations.

Questions:

- Which scientific investigations, in priority order (especially of relevance to an assumed mission theme of habitability), can be addressed using ice-bearing samples and the MSL landed system?
- Which measurements are needed on ice-bearing samples to support these investigations?
- What are the minimum sample collection hardware and processes needed to acquire the necessary ice-bearing samples?
- What are the minimum sample preparation steps required for ice-bearing samples?
- What are the issues associated with preservation of the scientific content of the samples between the time of their collection and the time of their analysis?
- Can common hardware be used to interact with both ice-free and ice-bearing samples? This would allow the decision of where to send the mission (i.e., in terms of a latitude band) to be deferred until very late in the mission development process.

Assumptions: For the purpose of this analysis, we have defined four model sample types: Weakly ice-cemented regolith, ice-saturated regolith, ice-supersaturated samples (up to 100% ice), and ice-bearing rocks. These sample types have different concentrations of ice, different texture, and different resistance to sampling devices.

Ice Science Priorities: The MIST team ranked the scientific objectives of studying an ice-bearing sample (using the potential capabilities of the MSL landed system). The following is a prioritized list, using the impact on astrobiology as the prioritization criterion.

1. Is ice present and in what abundance?
2. Are organic molecules present in the sample, and if so, what is their identity, and what is their relationship to the ice fraction of the sample?
3. Is some fraction of the water present in the sample in the liquid state (e.g., as fluid inclusions, or along grain boundaries)? If so, how much, and what is its composition?
4. How did the ice get into the ground? Was it trapped from the atmosphere? Is it buried surface ice? Did it percolate from surface standing water or from sheetwash?
5. How old is the ground ice?
6. Has the ground ice been processed, melted, or redistributed since deposition? If so, when and how?

In addition, the planetary scientists on the MIST team concluded that several additional high priority investigations (origin of the water, climate at the time the ice formed, exchange rates/processes, planetary modeling, etc.).could be supported by measuring the isotopic properties of the water.

Some assertions regarding ice sample science: Based on the collective experience of the MIST team, we pose the following assertions regarding deriving science value from an ice-bearing sample on the martian surface.

1. For the ice-related investigations described above, well-designed measurements on a small number of ice-bearing samples will be more useful than poorly designed measurements on a large number of samples.

2. None of the high-priority ice-related measurements require that ice-bearing samples be crushed.
3. It is not scientifically necessary to split a sample to make multiple ice-related measurements. Most of the logic for doing this for the refractory portions of geologic samples does not apply to the ice fraction. It is far more important that the samples are fresh than to have statistically equivalent splits.
4. Sample aging is always a problem with ice-bearing samples. An acceptable solution to minimizing these effects is to optimize the operational scenario (e.g., transfer ice samples at night, while it is cold). This will be far simpler than mechanical means of sample preservation (e.g. encapsulation, refrigeration).
5. It is impossible to design a simple sample preparation and distribution system in which dry and wet samples follow the same path. We never do this in Earth labs.
    - If the ice fraction of a sample melts in a system designed for dry samples, there is potential for serious damage (un-removable contaminants, and perhaps worse).
    - Note: It may be possible using thermodynamic arguments to show that the ice will sublimate rather than melt, and if so, an engineering solution is not required.

Discussion:

For the highest-priority astrobiology investigations, non-destructive measurements are essential. Textural relationships between ice crystals, any organic material present, liquid/salt inclusions, and any associated mineral material need to be observed. Microscopy, probably with different kinds of illumination, will be key. For the highest priority planetary science investigations, subliming the ice and running the vapor through a mass spectrometer is essential. Given the priorities of the Mars program, we do not see a good scientific reason to subject an ice-bearing sample to mechanical sample preparation steps such as crushing and splitting. Thus, the mechanical process of interacting with an ice-bearing sample is in some ways simpler than interacting with rocks, which need to be crushed and split for many types of measurements.

The most useful kinds of ice-bearing samples for the scientific objectives described above are ice-saturated regolith and ice-supersatured material. These two sample types cannot be effectively sampled without a drill. We do not have a good way of calculating the depth of penetration necessary to acquire these sample types, but in our judgement a subsurface access capability of 0.3-0.5 m is a minimum.

When a cold ice-bearing sample is moved from its natural state to the warmer environment of the rover, it will progressively degrade, first by addition (freezing of water vapor onto the sample), then by subtraction (sublimation). We were unable to model the rate of this degradation process in the time available to us, but it will be dependent on the integrated exposure to higher temperature over time and air circulation. How much time-temperature is acceptable?--Preliminary calculations suggest that several hours should be acceptable if ΔT is modest.

Recommendations:

1. We recommend including a means of determining whether or not ice is present in the acquired sample either at the site of sample collection, or at the front end of the lab.
2. Minimize the effects of sample degradation by:
    - Placing ice-critical instruments in a cold part of the rover.
    - Collecting and processing samples for ice-related measurements at night.
    - Processing and analyzing ice samples quickly. We recommend that instruments needing to receive raw ice-bearing samples have a "bypass" port, which would allow raw material to be introduced without passing through the sample preparation systems.
3. To protect the principal (dry) sample prep and analysis systems which are at the heart of MSL's scientific objectives, we recommend that samples be dried prior to introduction into crushing, splitting, or sieving operations.
    - The combination of time and temperature necessary to achieve the minimum necessary state of dryness needs more analysis and discussion. A part of this analysis needs to include assessment of the temperature at which one starts to lose information on hydrated phases.

Conclusion:

Our summary conclusion is that it is possible to design a single overall surface system that can interact with both ice-bearing and ice-free samples. However, this system will need to have more complexity than a system designed to interact only with ice-free samples. Such a system could be designed now, and we would be able to send it to a location selected years from now in response to future discoveries (possibly either ice-free or ice-bearing).

YEARLY COMPARISONS OF THE MARS NORTH POLAR CAP: 1999, 2001, AND 2003 MOC OBSERVATIONS. J. L. Benson and P. B. James, Ritter Astrophysical Research Center, Dept. of Physics and Astronomy, Univ. of Toledo, Toledo, OH 43606 (jbenson@physics.utoledo.edu; pbj@physics.utoledo.edu)

Introduction: The seasonal cycle of the martian north polar cap has been studied since the time of William Herschel, who published the first quantitative observations of the seasonal recession of the polar caps in 1784 [1]. Ground-based observations made after Herschel were summarized by Slipher in 1962 [2]. More recent ground-based observations of the north polar cap have been done by Iwasaki et al. [3, 4, 5, 6]. Mariner 9 [7] and Viking [8, 9] also made north polar observations. Cantor et al. used Hubble Space Telescope observations between 1990 and 1997 to determine several north polar recessions and Lambert albedos of the cap [10].

Mars Global Surveyor went into orbit around Mars in September 1997. The wide-angle cameras on the Mars Orbiter Camera (MOC) acquire images of the entire planet every day at a resolution of ~ 7.5 km/pixel in both red (575 nm – 625 nm) and blue (400 nm – 450 nm) bandpasses (WAR and WAB). Some polar cap observations were acquired during the aerobraking (AB) and science phasing (SPO) of MGS before systematic mapping began in March, 1999 at L_S = 110°.

More than two complete Martian years have now been monitored by MGS/MOC, including three summer seasons in the northern hemisphere. Data pertaining to the spring / summer recessions of the north cap during the first year of mapping has been reported previously [11]. The north polar recession in 2000 was very similar to previously observed recessions. The MOC observations confirmed an almost linear cap regression from L_S = 340° until L_S = 60°.

Using WAR images, we have studied the subsequent spring recession of the north seasonal polar cap and also made albedo measurements of the residual cap. We look for interannual variability between this and previous years observed by MOC. This comparison is especially interesting because an extensive planet encircling dust storm occurred in early northern fall of the second Martian year while there was no such large storm in the first year. Therefore, it may be possible to determine the effects of dust on the condensation and sublimation of the carbon dioxide in the cap.

Seasonal North Cap: The late winter and early spring portions of the north cap recession have been phases for which the largest interannual variability has been reported. The extent of the surface cap boundary in late winter has been controversial. Also, a halt in cap regression in early to mid-spring has been reported [3, 8]; that is, the boundary of the cap remains fixed at a latitude of about 65º for several weeks before the recession resumes. A global dust storm during the condensation phase of the north cap is one mechanism suggested to be responsible for this variability. However, it is difficult to separate interannual effects from longitudinal asymmetries in the cap due to the gradual change in the longitudes on Mars seen from a location on Earth.

We have determined the regression curves for the 2000-2001 and 2002-2003 recessions of the north polar cap (Figure 1); a planet encircling dust storm occurred in early fall in the second year. The regression curves from the two years are very similar, however, there are small differences between L_S=10º and L_S=50º. There is no sign of a halt in cap regression in either year.

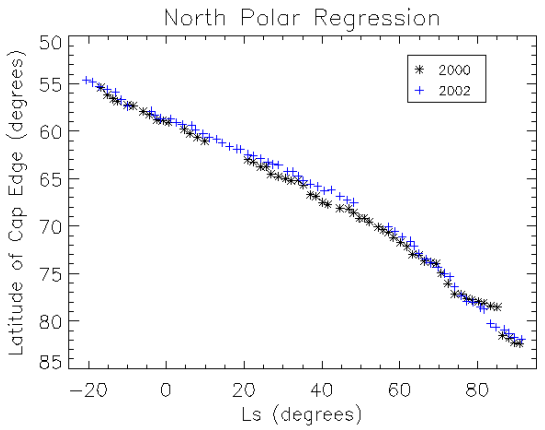

Figure 1: Regression of the north polar cap in 2000 (*) and 2002 (+). The latitude of the cap edge on a sterographic projection is ploted versus areocentric solar longitude. Recessions are similar, however, there are slight variations between L_S=10º and L_S=50º.

Residual North Cap: Mars Global Surveyor mapping began at L_S = 110º in 1999. Detailed comparisons of the caps in different years are complicated by frequent dust storms that may obscure the surface cap; fallout from these storms on the surface cap may also affect the apparent albedo for longer periods.

In Figure 2, the average Lambert albedo of the center (geographic pole) of the RNPC is plotted against L_S

for 1999 (*) and 2003 (Δ). Due to a change in sensitivity of the MOC WA Red Camera during the fall of 2001, those data are not included here, however, James and Cantor have reported these results [12]. The general behaviors of the albedo in this central region of the cap seem to be similar in the two years. The main exceptions are two data points from 1999 near L_S = 135°. There is a gap in the MOC WA red mapping subsequent to these events due to the Geodesy Campaign; so the question of the duration of this suppression is not answered by the red images alone, and additional investigation using the blue filter mapping images, which continued through the period, will be needed. The decrease after L_S > 160° is probably due to the fact that the Lambert approximation fails at the large incidence angles in late summer.

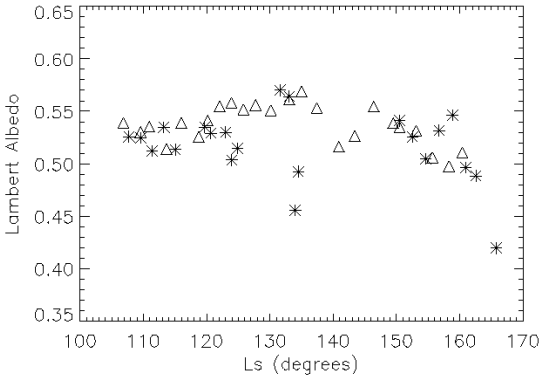

Figure 2: Average Lambert albedo for a 30 × 30 pixel^2 region around the geographic north pole as a function of L_S for 1999 (*) and for 2003 (Δ).

Acknowledgements: The authors were supported by grants from the Mars Data Analysis Program.

References: [1] Herschel, W. (1784) *Phil. Trans*., 24, 233-273. [2] Slipher, E. C. (1962) *The Photographic Story of Mars*, Northland Press. [3] Iwasaki, K. et al. (1979) *JGR*, 84, 8311-8316. [4] Iwasaki, K. et al. (1982) *JGR*, 87, 10265-10269. [5] Iwasaki, K. et al. (1984) *PASJ*, 36, 347-356. [6] Iwasaki, K. et al. (1999) *Icarus*, 138, 20-24. [7] Soderblom, L. A. (1973) *JGR*, 78, 4197-4210. [8] James, P. B. (1979) *JGR*, 84, 8332-8334. [9] James, P. B. (1982) *Icarus*, 32, 565-569. [10] Cantor, B. A. et al. (1998) *Icarus*, 136, 175-191. [11] James, P. B. and Cantor, B. A. (2001) *Icarus*, 154, 131-144. [12] James, P. B. and Cantor, B. A. (2001) *BAAS XXXIII*, Abstract #19.16.

EFFECTS OF ATMOSPHERIC AND SURFACE DUST ON THE SUBLIMATION RATES OF CO_2 ON MARS. B. P. Bonev[1], P. B. James[1], J.E. Bjorkman[1], G. B. Hansen[2], and M. J. Wolff[3], [1]Ritter Astrophysical Research Center, Dept. of Physics and Astronomy, Univ. of Toledo, Toledo, OH 43606, USA (bbonev@kuiper.gsfc.nasa.gov; pbj@physics.utoledo.edu; jon@physics.utoledo.edu), [2]Planetary Science Institute, Northwest Division, Univ. of Washington, Seattle laboratory, Seattle, WA 98195 (ghansen@rad.geology.washington.edu), [3]Space Science Institute, 3100 Marine Street, Boulder, CO 80303-1058, USA (wolff@colorado.edu).

Introduction: We present an overview of our modeling work dedicated to study the effects of atmospheric dust on the sublimation of CO_2 on Mars. The purpose of this study is to better understand the extent to which dust storm activity can be a root cause for interannual variability in the planetary CO_2 seasonal cycle, through modifying the springtime regression rates of the south polar cap. We obtain calculations of the sublimation fluxes for various types of polar surfaces and different amounts of atmospheric dust. These calculations have been compared qualitatively with the regression patterns observed by Mars Global Surveyor (MGS) in both visible [1, 2] and infrared [3] wavelengths, for two years of very different dust histories (1999, and 2001).

Atmospheric modeling: Our approach is to model the radiative transfer through a dusty atmosphere bounded by a sublimating CO_2 surface. Although we have done some preliminary monochromatic calculations [4], our main focus has been to employ a full spectrum model, which incorporates the main effect of atmospheric dust. This is the redistribution of the radiation incident to the surface from visible frequencies to the IR. We have adapted a monte-carlo radiative equilibrium algorithm, initially developed for modeling circumstellar envelopes [5], to the case of a plane-parallel dusty planetary atmosphere. This model was introduced in a case study [1] applied to the regression of the Mountains of Mitchel, one of the brightest regions in south seasonal polar cap. This work points out that although our model atmosphere is one-dimensional, our radiation transfer code is three-dimensional and includes wavelength-dependent dust opacity, anisotropic scattering and thermal dust emission. We have used the most recently calculated dust single scattering properties for both visible and IR wavelengths [6]. An important modification of the original code, has been the treatment of anisotropic scattering in the visible spectral region, which enabled incorporating the phase function appropriate for Martian dust [7].

Surface modeling: The surface albedo spectrum is a major parameter in this study. Its accurate modeling is of primary importance and without it, the effects of atmospheric dust cannot be assessed correctly. There are a number of parameters influencing the surface albedo spectrum [8], the most important of which is the amount of *surface dust intermixed in the frost*. The amount of surface intermixed dust and water, and the grain size of the CO_2 frost, can be constrained by data from at least three spectral regions: the thermal IR near 25 microns [8], the near-IR [9], and the visible ranges of the Mars Orbiter Camera (MOC) on MGS [10]. We initially conducted a limiting case study [1] of the sublimation of surfaces with zero and very high dust content. In [11] we have examined in depth the albedo changes with surface dust-to-ice mixing ratio and CO_2 frost grain size; the variation of the albedo with photon incident angle and the dependence on the ratio of direct/diffuse incident radiation. In monte carlo calculations the albedo dependence on the direction of the reflected photons is also important. This variable has been held as a free parameter by simulating different laws of surface reflection. A good constraint of the best directional distribution of the photons reflected would enable incorporating this factor accurately into our model.

Sublimation fluxes for different amounts of atmosheric and intermixed surface dust: We have calculated sublimation fluxes (SF) for a number of combinations between the total atmospheric dust optical depth and the type of the CO_2 ice surface. The SF have been normalized to the total flux incident on the atmosphere and calculated as a difference between the spectrally integrated fluxes absorbed and emitted by the surface (set to sublimate at 147 K). An example calculation is presented on Figure 1. It corresponds to a particular grain size, but this parameter has been varied as well [11]. The main model results reproduce qualitatively the observational comparison between 1999 (relatively dust free year) and the 2001 (global dust storm) south polar cap regression patterns, observed by MGS and described in [2, 11]:

1. The absorption of surface frost with a high dust content (1 wt% being the upper limit [8]) is dominated by visual photons. Therefore the attenuation of direct solar radiation by atmospheric dust results in retarded sublimation.

2. Conversely, the absorption of regions with low dust content is dominated by IR photons, owing to the

high visual albedos. In this case the visual-to-IR redistribution of the energy incident to the surface, caused by atmospheric dust, leads to increased sublimation rates.

3. There is a wide range of combinations between surface dust content and frost grain size for which the CO_2 sublimation rates show only subtle variations with the amount of atmospheric dust load. In these cases the surface absorption is distributed equally between visual and IR wavelengths, so the overall atmospheric dust effect is not important. It should be emphasized that the discussed region of the parameter space represents a "typical frost" [8] and consequently explains the apparent insensitivity of the *average decay rate* of the south seasonal cap to dust storm activity [2]. Strong coupling between sublimation and atmospheric dust exists primarily on *local scale* for regions with "deviant" surface albedos such as the Mountains of Mitchel (high visual albedo, faster regression in 2001 [1,3]), and the "Cryptic" region [12] (low visual albedo, slower regression in 2001 [3]).

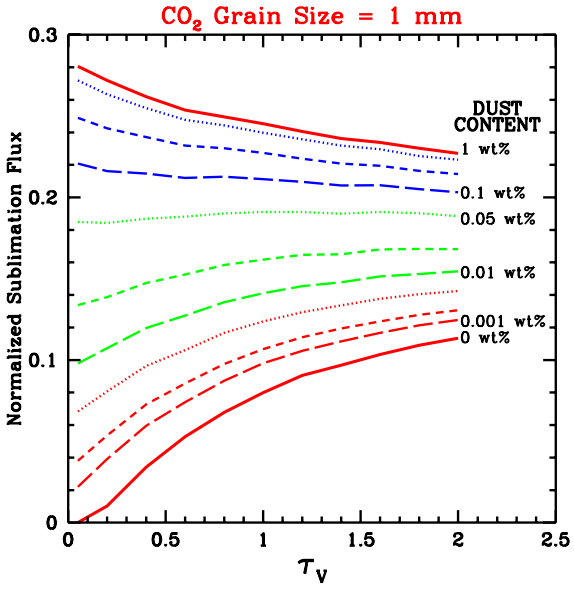

Figure 1. CO_2 Sublimation Flux vs. Total Atmospheric Dust Optical Depth at 550 nm for a frost grain size of 1 mm and various contents of intermixed surface dust.

A note should be made about the possibility that newly deposited surface dust played a role in the faster regression of bright regions (like the Mountains of Mitchel) by lowering the surface albedo and thus increasing the absorbed flux and consequently the sublimation rate. While this scenario cannot be ruled out, it fails to explain the slowing down of the dark regions such as the Cryptic region, which is consistent with the effect of atmospheric dust.

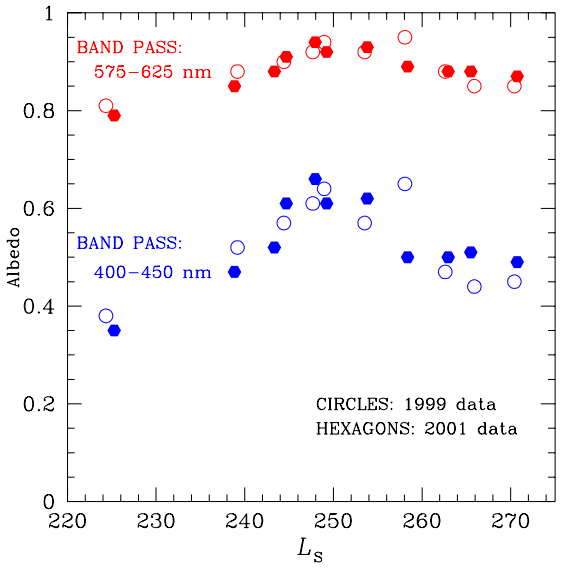

Figure 2. Top-of-the atmosphere Lambert albedos from 1999 and 2001 MOC data, averaged over a region within the perennial residual south polar cap.

In progress: In addition to the presented overview, we will discuss improvements of the atmospheric modeling, and some aspects of the study of the perennial residual south polar cap. The high maximum values of the red visual albedo of the residual cap (Figure 2) suggest small contents of intermixed surface dust and low sublimation rates at dust free conditions. The maximum values of the red and blue albedo measurements (like L_s~148°, 1999) most likely have minimal atmospheric contribution and can be used to constrain the ice properties through models of surface albedo spectra [8]. The likely higher sublimation the cap has undergone in 1972 (Mariner 9 observations) will also be addressed.

Acknowledgement: Four of the authors (BPB, MJW, PBJ, GBH, and JLB) were supported by grants from the Mars Data Analysis Program. JEB was supported by NSF Grant AST-9819928.

References: [1] Bonev, B. P. et al. (2002) *GRL*, *29*, 2017, doi:10.1029/2002GL015458. [2]. James, P. B. et al. (2003), *Intern. Mars Conf. VI,* #3093. [3] Titus, T. N. and Kieffer, H. H. (2002) *LPS XXXIII*, #2071. [4]. James, P. B. et al. (2000) *DPS 32, #51.10.* [5] Bjorkman, J. E. and Wood, K. W. (2001) *ApJ*, *554*, 615-623. [6] Wolff, M J. and Clancy, R. T. (2003) *JGR*, in press. [7] Tomasko et al. (1999) *JGR, 104, 8987-9007*. [8] Hansen, G. B. (1999) *JGR, 104*, 16,471-16,486. [9] Glenar et al. (2002), *DPS 34, #15.23*. [10] James et al. (2001) *JGR, 106, 23,635-23,652*. [11] Bonev, B. P. et al. (2003), *Intern. Mars Conf. VI,* #3111. [12] Kieffer, H. H. et al. (2000) *JGR, 105, 9653-9699*.

The most recent section of the south polar layered deposits. S. Byrne[1] and A.B. Ivanov[2], [1]Division of Geological and Planetary Sciences, California Institute of Technology, Mail-stop 150-21, Pasadena, CA 91125.. [2]Jet Propulsion Laboratory, MS168-416, Pasadena, CA 91106. **shane@gps.caltech.edu**, **anton.ivanov@jpl.nasa.gov**

Introduction: The polar layered deposits of both hemispheres contain a record of Martian environmental conditions. In this study we will assemble a fully three dimensional stratigraphic sequence for the topmost section of the southern layered deposits.

A prominent layer sticks out as a bench part-way down the section. We will correlate other layers relative to this one in exposures on opposite ends of the section. In this way we hope to learn how this part of the overall southern layered deposits is organized in three dimensions.

The necessary datasets which will be utilized will be hires topographic grids from the Mars Orbiter Laser Altimeter (MOLA) provided by the MOLA team and high resolution Mars Orbiter Camera (MOC) images with spatial resolutions of 1.4 to 12 m/px. Due to continuous repeat coverage of the polar orbiting Mars Global Surveyor and Mars Odyssey (MGS & MO) spacecraft this area has very high coverage. MOC frames almost totally cover the entire exposure which makes it ideal for this kind of study.

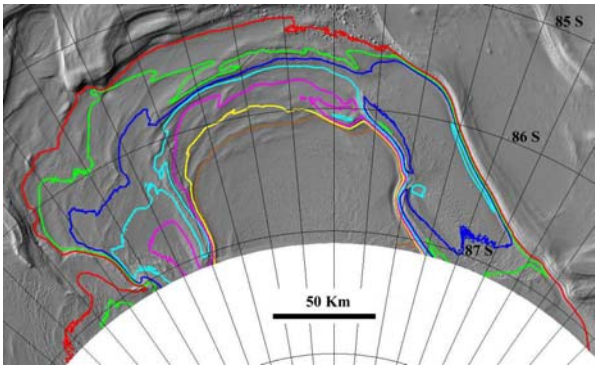

Figure1: MOLA derived shaded relief view of the top of the south polar layered deposits illuminated from the left. The coloured lines represent elevation contours from 4000m to 4600m (red to brown) at 100m intervals.

Regional context and marker bed: The layered sequence in the southern layered deposits can be divided into discrete sections based on elevation (see figure 1). The topmost section is centered on 87° S 5° E and its exposures span elevations of 4300m - 4600m. The highest point of the layered deposits (~4800m) also lies within this area. The top surface is covered with a thin skin of CO_2 ice which comprises part of the southern residual cap.

The layers comprising this section are exposed in scarps to the east and west at 350° E and 20° E as shown in figure 1. The northern edge of this section is not well exposed due to a smooth mantling cover and disruption from the McMurdo secondary crater field. The southern end of this section is well exposed on continuations of the eastern and western scarps however the lack of spacecraft data poleward of 87° S prohibits analysis in this region.

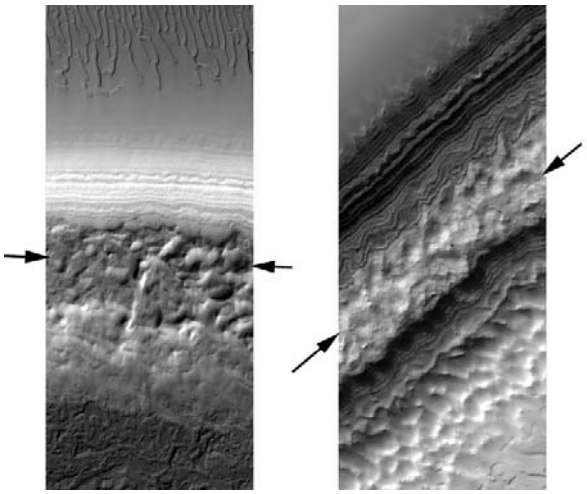

Figure 2: MOC images M08/06301 (left) and M08/02672 (right) from the western and eastern scarps respectively. Scale in both cases is the same (each image 2.8 km wide). Illumination from lower right and upper left respectively. Elevation decreases from top to bottom by 400-500 meters in both cases.

Figure 2 shows an example of two MOC frames separated by ~100 km. The same heavily pitted topographic step is visible part way down the scarp in both cases. This layer will serve as a marker bed by which the position of other layers can be measured.

Work to be presented: We will report on variations in elevations of layers within the topmost section of the south polar layered deposits. We will consider models where the layers are represented as inclined planes and surfaces containing low-order curvature.

We will document changes in strikes and dips as a function of elevation which can be interpreted as erosional unconformities. A lack of erosional unconformities within the section would imply a stable polar environment over the time it took this section to form.

CHALLENGES AND SOLUTIONS FOR THE HUMAN EXPLORATION OF THE MARTIAN POLES.

Charles Cockell, SETI Institute, NASA Ames Research Center, Moffett Field, CA 94035-1000.

Introduction: The Martian poles present special challenges for human scientific expeditions that bear similarities to operations in terrestrial polar regions. These challenges include mobility on snows and ices, the problem of accommodation in the deep field, methods for the use of local resources and problems of station maintenance. Because the polar regions are dynamic, substantial volatile sinks, the exploration of the polar regions by humans is a potentially high priority exploration goal. Furthermore, the high astrobiological potential of these regions makes them attractive targets for human exploration.

The exploration of the Martian poles might begin in the earliest stages of a human presence on the planet or missions of exploration might be launched from lower-latitude stations that would avoid the 9-month 24 hr darkness of polar winter, which imposes substantial long-term safety problems.

Mobility: I describe a series of concepts in response to these challenges [1-3]. Mobility on Martian snows and ices can be achieved with pressurized tracked rovers or unpressurized skidoos using methane or other fuels readily made from CO_2 and H_20, both abundantly available at the poles. Materials and supplies can be carried by Nansen sledge in an analogous way to Earth. By heating the underside of the sledges, a sublimed vapor layer can be used to assist in mobility and reduce the chances of freezing to the polar substratum ('polar hover').

Field stations: Field stations, depots and deep-field sites can be realized with pressurized 'ball' tents that allow two scientists to rest within a pressurized, heated environment. Larger versions of such easily assembled stations ('ball field stations') can be used for emergencies and the establishment of short-term camps on the polar ice caps. An augmentation of the ball tent is the Migloo - Martian igloo assembled from a pressurized tent surrounded with blocks of ice that can be used as a Solar Particle Event shelter, the ice reduces the radiation flux. These structures may also find use in deploying robust depots across the polar caps.

In-situ resourse use: Liquid water for drinking and for fuel and oxygen production can be gathered from the poles by two means – either 1) subliming the ice and snow by heating it and gathering the vapor for use in various manfacturing processes. This can be achieved with innovations such as 'sublimation netting' (Figure 1), a network of hollow, heated fibres that heat the ice and snow and draw it into a vacuum system or 2) pressurizing blocks of cut snow and ice and then heating directly into a liquid state, thus avoiding the cost of the latent heat of vaporisation.

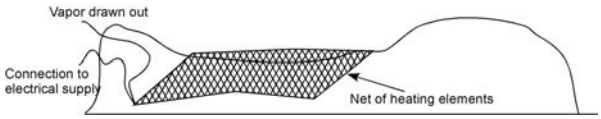

Figure 1. Sublimation netting can be used to gather water for in-situ resource utilization at the Martian poles.

Trans-polar assaults: As well as scientific exploration at specific points on the polar caps, future expeditions might be launched as exploratory trans-polar expeditions across the Martian poles. These expeditions would gather samples across a polar transect and complete traverses that in distance are similar to Trans-polar Antarctic expeditions. I discuss operations at the Martian poles during the 24 hr darkness of polar winter and the challenges presented to overwintering operations.

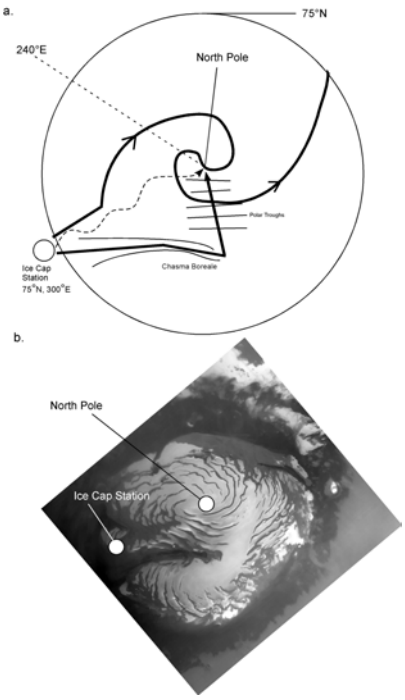

Figure 2. Trans-polar expeditions provide opportunities for polar sampling and purely exploration-driven assaults.

References: [1] C.S. Cockell, (1995) *JBIS*, 48, 359-368. [2] C.S. Cockell, (2001) *Acta Astronautica*, 49, 693-706. [3] C.S. Cockell and A.A. Ellery, (2003) *JBIS*, 56, 33-42.

SIMULATIONS OF THE SEASONAL VARIATIONS OF THE MARS SOUTH POLAR CAP: PRELIMINARY RESULTS. K. Dassas , F. Forget , *Laboratoire de Meterologie Dynamique du CNRS, Universite Paris 6, BP99, 75252 Paris Cedex 05, France (dassas@lmd.jussieu.fr).*

Introduction

Every martian year, as much as 30% of the CO_2 atmosphere of Mars condenses in the polar caps of each hemisphere during their respective polar nights. During the spring and summer seasons in a given hemisphere, the seasonal CO_2 cap sublimates back into the atmosphere. While the north polar cap remains roughly circular and centered on the geographic pole during its recession, the south polar cap becomes assymetric with strong variations with space and time. In particular, the preservation of a permanent CO_2 deposit all year long near the south pole raises important issues such as the potential ability of these deposits to buffer the atmosphere. The TES observations of the south polar region during its recession have also confirmed that two regions have different behavior than the rest of the cap in terms of albedo and CO_2 budget. These are the Mountains of Mitchel, a high albedo area where the frost is left behind after the rest of the polar cap recedes each spring, and the Cryptic region, an extended low albedo area which sublimates earlier than the rest of the cap [1]. As of today , the existence and location of the residual cap, the mountains of Mitchel, and the Cryptic region remain poorly understood. No obvious correlations have been found between these areas of interest and topography, geology, thermal inertia or ground albedo [1-2].

Current situation

In the LMD martian general circulation model [3-5], the condensation and sublimation of carbon dioxide on the ground is primarily controlled by relatively simple physical processes. When the surface temperature falls below the condensation temperature, CO_2 condenses, releasing the latent heat required to keep the solid-gas interface at the condensation temperature. Conversly, when CO_2 ice is heated, it partially sublimes to keep its temperature at the frost point temperature. In the atmosphere, condensation may result from radiative cooling on the one hand (especially when the atmosphere is dust laden) and from adiabatic cooling in upward motions on the other hand. The radiative effect of CO_2 snow fall and fresh snow can be taken into account by lowering the emissivity [3]. Although the LMD GCM represents pretty well the boundaries and the total mass of the polar caps, it doesn't reproduce neither the Cryptic region nor the mountains of Mitchell or the residual polar cap. The modeled south polar cap completely sublimes by the beginning of summer.

Investigation

To better understand and simulate polar cap features like the Cryptic region, the mountains of Mitchel or the perenial CO_2 ice cap, different investigations have been done.

What happen's during the polar night?

Using the LMD GCM, simulations have been performed during the polar night (Ls90-120) in order to highlight possible enhanced or reduced CO_2 condensation rate in regions of interest. No obvious correlations between atmospheric or ground condensation rate and neither the Cryptic region nor the mountains of Mitchel have been found. Such a work could be of interest to compare with the Mars clouds detected by the Mars Orbiter Laser Altimeter (MOLA) [6].

New albedo parametrization.

Previously in GCM, the ice albedo parametrization was not dependent on the incident solar flux. According to the observations the CO_2 ice albedo increases as the CO_2 ice is exposed to increasing insolation [6]. We added this parametrization in the GCM. At the same time, we have simulated the fact that slab CO_2 ice becomes transparent when it becomes thin by defining the albedo as a combination of the ice and underlying ground albedos depending on a chosen thickness of the CO_2 ice layer.

Taking account slope orientation.

The previous parametrization of the incident solar flux surface was not taking account the slope (orientation and absolute value). We have performed simulations with a new slope dependent parametrization. Slopes have been calculated using the MOLA topography data (32 pixels / degree).

Future work

In order to better understand the seasonal variations of the south polar cap, we will continue this project and, in particular, perform very high spatial resolution simulations in order to highlight the slope effect or the spatial variations of atmospheric condensation. We also want to improve CO_2 ice microphysic representation, and some work should be done to determine the role of dust. Once all these processes will be taken into account, the GCM should be able to predict features like the Mountain of Mitchel or the Cryptic region. Otherwise, these features will have to be considered as a

major enigma of the martian climate system.

References [1] Kieffer H. et al (2000) JGR, 105, 9653-9699. [2] James P. et al (2001) JGR, 106, NO. E10, 23,635-23,652. [3] Hourdin F. et al (1993) JAS, 50, 3625-3640. [4] Forget F. et al (1998) Icarus, 131, 302-316. [5] Forget F. et al (1999) JGR, 104, 24,155-24,176. [6] Neumann et al (2003) JGR, 108, NO. E4, 5023. [7] Paige D.A (1985) Science, 228, 1160-1168.

EPISODIC ENDOGENETIC-DRIVEN ATMOSPHERIC AND HYDROLOGIC CYCLES AND THEIR INFLUENCE ON THE GEOLOGIC RECORDS OF THE NORTHERN AND SOUTHERN HEMISPHERES, MARS

J. M. Dohm, *Department of Hydrology and Water Resources, University of Arizona, Tucson, Arizona (jmd@hwr.arizona.edu)*, **A. G. Fairén**, *CBM, CSIC-Universidad Autónoma de Madrid, 28049-Cantoblanco, Madrid, Spain,* **V. R. Baker,** *Department of Hydrology and Water Resources, University of Arizona, Tucson, Arizona,* **J. C. Ferris**, *United States Geological Survey, Denver, Colorado,* **R.C. Anderson**, *Jet Propulsion Laboratory, Pasadena, California,* **E. R. Uceda,** *Servicio de Endocrinología, Hospital Ramón y Cajal, Madrid.*

Diverse evidence shows a direct correlation between episodic endogenetic events of the Tharsis magmatic complex (TMC)/Superplume [1], flood inundations in the northern plains [2], and glacial/lacustrine/ice sheet activity in the south polar region, which includes Hellas and Argyre impact basins (**Fig. 1**) [3-5], corroborating the MEGAOUTFLO hypothesis [6,7]. The TMC encompasses a total surface area of approximately 2 X 10^7 km^2, which is slightly larger than the estimated size of the Southern Pacific Superplume [8]. These hydrologic events include (1) a Noachian to possibly Early Hesperian oceanic epoch and related atmospheric and environmental change (a water body covering about 1/3 of the planet's surface area [9]) related to the incipient development of Tharsis Superplume and the northwestern sloping valleys (NSVs) [10,11] and possibly early circum-Chryse development [12-14], the northwest and northeast watersheds of Tharsis, respectively, (2) a smaller ocean [6-7; 15-17] inset within the former larger ocean related to extensive Late Hesperian to Early Amazonian effusive volcanism at Tharsis [18] and Elysium [19-20] and incisement of the circum-Chryse outflow system [e.g.,12-13]. During this time, magmatic/plume-driven tectonic activity transitioned into more centralized volcanism [4,21]. This Late Hesperian water body may have simply diminished into smaller seas and/or lakes [22] during the Amazonian Period, or renewed activity at Tharsis [21] and Elysium [20,23] resulted in brief perturbations from the prevailing cold and dry climatic conditions to later form minor seas or lakes [2]. All of the hydrologic phases transitioned into extensive periods of quiescence [1,2].

Dynamic, pulse-like, magmatic activity, especially at Tharsis [10] is partly the result of a stagnant-lid lithospheric regime where the internal heat of the planet builds over time to catastrophically erupt magmas and volatiles at the martian surface [1,6,7]. This is not to be unexpected, as pulses of activity are also documented for the Southern Pacific Superplume on Earth where present plate tectonism is recorded [8]. On Mars, the primary releases of the stored-up internal heat of the planet occur at dominant vent regions such as at Tharsis and Elysium and along pre-existing zones of weaknesses related to earlier magmatism and tectonism. This may include both impact events and plate tectonism during the earlier stages of planetary development [1,24]. Persistent periods of quiescence transpired between these violent outbursts sending the planet back into a dormant deep freeze [1,25], with the exception of areas where elevated geotherms persist and local hydrologic activity occurs.

Following a persistent deep freeze and ever thickening cryosphere, an Ontong Java-sized event on Mars (especially considering it is unvegetated and less than half the size of Earth, allowing a far greater impact to the climatic system) would trigger enhanced atmospheric conditions and hydrologic dynamics. A prime example of this process is observed during the Late Noachian/Early Hesperian; a time when magmatic-driven activity included the emplacement of older wrinkle ridged materials in the Thaumasia Planum region, the formation of the Thaumasia plateau, and major development of the primary centers of activity, Syria and central Valles (Stage 2 of Tharsis Superplume evolution; see [4,10-11,21]).

Though variation in the orbital parameters of Mars must be considered as a contributing influence on environmental change [26], a direct correlation between endogenic activity at Tharsis (and to a lesser extent Elysium) and global aqueous activity on Mars is observed in the geologic and paleohydrologic records of Mars (schematically portrayed in **Fig. 1**), including: (1) inundations in the northern plains and relatively short-lived climatic perturbations [1,2,6-7,25], (2) growth and retreat of the south polar ice sheet [5], (3) glacial and lacustrine activity in and partly surrounding Hellas [27] and Argyre [3-4], (4) outflow channel activity at NSVs [10-11] and circum-Chryse [e.g.,12-13], (5) formation of the Tharsis Montes aureole deposits [28], and development of impact crater lakes [29,30]. As such, any theoretic modelling of martian atmospheric or surface conditions must take into account endogenetic-driven activity as distinctly expressed in the geologic record.

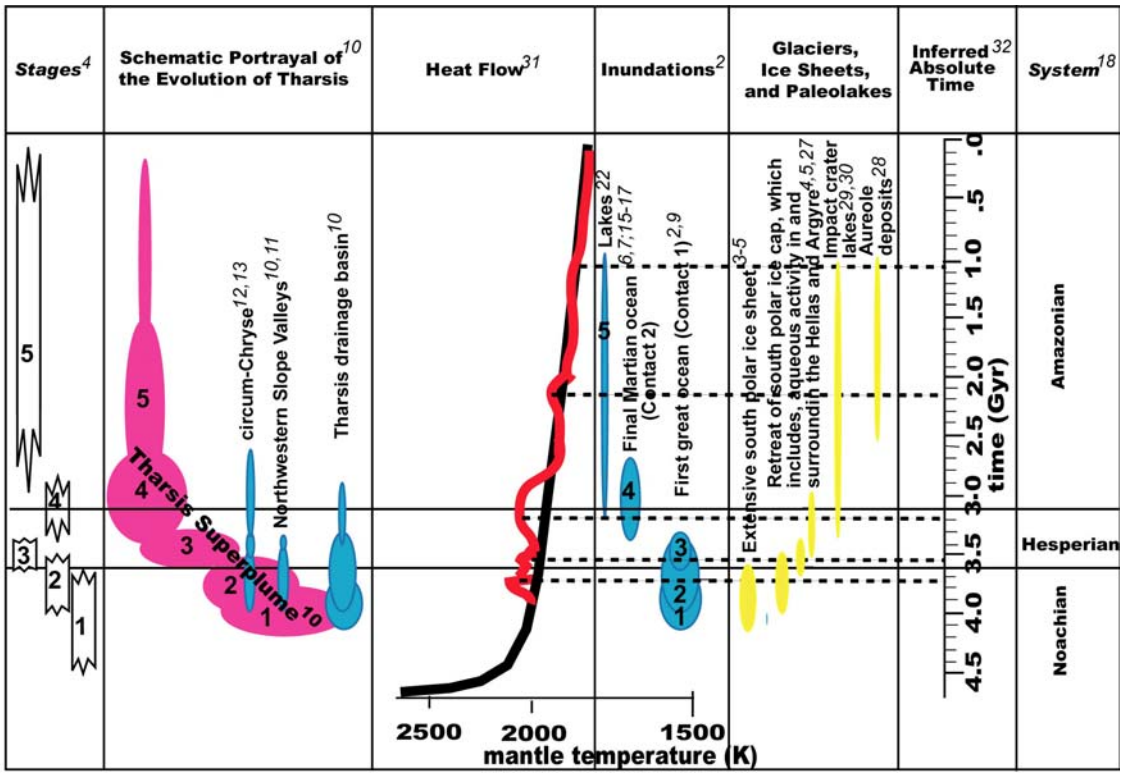

Figure 1. Schematic diagram portraying the spatial and temporal occurrence of major geologic and hydrologic events in martian history.

References. [1] Baker, V.R., *et al*. (2002). A theory for the geological evolution of Mars and related synthesis (GEOMARS). *Lunar Planet. Sci. Conf.*, XXXIII, #1586 (abstract) [CD-ROM]. [2] Fairén, A.G., et al. (2003). Episodic flood inundations of the northern plains of Mars. *Icarus*, in press. [3] Kargel, J.S., and Strom, R.G. (1992). Ancient glaciation on Mars. *Geology*, 20, 3-7. [4] Dohm, J.M., et al., (2001a). Geologic, paleotectonic, and paleoerosional maps of the Thaumasia region of Mars: USGS Misc. Inv. Ser. Map I-2650, scale 1:5,000,000. [5] Milkovich, S.M., et al. (2002). Meltback of Hesperian-aged ice-rich deposits near the south pole of Mars: evidence for drainage channels and lakes. *J. Geophys. Res*., 107, 2001JE001802. [6] Baker, V.R., *et al.* (1991). Ancient oceans, ice sheets and the hydrological cycle on Mars. *Nature*, 352, 589-594. [7] Baker, V.R., *et al.* (2000). Mars' Oceanus Borealis, ancient glaciers, and the MEGAOUTFLO hypothesis. *Lunar Planet. Sci. Conf.*, XXXI, #1863 (abstract) [CD-ROM]. [8] Maruyama, Shigenori, 1994. Plume tectonics, J. Geol. Soc. of Japan, 100, 24-49. [9] Clifford, S. M., and Parker, T. J. (2001). The evolution of the Martian hydrosphere: Implications for the fate of a primordial ocean and the current state of the northern plains. *Icarus*, 154, 40–79. [10] Dohm, J.M., *et al*. (2001b). Ancient drainage basin of the Tharsis region, Mars: Potential source for outflow channel systems and putative oceans or paleolakes. *J. Geophys. Res*., 106, 32,943-32,958. [11] Dohm, J.M., *et al*. (2001c). Latent outflow activity for western Tharsis, Mars: Significant flood record exposed. *J. Geophys. Res*., 106, 12,301-12,314. [12] Rotto, S.L., and Tanaka K.L. (1995). Geologic/geomorphologic map of the Chryse Planitia region of Mars. *U.S. Geol. Surv. Misc. Invest. Ser.* Map I-2441. [13] Nelson, D. M., and Greeley, R. (1999). Geology of Xanthe Terra outflow channels and the Mars Pathfinder landing site. *J. Geophys. Res*., 104, 8653-8669. [14] Zuber, M.T., et al. (2000). Internal structure and early thermal evolution of Mars from Mars Global Surveyor topography and gravity. *Science*, 287, 1788-1793. [15] Parker, T. J., *et al.* (1987). Geomorphic evidence for ancient seas on Mars. In *Symposium on Mars: Evolution of its Climate and Atmosphere, LPI Tech. Rept. 87-01*, 96-98, 1987. [16] Parker, T.J., *et al.* (1993). Coastal geomorphology of the Martian northern plains. *J. Geophys. Res*., 98, 11061-11078. [17] Head, J.W., *et al.* (1999). Possible ancient oceans on Mars: Evidence from Mars Orbiter laser altimeter data. *Science*, 286, 2134-2137. [18] Scott, D.H., and Tanaka, K.L. 1986. Geologic map of the western equatorial region of Mars, *USGS Misc. Inv. Ser. Map I-1802-A (1:15,000,000)*. [19] Greeley, R, and Guest, J. E. 1987. Geologic map of the eastern equatorial region of Mars, *USGS Misc. Inv. Ser. Map I-1802B (1:15,000,000)*. [20] Tanaka, K.L., et al. (2003). Resurfacing history of the northern plains of Mars based on geologic mapping of Mars Global Surveyor data. *J. Geophys. Res*., 108, 8043, doi: 10.1029/2002JE001908. [21] Anderson, R.C., *et al.* (2001). Primary centers and secondary concentrations of tectonic activity through time in western hemisphere of Mars. *J. Geophys. Res.,* **106**, 20,563-20,585. [22] Scott, D.H., *et al.* (1995). Map of Mars showing channels and possible paleolake basins. U.S. Geol. Surv. Misc. Invest. Ser. MAP I-2461. [23] Skinner, J. A., and Tanaka, K. L. (2001). Long-lived hydrovolcanism of Elysium. *Eos. Trans. AGU* ***82***, Fall Meet. Suppl., Abstract P31B-07. [24] Fairén, A.G., et al. (2002). An origin for the linear magnetic anomalies on Mars through accretion of terranes: implications for dynamo timing. *Icarus*, 160, 220-223. [25] Baker, VR. (2001). Water and the Martian landscape. *Nature*, 412, 228-236. [26] Touma, J., and Wisdom, J. 1993. The chaotic obliquity of Mars. *Science*, 259, 1294-1296. [27] Moore, J. M., and Wilhelms, D. E. 2001. Hellas as a possible site of ancient ice-covered lakes on Mars. *Icarus*, 154, 258-276. [28] Scott, D.H., et al. (1998). Geologic map of the Pavonis Mons volcano, Mars: *USGS Misc. Inv. Ser. Map I-2561* (1;2,000,000 scale). [29] Cabrol, N. A., and Grin, E. A. (1999). Distribution, classification and ages of Martian impact crater lakes. *Icarus*, 142, 160-172. [30] Cabrol, N. A., and Grin, E. A. (2001). The evolution of lacustrine environments on Mars: is Mars only hydrologically dormant? *Icarus*, 149, 291-328. [31] Schubert, G., and Spohn, T. 1990. Thermal history of Mars and the sulfur content of its core. *J. Geophys. Res.* 95, 14,095-14,104. [32] Hartmann, W. K., and Neukum, G. 2001. Cratering chronology and the evolution of Mars. *Space Sci. Rew*., 96, 165-194.

A MICROPHYSICALLY-BASED APPROACH TO INFERRING POROSITY, GRAIN SIZE, AND DUST ABUNDANCE IN THE SEASONAL CAPS FROM ATMOSPHERICALLY-CORRECTED TES SPECTRA.

J. Eluszkiewicz[1] and T. N. Titus[2], [1]Atmospheric and Environmental Research, Inc., 131 Hartwell Ave., Lexington, MA 02421, jel@aer.com, [2]U.S. Geological Survey, 2255 North Gemini Dr., Flagstaff, AZ 86001, ttitus@usgs.gov.

Introduction: One of the highlights of the TES observations in the polar regions has been the identification of a "cryptic" region in the south where CO_2 appears to be in the form of a solid slab rather than a fluffy frost [1]. While the exact mechanism(s) by which the cryptic region is formed are still subject of some debate, it appears certain that a type of rapid metamorphism related to the high volatility of CO_2 ice is involved. The high volatility of CO_2 ice under martian conditions has several Solar System analogs (N_2 on Triton and Pluto, SO_2 on Io), thus making the martian cryptic region somewhat less cryptic and certainly non-unique among planetary objects. In an end-member scenario, both the formation and the spectral properties of the cryptic region (and of other areas in the seasonal caps) can be quantitatively modeled by considering sintering of an ensemble of quasi-spherical CO_2 grains [2]. This model includes the special case of instanteneous slab formation, which occurs when the grains are sufficiently small (in the submicron range) so that their sintering timescale is short relative to the deposition timescale (a situation analogous to the "sintering" of water droplets falling into a pond).

Physics of Sintering: Originally, the idea of annealed slabs of CO_2 in the martian seasonal caps was proposed based on an analysis of densification timescales [2]. Recently, we have also evaluated the role played by the non-densifying sintering mechanism caused by vapor transport (Kelvin effect). The main conclusion from this recent work is that the seasonal CO_2 deposits on Mars rapidly metamorphose into an impermeable slab regardless of the initial grain size. The slab forming by this mechanism is expected to contain quasi-spherical voids that then undergo slow elimination by the densifying mechanisms. This densification process *is* strongly grain-size dependent, which can be used to explain the persistence of both low- and high-emissivity areas (e.g., the cryptic region and Mountains of Mitchell, respectively). The proposed texture for the martian CO_2 deposits is consistent with both TES and other observations (in particular, the porous texture of the slab is consistent with the mean density of the seasonal deposits inferred from the MOLA data being less than the theoretical density of solid CO_2 [3]) and it has important consequences for the modeling of the physical properties of the martian seasonal frost. Specifically, the radiative properties of the frost (e.g., albedo and emissivity) are more properly modeled by treating radiative transfer in a slab of solid CO_2 containing spherical voids (and other impurities such as dust grains) rather than by the usual model of spherical CO_2 and dust grains *in vacuo*. In the present study, this problem is tackled by finding the Mie solution for a spherical particle embedded in an absorbing host medium [4]. The Mie solution is then applied in a multiple scattering code [5] to compute the radiative properties of the martian CO_2 deposits.

Application of the New RT Model: The chief advantage of the new RT model is its connection to the microphysical model of the cap texture and, consequently, its predictive capability. In particular, the new model does not require the notion of meter-sized Mie boulders of solid CO_2 in order to explain the high emissivities in the cap spectra (e.g., in the cryptic region) but instead relates them to low porosity. The strong porosity dependence of the computed emissivity suggests that the density evolution obtained from the sintering model can be coupled with the radiative transfer calculations to predict the evolution of emissivities. Preliminary results presented at the 6th Mars Conference [6] have demonstrated the capability of the new model to mimic the observed evolution of the cap emissivity (represented as the depth of the TES 25-μm band, BD_{25}).

Modeling the Shape of TES Spectra: In addition to generating a semi-quantitative agreement with the evolution of BD_{25}, the new model is capable of providing a quantitative match to the shape of the TES spectra. For this more quantitative test, it is important to remove the component of the spectra related to atmospheric dust, which we accomplish using an approach based on the emission phase function (EPF) [7]. To date, 105 EPF-corrected spectra of the caps have been generated. An example of an EPF-corrected spectrum and the model spectra computed using the new RT model are shown in Figure 1. The refractive indices for solid CO_2 used in the calculations are as in [8], while the dusty spectra have been computed using optical constants for palagonite [9]. Application of the new model to match the TES spectra can in principle lead to maps of the porosity, void size, and dust content for the polar caps. In the example shown in Figure 1, a fairly good match to the observed spectrum is obtained for a slab containing 5-μm voids at 1% porosity with a

fractional abundance of 1-μm dust grains of 5 x 10^{-4} by volume (the presence of dust is responsible for the shift of the frequency of mimimum emissivity long-ward of 25 μm). Of course, the RT solution for these parameters is non-unique, and this will necessitate the development of a maximum-likehood inversion method utilizing *a priori* information. The results from the sintering model might in fact be used as an *a priori* constraint (i.e., in a given location, the solution for porosity at different times should be consistent with the porosity evolution predicted by the sintering model). In addition, several important factors ne-glected so far (e.g., variable cap thickness, nonuniform density distribution with depth, presence of a thermal gradient) should be included, some of which could further improve the agreement between the coupled microphysical/radiative transfer model and TES obser-vations. Ultimately, the new model will provide a powerful observationally-based tool for the modeling of the coupled surface-atmosphere system on Mars.

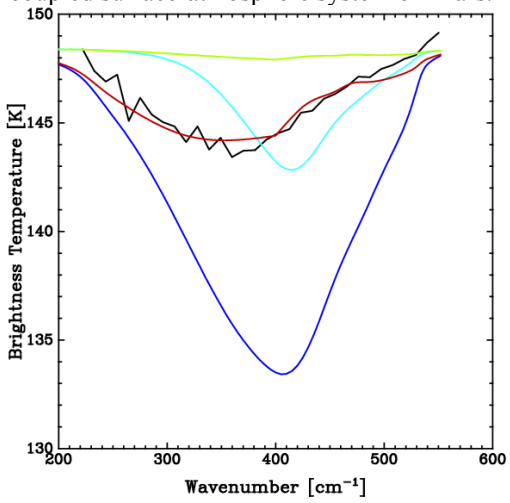

Figure 1: Black line: Observed spectrum. Dark blue line: computed spectrum with 5-μm voids, no dust. Light blue line: computed spectrum with 1-μm voids, no dust. Green line: Computed spectrum with 1-μm voids, 5 x 10^{-4} by volume of dust. Red line: Computed spectrum with 5-μm voids, 5 x 10^{-4} by volume of dust. All computed spectra assume a kinetic temperature of 146 K, slab thickness of 1 meter, 1% porosity, and dust grain size of 1 μm.

Acknowledgement: One of the authors (JE) has been funded by the Mars Data Analysis Program.

References: [1] Kieffer H. et al. (2000) *JGR 105,* 9653. [2] Eluszkiewicz J. (1993) *Icarus 103,* 43. [3] [3] Smith D. E. et al. (2001) *Science 294,* 2141. [4] Yang P. et al. (2002) *Appl. Opt. 41,* 2740. [5] Stamnes K. et al. (1988) *Appl. Opt. 27,* 2502. [6] Elusz-kiewicz J. and T. N. Titus (2003) 6th Mars Conference (www.lpi.usra.edu/meetings/sixthmars2003/pdf/3046.pdf). [7] Titus T. N. and H. H. Kieffer (2001) 33rd DPS Meeting. [8] Hansen G. B. (1997) *JGR 102,* 21,569. [9] Roush T. et al. (1991) *Icarus 94,* 191.

THE ABILITY TO PROBE THE MARTIAN POLAR SUBSURFACE VIA GROUND-PENETRATING RADAR. W. M. Farrell and P. R. Mahaffy, NASA/Goddard Space Flight Center, Greenbelt MD 20771, William.Farrell@gsfc.nasa.gov, Paul.R.Mahaffy@gsfc.nasa.gov

Introduction: Ground-penetrating radar (GPR) offers the exciting possibility of remote sensing below the Martian surface for trapped aquifers. A GPR is currently heading to Mars onboard Mars Express (MEX) and a GPR is in consideration to be onboard Mars Reconnaissance Orbiter (MRO) in 2005. While such orbital systems offer great potential for polar stratigraphy studies, their ability to penetrate deep into the Martian polar ice is a function of both the intervening ionospheric density and the overlying ground ice conductivity. The influence of both signal-altering layers will be discussed.

Polar Ice and Water: Clifford[1,2] has suggested that the trapped basal lakes may form at the bottom of the polar cap, along the ice/regolith interface. Such deep aquifers form either due to insulation effects from the overlying ice, local geothermal hot spots, or frictional heating from glacial sliding. Chasma Boreale and Australe have been suggested to be of possible fluvial origin[3], formed by discharging from a past-trapped aquifer within the cap. Basal lakes and deep ice cap melting may ultimately feed a deeper water table that ultimately supplies the cryosphere at lower latitudes[2]. Evidence for this areal extended ice cryosphere has recently been obtained by the GRS experiment onboard Mars Odyssey[4,5]. Similar basal lakes have been found in Antarctica and allegorical discharging lakes are found in Iceland[1,2].

GPR Signal Propagation: In order for orbiting GPR's to examine the polar subsurface for trapped aquifers, their radio signal must first propagate through the attenuating ionosphere. The operating frequency for the MEX/Mars Advanced Radar for Subsurface and Ionospheric Sounding (MARSIS) is 1-5 MHz with a transmitting power of 15 W. The ionospheric plasma frequency, fp, the blocking frequency below which the ionosphere is opaque, extends from about 3 MHz on the dayside of Mars but quickly drops to about ~300 kHz just past (about 10^o from) the terminator. Hence, to minimize the effect of the ionosphere, sounding the polar subsurface from orbit should occur when the overlying polar ionosphere is not illuminated by the sun. Ideal observation periods for MARSIS nighttime polar sounding will be displayed in the presentation.

Besides the ionosphere, the overlying polar ice over a basal lake also attenuates GPR signals. It is demonstrated that the ability of the MARSIS 15 W transmitter to yield a detectable return signal (above the cosmic background level) from an aquifer located at depth, d, varies as $d \sim k\ \sigma^{-1}$, where k is 0.01 S, for a MEX altitudes of 800 km and a transmission frequency of 4 MHz. Consequently, if the polar ice has a consistency comparable to freshwater ice, with $\sigma \sim 10^{-3}$ S/m, a return signal from an aquifer is possible only in the first few meters of the cap. For depths > 10 m, the ice attenuates the signal (both incoming and outgoing) to the extent that the reflected pulse cannot return to the receiver at strengths above the ambient background noise. In contrast, if the cap consistency is more like firm snow, with $\sigma \sim 10^{-5}$ S/m, aquifer detection with a return signal above the noise level is possible to a depth of about 1 km. Clearly, the as-yet-determined character and consistency of the overlying ice will have a significant impact on the successful detection of a polar aquifer.

Future Concepts: There have been other proposed strategies for sounding the polar subsurface. During last year's Scout Mission Opportunity, a multi-institutional team proposed the Mars-POLAR Montgolfier balloon mission to perform a 30-60 day overflight of the north polar region at 4 km altitude. Included in the payload was a 3W Radio Beacon Sounder (RBS) that had the following advantages over their orbital counterparts:

-Proximity to the source by a factor of 100 increases the delivered signal strength to the ground by 30 dB compared to orbital instruments.

-Platform below the shielding, contaminating, and attenuating effects of the ionosphere.

-Ease in deployment of large antenna via direct integration into the balloon, thereby reducing deployment mass and risks that plague orbital sounder antenna deployments.

The feasibility of aquifer detection for a balloon-based system will be compared and contrasted to its orbital counterpart.

References: [1] Clifford, S.M. (1987) *JGR, 92,* 9135. [2] Clifford, S. M. (1993) *JGR, 98,* 10973. [3] Anguita F. et al. (2000) *Icarus, 144,* 302. [4] Mitrofanov, I., et al. (2002), *Science, 297,* 78. [5] Feldman, W. C., et al., *Science, 297,*75.

EXPERIMENTAL INSTRUMENT ON HUNVEYOR FOR COLLECTING BACTERIA BY THEIR ELECTROSTATIC COAGULATION WITH DUST GRAINS (FOELDIX): OBSERVATION OF ELECTROSTATICAL PRECIPITATED COAGULATED UNITS IN A NUTRIENT DETECTOR PATTERN. ***T. Földi[1], Sz. Bérczi[2], E. Palásti[1]*** [1]FOELDIX, H-1117 Budapest, Irinyi József u. 36/b. Hungary, [2]Eötvös University, Department G. Physics, Cosmic Materials Space Res. Gr. H-1117 Budapest, Pázmány Péter s. 1/a, Hungary, (berczi szani@ludens.elte.hu)

ABSTRACT

Electrostatic coagulation properties of dust above planetary surfaces [1-5] were studied by FOELDIX-1 instrument of Hunveyor. We developed FOELDIX-1 by a detector unit in order to observe biomarkers on Mars by collecting dust thrown out from dusty regions. The dust collector experiment [6], with the observation capability of the size dependent dust particles [7], was developed by a nutrient containers which forming a pattern can show various types of bacteria in the inner detector-wall of the FOELDIX-1 instrument [8]. Coagulation of electrostatically charged dust particles, rare H_2O molecules and suggested extremophile bacteria from the dusty Martian surface is transported by our experimental assemblage through the space with electrodes and allows to precipitate in the vicinity of some specially charged electrodes [9]. If living units form a community, a consortia of bacteria and fungla spores with the attached soil then the cryptobiotic crust components of Mars may also be found and distinguished by this measuring technology.

INTRODUCTION

Levitating charged dust particles were measured on Surveyors [1], Apollo's LEAM [2] and their models were shown [3-5], and windstorms on Mars are known since old times and were photographed. We also studied levitating dust particle phenomenon in the experiment of FOELDIX-1 where coagulation of lunar quasiatmospheric dust were modelled [6,8]. We placed the FOELDIX-1 instrument to the Hunveyor electrostatic assemblage. To search the possibility of life on Mars we developed our instrument with bacteria and spora detector unit.

The FOELDIX detector unit consists of spots with nutrient containers. They are placed on the inner wall of the dust collector. They form a coordinate system. (In terrestrial conditions the containers can be replaced with other ones.) In principle the detector unit is similar to the Magnetic Properties Experiment of the Mars Pathfinder, where magnetic materials were fixed on a curtain on the surface of the lander. Magnetic materials were arranged in a characteristic pattern of spots. Magnetic forces glued the magnetized particles on the spots. The repeated dust interaction with this curtain amplified the pattern of the colored dust particles attracted on the spots till the visibility of the pattern. Even by camera observation of the curtain the magnetic spot pattern - with various megnetisation strength of the spots in the curtain magnets - allowed estimation of the magnetisation of the dust particles flown by winds [10].

THE SOIL AND BACTERIA TOGETHER

Extremophile bacteria are among the main constituents of the cryptobiotic crust on the Earth. The FOELDIX instrument has a benefit to colllect the fragments of such living consortia in glued units. This way not only dust but the glued bacteria or other living units (i.e. fungla spores) can be collected into the instruments container. Selected detecting mechanism is necessary to distinguish the various components of the cryptobiotic type living unit fragments of the windblown dry powder material. Therefore a detecting surface with a selective nutrient spot arrangement was constructed for the FEOLDIX. On the Hunveyor we measure the CBC collecting capacity of the instrument in the Great Hungarian Plain where dry alkaline grounds can be found, especially in the Hortobágy.

THE MEASURING DETECTOR ARRANGEMENT

In our measuring detector an inner wall-curtain with various nutrients are fixed in the vicinity of special electrodes. These electrodes allow the coagulated dust and bacteria grains (and other complex particles) to precipitate from the streaming particles in the instrument. The coagulated materials with various bacterial components can grow on the nutrient spots with different effectivity. Repeated interaction of the precipitated dust-and-bacteria coagulates will change the color and extent of the nutrient spot regions and amplifies the pattern of the nutrients till the visibility of the arrangement of spots. Microcamera observation of the detector's spot pattern will show the types of bacteria (or fungla spores) existing inside the coagulated dust particles.

COAGULATION OF PARTICLES CONTAINING DUST+BACTERIA+WATER-MOLECULES

On the inner surface of the electron tube, even in the case of hypervacuum, a monomolecular water molecule layer can be found (Tungsram Factory, [11]). These water molecules are small negative ions and have far longer lifetime then that of the small positive ions [12].

In the vicinity of a dusty planetary surface there exist a space charge of electron cloud. The rare water molecules will act as if they were negatively charged and they preserve their charge. The negatively charged water molecules frequently collide with particles of a positively charged dust cloud producing a complex coagulated particle. This particle is a loose aggregate of ions, has great mass and has lower velocity compared to the small mass particles. While colliding with a negatively charged water molecule the water molecule will attach to the larger one. This process enlarges the complex aggregate larger and larger (we measured coagulation up to 450.000 times mass in the FOELDIX instrument). The living units are embraced and included into this coagulated large particles. Living units are shielded by the dust components from UV and other radiations, and presence of water allows to continue life activity, too.

LOCATION OF PROMISFUL OBSERVATION CHANCES FOR MARTIAN LIVING ORGANISMS: SOUTH POLE

On the MOC MGS images there are promisful regions where to land in order to observe Martian life components of bacteria or fungal spores with dust. In winter these dark dunes are covered with frost. Dark dune spots are formed in

late winter and early spring show a structure on the frost covered surface where the soil material is partially exposed on the surface. This uncovered region is the dark spot itself. In these periods wind blows out the dark dune material from the spots and the ejected dark dust forms a thin layer on the surface of the frost cover.

Dark dune spots (DDSs) were estimated as probable sites for biogenic activity [13-15] and the suggested Martian surface organisms (MSOs) were considered as promisful candidates of the recent life on Mars. If the MSOs exist, then they must be flown out from the dark dune spots during the late winter and early spring period of DDS activity.

PRESENCE OF WATER ON DDS SITES

As we referred earlier the water molecule content of the atmosphere helps the electrostatic coagulation of the dust particles [16]. The Southern Polar region of Mars where the DDS sites were found and studied is therefore promisful source for the FOELDIX experiment because Mars Odyssey also found higher concentration of water in this region [17-19]. Although the 2003/2004 Mars missions will not go to the polar regions, a more detailed imaging may reveal special sites with extensive wind activity in the given late winter early spring period [20, 21].

SUMMARY

The new FOELDIX instrument with the bacteria and spore detector unit is capable to observe various Martian living units coagulated by the instrument and deposited by special electrodes on nutrient spots of the detector. The growing spots can be observed by microcamera units built into the FOELDIX instrument. Such detector can measure not only bacteria but the soil type which is glued with the bacteria. Therefore it is probable that components of the cryptobiotical crust units may be discovered by this measuring technology.

ACKNOWLEDGMENTS

This work was supported by the MÜI-TP-190/2002 and 190/2003 funds of the Hungarian Space Office.

REFERENCES:

[1] Criswell, D. R. (1972): Horizon glow and motion of Lunar dust. *Lunar Science III*. p. 163. LPI, Houston; [2] Rhee, J. W., Berg, O. E., Wolf, H. (1977): Electrostatic dust transport and Apollo 17 LEAM experiment. Space Research XVII. p. 627; [3] Horányi M., Walch, B., Robertson, S. (1998): Electrostatic charging of lunar dust. *LPSC XXIX*. LPI, CD-ROM, #1527; [4] Reid, G. C. (1997): On the influence of electrostatic charging on coagulation of dust and ice particles in the upper mesosphere. *Geophysical Res. Letters*, **24,** No. 9. p. 1095; [5] Sickafoose, A. A., Colwell, J. E., Horányi, M. Robertson, S. (2001): Dust particle charging near surfaces in space. In *LPI XXXII*, #1320, LPI, CD-ROM; [6] T. Földi, R. Ezer, Sz. Bérczi, Sz. Tóth. (1999): Creating Quasi-Spherules from Molecular Material Using Electric Fields (Inverse EGD Effect). *LPSC XXX*. LPI, CD-ROM, #1266.; [7] T. Földi, Sz. Bérczi, E. Palásti (2002): Time Dependent Dust Size Spectrometry (DUSIS) Experiment: Applications in Interplanetary Space and in Planetary Atmospheres/Surfaces on Hunveyor. *Meteoritics & Planetary Science,* **37**, No. 7. Suppl., p. A49.; [8] Földi T., Bérczi Sz., Palásti E. (2001): Water and bacteria transport via electrostatic coagulation and their accumulation at the poles on the dusty planet. *LPSC XXXII*, #1059, LPI, CD-ROM; [9] Földi T., Bérczi Sz. (2001): The source of water molecules in the vicinity of the Moon. *LPSC XXXII*, #1148, LPI, CD-ROM; [10] Hviid, S. F.; Knudsen, J. M.; Madsen, M.B.; Hargraves, R. B. (2000): Spectroscopic Investigation of the Dust Attracted to the Magnetic Properties Experiment on the Mars Pathfinder Lander. *LPSC XXXI*, #1641, LPI, CD-ROM; [11] Bródy I., Palócz K. (1953): Lecture on Techn. Univ. Budapest (personal communication); [12] Israel, H. (1957): *Atmospherische Elektricitet*. Leipzig.; [13] Horváth A., Gánti T., Gesztesi A., Bérczi Sz., Szathmáry E. (2001): Probable evidences of recent biological activity on Mars: Appearance and growing of Dark Dune Spots in the South Polar Region. *LPSC XXXII*, #1543, LPI, CD-ROM; [14] A. Horváth, T. Gánti, Sz. Bérczi, A. Gesztesi, E. Szathmáry (2002): Morphological Analysis of the Dark Dune Spots on Mars: New Aspects in Biological Interpretation. *LPSC XXXIII*, #1108, LPI, CD-ROM; [15] A. Horváth, Sz. Bérczi, T. Gánti, A. Gesztesi, E. Szathmáry (2002): The "Inca City" Region of Mars: Testfield for Dark Dune Spots Origin. *LPSC XXXIII*, #1109, LPI, CD-ROM; [16] T. Földi, Sz. Bérczi (2001): Quasiatmospheric Electrostatic Processes on Dusty Planetary Surfaces: Electrostatic Dust and Water molecule Coagulation and Transport to the Poles. *26th NIPR Symposium Antarctic Meteorites*, Tokyo, p. 21-23.; [17] Mitrofanov, I. G. et al., (2003): Global Distribution of Shallow Water on Mars: Neutron Mapping of Summer-Time Surface by HEND/Odyssey. *LPSC XXXIV,* #1104, LPI, CD-ROM; [18] Kuzmin, R. O.; Mitrofanov, I. G.; Litvak, M. L.; Boynton, W. V.; Saunders, R. S. (2003): Mars: Detaching of the Free Water Signature (FWS) Presence Regions on the Base of HEND/ODYSSEY Data and Their Correlation with Some Permafrost Features from MOC Data. *LPSC XXXIV,* #1369, LPI, CD-ROM; [19] A. Horváth, T. Gánti, Sz. Bérczi, A. Gesztesi, E. Szathmáry (2003): Evidence for Water by Mars Odyssey is Compatible with a Biogenic DDS-Formation Process. *LPSC XXXIV*, #1134, LPI, CD-ROM; [20] Córdoba-Jabonero, C.; Fernández-Remolar, D.; González-Kessler, C.; Lesmes, F.; C. Manrubia, S.; Prieto Ballesteros, O.; Selsis, F.; Bérczi, S.; Gesztesi, A.; Horváth, A. (2003): Analysis of geological features and seasonal processes in the Cavi Novi region of Mars. EGS Conference, Nizza, EAE03-A-13011.; [21] Horvath, A.; Manrubia, S. C.; Ganti, T.; Berczi, S.; Gesztesi, A.; Fernandez-Remolar, D.; Prieto Ballesteros, O.; Szathmary, E. (2003): Proposal for Mars Express: detailed DDS-test in the "Inca City" and "Csontváry" areas. EGS Conference, Nizza, EAE03-A-14142.;

3D SIMULATIONS OF THE EARLY MARS CLIMATE WITH A GENERAL CIRCULATION MODEL. F. Forget[1] , R. M. Haberle[2], F. Montmessin[2], S. Cha[2], E. Marcq[1,2], J. Schaeffer[2], Y. Wanherdrick[1], [1] *Laboratoire de Météorologie Dynamique,IPSL, UPMC BP99, place Jussieu, 75252 Paris cedex 05 (forget@lmd.jussieu.fr)*, [2] *NASA Ames Research Center, Space Science Division, Moffett Field, California*, ..

Introduction

The environmental conditions that existed on Mars during the Noachian period are subject to debate in the community. In any case, there are compelling evidence that these conditions were different than what they became later in the amazonian and possibly the Hesperian periods. Indeed, most of the old cratered terrains are disected by valley networks (thought to have been carved by flowing liquid water), whereas younger surface are almost devoid of such valleys. In addition, there are evidence that the erosion rate was much higher during the early noachian than later [1]. Flowing water is surprising on early Mars because the solar luminosity was significantly lower than today. Even with the thick atmosphere (up to several bars) that is expected to have existed on Mars at the time, simple 1D models based on a purely gaseous atmosphere predicted climate conditions too cold to allow liquid water to flow [2]. On this basis, some authors have suggested that the difference resulted from a stronger geothermalism during that period, and that a warm climate was not necessary to explain the valley network [3]. However, other authors claim that a warm, wet early climate capable of supporting rainfall and surface runoff is the most plausible scenario for explaining the entire suite of geologic features in the Martian cratered highlands [1].

To help understand this key issue in Mars science, it is important to extend the initial climate simulations that concluded that early Mars must have been cold [2,3], since these calculations were performed with very simple 1D models [4]. Such improvements have been performed by several authors, and in particular it has been suggested that the CO_2 ice clouds that must have formed in such an atmosphere could have produced a strong "scattering" greenhouse effect sufficient to warm the planet above the freezing point of water [5]. However, there again, these simulations were performed with simple 1D models, from which it is difficult to predict the environmental conditions.

A Global Climate model for early Mars

To improve our understanding of the early Mars Climate, we have developped a 3D general circulation model similar to the one used on current Earth or Mars to study the details of the climate today. Our first objective is to answer the following questions : how is the Martian climate modified if 1) the surface pressure is increased up to several bars (our baseline: 2 bars) and 2) if the sun luminosity is decreased by 25account the heat possibly released by impacts during short periods, although it may have played a role [6]

For this purpose, we have coupled the Martian General Circulation model developped at LMD [7] with a sophisticated correlated k distribution model developped at NASA Ames Research Center. It is a narrow band model which computes the radiative transfer at both solar and thermal wavelengths (from 0.3 to 250 microns). The correlated-k's for each bands are generated from a line-by-line code using the HITEMP data base from HITRAN. In addition, pressure induced absorption by CO_2 in included using a simple parameterisation from an analytical formula produced by Moore et al. (1971). This is a major source of uncertainty.

In addition to the radiative transfer and to the parameterisation that are usually included in such a climate models (dynamical core to solve the 3D fluid dynamic equations, subgrid scale turbulent and convective mixing, surface heat balance and subsurface heat conduction, etc...), we have included parameterisations to account for the condensation, transport, gravitational sedimentation and radiative effects of the CO_2 ice clouds that readily form in a thick CO_2 atmosphere. model. Using the correlated k distribution model allowed us to compute the complex radiative transfer processes (scattering in the thermal infrared) that cannot usually be accounted for with the usual GCM's wide band model.

Results

Preliminary results obtained assuming a 2 bars atmosphere suggest that, even without taking into account the radiative effect of CO_2 clouds, temperature near or above the freezing point of water may be obtained seasonally in the summer hemisphere. The diurnal amplitude of surface temperature is small, and therefore warm temperatures may last for long periods. CO_2 ice clouds are found to form almost everywhere on the planet in the upper atmosphere above 40 km. Their radiative effect on the climate is very model dependent but, in most cases, should correspond to a warming of the surface.

Ultimately, such a model may enable us to simulate the water cycle by applying parameterisations currently used in Earth models. It will be interesting to investigate wether snow or rain could have occur on such a planet.

Reference

[1] Craddock and Howard, *J.G.R* 107 [2002]
[2] Kasting, *Icarus* **94**,1 (1991)
[3] Squyres and Kasting, *Science* **265**, 744 (1994).
[4] Haberle, *J.G.R* 103, 28467, (1999)
[5] Forget and Pierrehumbert, *Science* 278, 1273 (1997)
[6] Segura et al. *Science* 298, 1977 (2002)
[7] Forget et al. *J.G.R* 104, 24,155 (1999)

ON THE CO_2 HYDRATE PHYSICAL CHEMISTRY AT MARTIAN CONDITIONS. G. Genov and W. F. Kuhs, GZG Abt. Kristallographie, Georg-August-Universität Göttingen, Goldschmidtstr. 1, 37077 Göttingen, Germany (ggenov@gwdg.de; wf.kuhs@geo.uni-goettingen.de)

Introduction: In 1970 Miller and Smythe [1] concluded that the CO_2 hydrate is stable on Mars and that the mixture of pure condensates of CO_2 and H_2O is unstable at the poles. Moreover, some limited kinetic data suggested that the hydrate formation process was fast enough in a meteorological time-scale, which meant, it would lead to a diurnal and annual hydrate cycle. Some authors even put forward the idea that most of the ice in the polar caps was in a hydrate form [2]. Unfortunately, the hydrate and the ice are quite undistinguishable with conventional spectroscopic methods. Moreover, very little is known about the physico-chemical properties of CO_2 hydrates at low temperatures encountered on Mars. We have started to investigate the thermodynamic, physical and kinetic properties of CO_2 hydrate under Martian surface and subsurface p-T conditions.

Possible Importance Of CO_2 Hydrates: Presently is believed that the Martian polar caps consist of water ice, solid CO_2, CO_2 clathrate and dust in unknown proportions, probably different for both caps. The CO_2 clathrate, being the strongest of the three ices could probably affect the rheologic properties of the polar ice layers [3-6] as it was suggested for the north [7] and the south polar caps [8]. If the quantity of the CO_2 hydrate in these regions is large enough it will also influence the process of their basal melting [4, 5]. This is because the hydrates are several times better thermal insulators than water ice and the period needed for establishing a steady-state geothermal gradient in the inner parts of the caps will be much longer.

About The Hydrate Formation: The hydrate formation process is generally believed to start after a certain induction period, needed for some clathrate super nuclei to form. Then the further growth of those nuclei runs in three stages as shown on **Fig. 1**. Guided by the relevance of clathrate hydrate formation from water ice for Mars, a series of kinetic *in-situ* neutron diffraction experiments for CO_2 hydrate formation at higher temperatures were performed. To complement those, a series of pVT formation kinetic experiments were carried out [9]. As a result, applying the model of Salamatin & Kuhs [10, 11], values for the reaction rate coefficients for the different reactions were obtained (**Fig. 2**). A strong bias, of the two points at 272 K and 263 K, from the Arrhenius fit is observed because of the existence of a quasi liquid layer on the surface of the reacting water ice. Thus, two values for the activation energies were obtained – for the high temperature part – 53.5 kJ/mol, and for the low temperature one – 15.5 kJ/mol.

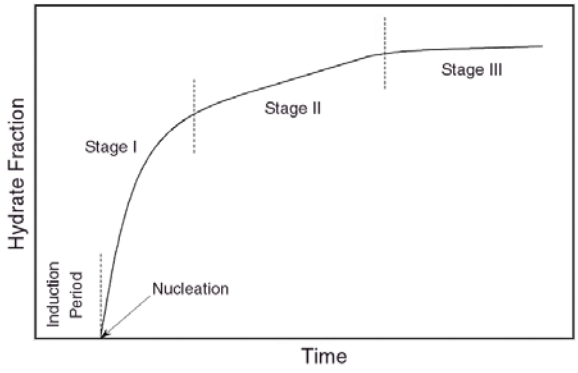

Fig. 1 Stages of the hydrate growth kinetics and induction period.

The delay in formation due to the induction period could be extremely important. Preliminary experiments

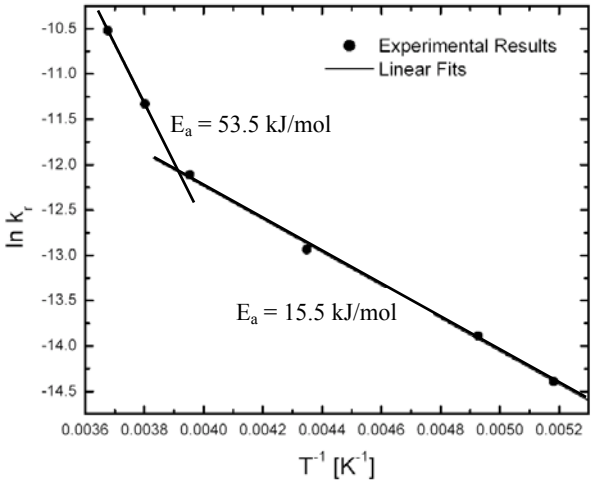

Fig. 2 Plot of the model results for the reaction rate coefficients vs. the temperature.

indicate that the induction period could be several hours up to days at temperatures near 170K and pressures not well exceeding the decomposition pressure of CO_2 hydrate. This may well question the possibility of forming CO_2 hydrate during the Martian night in the diurnal cycle. In our high temperature *in situ* neutron experiments at higher temperatures no induction period was observed within the experimental resolution of 20 s.

Clearly, the induction time depends on temperature and excess pressure and further work is needed to quantify this effect, which is presently under way. Including the effect of induction time in an extended version of the model of Salamatin & Kuhs, we will eventually be in a position to give a realistic prediction for the timescales and kinetics of the hydrate formation at Martian conditions. The kinetics of the growth following the nucleation period is more easily accessible and first estimates will be given in our contribution.

References: [1] Miller S. L. & Smythe W. D. (1970) *Science 170,* 531-533.

[2] Jakosky, B. M. et al. (1995) *J. Geophys. Res., 100, pp. 1579-1584.*

[3] Durham W. B. (1998) *ICMPS, Abstract # 3024*

[4] Kargel J. S. & Tanaka K. L. (2002) *LPS XXXIII, Abstract # 1799*

[5] Kreslavsky M. A. & Head J. W. (2002) *LPS XXXIII Abstract, # 1779*

[6] Kargel J. S. (1998) *ICMPS, Abstract # 3048*

[7] Milkovich S. M. et al. (2002) *LPS XXXIII, Abstract # 171*

[8] Brightwell S. N. et al. (2003) *LPS XXXVI, Abstract # 2077.*

[9] Genov G. & Kuhs W. F. (2003) *VTth ICM, Abstract # 3098.*

[10] Salamatin, A. N. & Kuhs W. F. (2002) *Proc.IV ICGH, pp 766-770*

[11] Staykova, D. K. et al. (2003) *J. Phys. Chem. in press.*

RECONCILING THE MOLA, TES, AND NEUTRON OBSERVATIONS OF THE NORTH POLAR CO_2 MASS BUDGET ON MARS. R.M. Haberle[1], B. Mattingly[2], and T.N. Titus[3]. [1]Space Science Division, MS 245-3, NASA/Ames Research Center, Moffett Field CA, 94035, Robert.M.Haberle@nasa.gov. [2]Dept. Meteorology, San Jose State University, San Jose CA, 95192, bridgemat@yahoo.com. [3]U.S. Geological Survey, 2255 North Gemini Drive, Flagstaff AZ, 86001, ttitus@usgs.gov.

Introduction: There are now three independent observations of the CO_2 polar cap mass budget of Mars' north polar cap. The first is based elevation changes detected by the Mars Orbiter Laser Altimeter (MOLA) on the Mars Global Surveyor (MGS) [1]. The second is based on MGS Thermal Emission Spectrometer (TES) broadband observations of the solar and infrared radiation fields at the top of the atmosphere [2,3]. The third is based on neutron counts measured by the neutron spectrometer (NS) on Odyssey [4]. If one assumes a cap density of 910 kg/m^3 [1], then the peak mass loading poleward of 85°N inferred from the MOLA data is ~1090 kg/m^2, which compares to ~1150 kg/m^2 inferred from TES for the same region, and ~700 kg/m^2 from the NS data. TES and MOLA are in good agreement, but are about 60% higher than the NS data. Is there a way to reconcile these discrepancies?

Role of surface heat storage: The TES data are based on an energy balance. The net radiative loss (gain) in a column is balanced by latent heating due condensation (sublimation) of CO_2. In calculating the mass budget, the other main energy sources, atmospheric heat transport and subsurface conduction, were neglected [2,3]. At the pole, atmospheric heat transport is indeed a small term. However, subsurface heat conduction can be significant because at the North Pole water ice, which has a high thermal conductivity compared to bare soil, is a dominant component of the subsurface. Thus, heat conducted down into the ice during summer will slowly bleed back out during fall and winter reducing the amount of CO_2 that condenses on the pole.

We have taken a first cut at quantifying this effect by fitting a curve to Paige's [5] estimates of the conducted energy flux in his analysis of Viking IRTM data. For a thermal inertia of ~2100 (SI units) this curve shows a peak upward conducted heat flux of about 30 W/m^2 at L_s=180°, which is just after the time CO_2 begins condensing. This then gradually tapers off to less than several W/m^2 near the end of spring just before the CO_2 ice completely sublimes. We then added this term to the TES radiation fields and recalculated the CO_2 mass budget. We find that subsurface heat conduction at the North Pole can reduce the amount of CO_2 that condenses by about 400 kg/m^2, which brings the TES data in close agreement with the NS data.

CO_2 ice density: That leaves the MOLA data much higher the both TES and NS. However, the MOLA data are based on elevation changes and are not direct measurements of the mass loading. To relate the elevation changes to a mass loading requires knowledge of the ice density. The MOLA data can be reconciled with TES and NS if the CO_2 ice density is ~600 kg/m^3. Feldman et al. [4] suggested that low ice densities could be a way to explain the difference between MOLA and NS.

The MOLA combined gravity/elevation measurements infer a mean cap density of 910 ± 230 kg/m^2 [1]. Thus, 600 kg/m^3 is below the lower limit of the MOLA measurements. However, the MOLA-derived density is an average for the entire seasonal cap. It is possible that the density of the north polar deposits is less than the average of the entire seasonal cap. A good physical basis for this is the much more frequent occurrence of "cold spots" at the North Pole compared to lower latitudes [6]. Snowfall is a strong candidate for the origin of these cold spots. If true, it means that a much greater fraction of the north polar deposits originate from the atmosphere as snowfall rather than direct condensation onto the surface. Surface accumulations resulting from snowfall have lower densities than those originating from direct deposition.

Conclusion: Of the three measurements that bear on the north polar CO_2 mass budget, the NS provides the most direct measurement of the mass loading. Yet it shows much less CO_2 accumulating on the pole than initially predicted by either MOLA or TES. These differences can be reconciled by (a) including subsurface heat conduction in the TES calculations, and (b) using a lower ice density to convert MOLA elevation data to a mass loading.

References: [1] Smith D.E., Zuber M.T. and Neumann G.A. (2001) *Science, 294,* 2141-2148. [2] Kieffer, H.H. and Titus, T.N. (2001) *Icarus, 154*, 162-180. [3] Titus, T.N. (2003) *International workshop: Mars atmosphere modelling and observatiions,* Granada, Spain. [4] Feldman W.C., et al. (2003) *JGR,* submitted. [5] Paige, D.A. (1985) *Ph.D. Thesis*, UCLA, 206p. [6] Titus T.N. and Kieffer, H.H. (2003) *6th International Mars Conference*, Pasadena Ca.

ALBEDO VARIATIONS ON THE MARTIAN NORTHERN POLAR CAP AS SEEN BY MGS. A.S. Hale D. S. Bass, and L. K. Tamppari[3], [1]NASA Jet Propulsion Laboratory (MS 264-235, 4800 Oak Grove Drive, Pasadena, CA 91109 amy.s.hale@jpl.nasa.gov), [2]NASA Jet Propulsion Laboratory (MS T1722, 4800 Oak Grove Drive, Pasadena, CA 91109 deborah.s.bass@jpl.nasa.gov), [3]NASA Jet Propulsion Laboratory (MS 301-422, 4800 Oak Grove Drive, Pasadena, CA 91109 leslie.k.tamppari@jpl.nasa.gov [1]

Introduction The Viking Orbiters determined that the surface of Mars' northern residual cap is water ice. Many researchers have related observed atmospheric water vapor abundances to seasonal exchange between reservoirs such as the polar caps, but the extent to which the exchange between the surface and the atmosphere remains uncertain. Early studies of the ice coverage and albedo of the northern residual Martian polar cap using Mariner 9 and Viking images reported that there were substantial internannual differences in ice deposition on the polar cap [1], a result that suggested a highly variable Martian climate. However, some of the data used in these studies were obtained at differing values of heliocentric solar longitude (L_s). Reevaluation of this dataset in [2] indicated that the residual cap undergoes seasonal brightening throughout the summer, and indicated that this process repeats from year to year. In this study we continue this work with data acquired with Mars Global Surveyor's Mars Orbiter Camera (MOC) and Thermal Emission Spectrometer (TES) instruments.

We use MOC Wide Angel (WA) red filter images of the cap obtained at different values of L_s and different Martian years, and TES albedo data of the north polar region. Previous work in this study has concentrated on MOC images of the cap edge and frost covered outliers [3]; in this phase we systematically investigate images from the cap center (defined for our purposes to be the area northward of 80 degrees latitude) in order to assess any latitudinal trends in seasonal brightening. We have examined data from both instruments from mapping year 1 and 2, though we have ignored MOC data acquired between September 2000 and May 2001, as the MOC camera experienced a state change between those dates that make albedo comparisons with data taken at other times problematic (Cantor, private communication).

Result 1: MOC: Previous work [3] examined brightening of cap edge areas of approximately 40% throughout the northern summer, with the greatest increase occurring in early summer. This result is in agreement with that obtained by [1] for Viking and Mariner 9 data. The region shown in **Figure 1** shows this brightening [3].

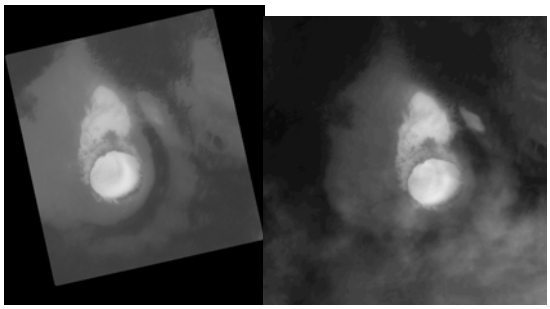

a. b.

. **Figure 1:** MOC images showing the crater at approx. 77 degrees north and 270 degrees west. The left image (a) shows L_s = 108; the image on the right (b) shows L_s =161. An approximate 40% brightening is seen.

In contrast, examination of center cap images to date shows a different trend; center cap images appear to remain at the same albedo as the summer progresses. For example, the region shown in **Figure 2** shows a decrease in brightness of approximately 2.5 % between L_s = 121 and L_s = 155. This change is not within the MOC detectability limits (Malin and Edgett 2001), and so we conclude that this region has experienced no detectable albedo change. This result is in disagreement with that obtained by [1] for Viking and Mariner 9 data that suggested cap edge albedo was controlled by cap center albedo; the reasons for discrepancy are still being explored and will be discussed in our presentation. In all comparisons, the DN values of same pixels of the calibrated processed ISIS level 2 cubes were compared in qview.

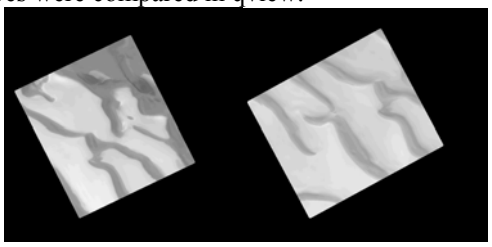

a. b.

Figure 2: MOC images showing the area at approx. 86 degrees north and 141 degrees west. The left image (a) shows L_s = 121, the right one (b) L_s=155. No brightening within reliable detection limits is seen for the same areas

Result 2: TES: The story of north polar water ice frost appears to be even more complex when other datasets are examined. We generated TES lambert albedo maps for the northern polar region; maps were binned in 2 by 2 degrees of latitude and longitude, and 10 degrees of L_s. The spatial resolution of the TES instrument is much less than that of MOC (approximately 3 km per pixel), but larger regional trends can still be seen (**Figure 3**).

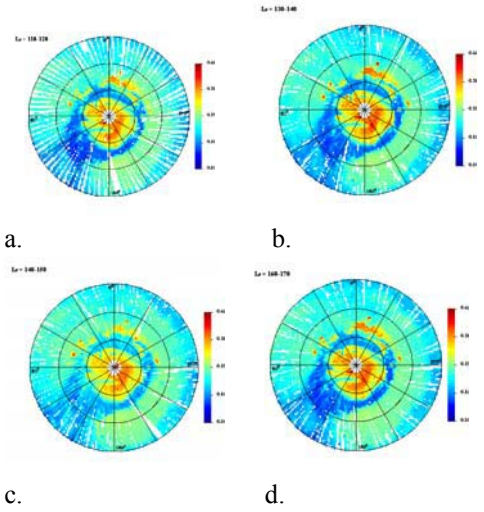

a. b.

c. d.

Figure 3: TES lambert albedo data showing the Martian north polar region. The plot on the top left (a) shows L_s 110-120; the plot on the top right (b.) L_s =120-130. The bottom left image (c) shows L_s 140-150, and image d shows L_s = 160-170 The latitude range shown is from 60 to 90 degrees north. All data from second mapping year.

The TES data show a complex picture, with the cap region appearing to brighten early in the summer, then decrease in albedo later in the season, and then brighten again as the summer ends. This is consistent with behavior documented previously [4]. Work is ongoing correlating TES pixels with areas observed by MOC, as is analysis of how the regional view of TES and the localized view of MOC agree and disagree, and we will present the results in our presentation.

Conclusions: The results reported here describe far more complexity in water ice albedo variability than had previously been appreciated. It is clear that the entire cap may not be treated as a monolithic body, but rather, individual locations show a variety of influences. One possibility is that topographic effects may have an effect; water cycle processes may also have a latitudinal dependence. In other research not presented here we are also investigating is the role of atmospheric effects on surface albedo. Clearly, whatever processes are affecting the cap albedo may have latitudinal dependence, and may have important implications for the Martian water cycle. We will present results regarding the full TES albedo data set, as well as other sites observed by MOC. Additionally we will present out interpretation of regional and local process interaction.

References: [1] Bass D. S et al. (2000) *Icarus, 144,* 382-396. [2] Cantor B. et al. (2002) *JGR., 107*. [3] Hale et al. (2003) 34th LPSC Abstract # 1422. [4] Kieffer and Titus (2001) *Icarus, 154,* 162-180.

SPECULATIONS ON ORBITAL FORCING OF SUBLIMATION FROM THE POLAR CAPS M. H. Hecht, Jet Propulsion Laboratory, California Institute of Technology (michael.h.hecht@jpl.nasa.gov)

Introduction: Calculation of the periodic variations in the martian orbital parameters by Ward [1] and subsequent refinements to the theory [2,3] have inspired numerous models of variation of the martian water cycle. The limitations of models such as this can not be overstated. Albedo, for example, has a much greater influence on temperature than orbital forcing, and seems to be linked to insolation, possibly via its influence on dust transport [4]. To make further progress, either new constraints must be identified, or additional clues must be obtained from remote sensing and *in situ* exploration.

The MGS and Odyssey missions have provided us with several such critical pieces of information. The discovery of what can only be described as an ice sheet underlying a lag deposit over enormous areas of both hemispheres is one such clue [5], along with indications from surface features of recent, wide-scale modification by water [6]. Another is the observation of mantling of gullied slopes, presumably a vestigial layer of frost and snow protected by a similar lag deposit [7]. More speculative, perhaps, are suggestions from analysis of MOLA data of a net seasonal increase in thickness of the northern cap [8], or correlation of PLD structures with orbital variations dominated by precession of the L_s of perihelion [3]. Speculative implications of these new data are summarized in the sections below.

Critical oscillations: Most orbital forcing models have focused on variations in planetary obliquity (on both a short-term, 110 kyr time scale and larger oscillations occurring over millions of years) [9-11]. The fastest mode of variation, perihelion precession, has generally been deemphasized because it does not change the integrated annual insolation. But as a result of this precession, the asymmetry in peak summer insolation between the poles exceeds 50% today, with the maximum cycling between poles every 25.5 kyrs. Variations in planetary eccentricity also play a role, defining the magnitude of the excursions associated with this perihelion precession.

Fanale, for example, concluded that precession of the longitude of perihelion may be sufficient to increase water removal from the poles by factors of 50-100 [9]. He calculated the peak vapor pressure at the North Pole by assuming a surface of pure water ice or CO_2 ice with distinct optical properties, incorporating only radiative balance and latent heat of CO_2 deposition. It was further assumed that the zonal humidity was proportional to that peak water vapor, which was in turn a simple function of the ice surface temperature. This assumption is reasonable because the energy deposited as sunlight into the polar cap must ultimately be accommodated in the form of sublimation. If advection or vertical transport is insufficient to remove the generated water vapor, for example, it will recondense as fog, pumping heat into the atmosphere and either generating convective currents or increasing the saturation vapor pressure.

Figure 1 shows the results of calculations using a protocol similar to Fanale's, but with the critical addition of tracking latent heat of water condensation and sublimation. All three curves represent an extrapolation back only 150 kyrs. Rather than extrapolating back far enough to reflect large changes in obliquity, the obliquity was forced to specific values. Thus one curve represents the calculated obliquity, a second holds the obliquity at the current value of 25°, and the third holds the obliquity at 40°. The data is expressed in terms of the amount of heat from insolation that is converted to sublimation under these circumstances. It can be seen that, at constant obliquity, the sublimation rate can increase by a factor of 100 with the passage of only 20 kyrs. Changing the obliquity from 25° to 40° adds another factor of only approximately 5.

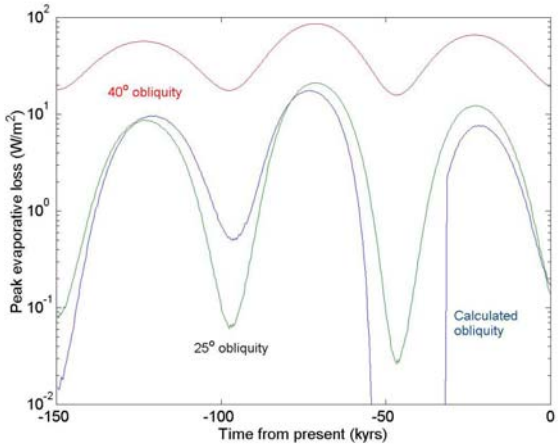

Figure 1: Calculated peak evaporative loss at the North Pole of Mars, expressed as an evaporative heat measure over 150,000 years. The calculation balances radiation, latent heat of CO_2 and H_2O, and insolation using orbital parameters from Ward [1], albedo and emissivity values suggested by Fanale et al [9]. To show the relative effect of precession and obliquity, the three curves represent calculated obliquity and obliquity fixed at 25° or 40°.

Lag deposits and ice cap evolution: Odyssey results suggest that the vast majority of ice on Mars is sequestered beneath either a lag deposit of dust or a buffer layer of CO_2. The reason for this seems straightforward – the water table will retreat to a depth such that the annual thermal wave does not result in temperatures above the dewpoint [12]. In other words, the boundary of the cryosphere will tend to adiabatically adjust to the changing heat balance. The southern hemisphere is currently favored by summer perihelion, and not surprisingly exposed water is scarce. To the extent that cap evolution can track climate change, the boundary of the exposed northern polar cap would represent the latitude above which the surface temperature doesn't exceed the frostpoint.

The appearance of the PLD and the apparent high resurfacing rates of the cap itself [13] suggest that the age of the cap isn't geologically great. There are few polar features suggestive of flow, implying that the cap periodically retreats by other processes, presumably sublimation and transport to lower latitudes or the opposing hemisphere. The time scale for disappearance and reconstruction of the cap has never been resolved, but could range from many millions of years to the rapid 51,000 year cycle of precession.

As the northern hemisphere warms up due to orbital precession, two things may occur. The boundaries of the cap may be encouraged to retreat to higher latitude, and measurable amounts of water may be seasonally removed from the polar cap. If formation of a lag deposit halts the surface erosion of the cap, then further erosion may be limited to the scarps and slopes at the edges of the cap, effectively eroding the cap from the outside. Only by vigorous removal on the perimeter, where gravitational forces remove the residue, could the cap be substantially modified on the timescale suggested by the geological record. Supporting such a view is the observation that as ice sublimates, surface facets will tend to grow normal to the sun direction, maximizing further erosion [14]. We might imagine, therefore, that as the summers become hotter in the north over the next 20,000 years, the diameter of the northern cap will become smaller, with material being vigorously removed from the edges and redeposited on top. Indeed, if the net increase in thickness of the cap suggested by the MOLA data were verified, it would not be inconsistent with such a mechanism. It is also not unreasonable that the cap would bifurcate into two regions – a high latitude, actively growing region with thermally stable exposed ice, and a lower latitude region with suppressed growth, where a lag deposit protects the ice from further erosion.

Conclusions: Models of peak seasonal sublimation from the north polar cap suggest that the important cycle of water injection may be 25.5 or 51 kyrs, depending on whether one or two poles are involved. If the process is limited by hemispheric depletion of available dust-free water, the result may be periodic pulses of water injection. The tendency of the surface to form lag deposits above ice layers is consistent with an equilibrium water table determined by the frostpoint. As temperatures warm, this stability level will retreat below the surface at higher latitudes, encouraging polar cap retreat. The ability of the cap to shrink from the surface may also be limited by lag formation, suggesting that the cap grows and shrinks from the perimeter, with the sublimed material being transported from perimeter to top surface. Favorable geometries with respect to the sun would make this an efficient form of water transport.

References: [**1**] Ward W.R. (1974), *J. Geophys. Res. 79*, 3375-3386. [2] Laskar J. (1990), *Icarus 88,* 266-291. [3] Laskar J., Levrard B., Mustard J.F. (2002), *Nature 419*, 375-377. [4] Kieffer H.H., Zent A.P. (1992), in *Mars*, ed. H. H. Kieffer et al., 1180-1218. [5] Boynton, W. et al. (2002), *Science* **297** 81-85. [6] Kreslavsky M. and Head J. (2000), JGR 105, 26695. [7] Christensen P.R. (2002), *Nature **422***, 45-48. [8] Smith, D. E., M. T. Zuber, G. A. Neumann (2001), *Science* **294**, 2141. [9] Fanale F.P. et al. (1986), *Icarus 67*, 1-18. [10] Carr, M.H. (1982), *Icarus 50*, 129-139. [11] Hecht M. H. (2002), *Icarus 156*, 373-386. [12] Leighton R.B., Murray B.C. [1966], *Science 153* 136-144 [13] Herkenhoff, K. E. and J. J. Plaut (2000), *Icarus* **144**, 243-253. [14] Ingersoll A.P., Svitek T., Murray B.C. (1992), *Icarus 100*, 40-47.

Acknowledgements: This work was performed at the Jet Propulsion Laboratory, California Institute of Technology, under funding from NASA. Useful discussions with Frank Carsey are greatly appreciated.

THE MARS IMAGER FOR CLOUD AND AEROSOL (MICA). V. J. Hipkin[1], J. R. Drummond[1], J. Hackett[2], R. Deschambault[2], J. Abbatt[1], G. Besla[1], C. T. McElroy[1], S. M. L. Melo[1], K. Strong[1], J. J. Caldwell[3], J. C. McConnell[3], D. V. Michelangeli[3], P. Bernath[4], J. Sloan[4], W. Ward[5] and B. Tolton[6]. [1]University of Toronto, Toronto, Ontario, [2]COMDEV Ltd, Cambridge, Ontario, [3]York University, Toronto, Ontario, [4]University of Waterloo, Waterloo, Ontario, [5]University of New Brunswick, Fredericton, New Brunswick, [6]Synodon Ltd, Edmonton, Alberta

Introduction: Cloud and dust play an important role in the Mars polar atmosphere. Of particular interest is the evolution of cap-edge dust storms observed during the Mars Global Surveyor mission [1] and the development of the polar hood.

This poster describes the Mars Imager for Cloud and Aerosol (MICA), a four-band visible camera designed to characterize Mars cloud and dust by imaging the limb at sunrise and sunset. It will be capable of producing profiles of Mars aerosol optical properties from 0-75km with a vertical resolution better than 600m. MICA will follow on from Mars Express and MRO cloud and aerosol vertical profile mapping, providing new information, higher vertical resolution and adding to the Mars cloud and dust climatology.

MICA instrument design: Two-band twilight limb images from Viking were analyzed by Jaquin et al [2] and used to produce detailed aerosol extinction profiles. The power of this technique lies in the strong scattering response of small particles to visible light, and in viewing this signal against the dark limb. It allows very thin particle layers to be observed with high signal to noise.

The MICA design uses multiple bands and a new occulting disk technique to provide enhanced dust characterization capabilities. The full dynamic range of the camera is optimized for scattered light. A pinhole in the occulting disk attenuates direct sunlight, reducing its intensity to levels produced by scattering. The resulting composite image contains both a detailed image of the sun and a sensitive wide-angle image of the distribution of thin cloud and aerosol layers (Figure 1). Absolute calibration is possible through viewing the sun at high angle above the atmosphere. The calibrated solar image produces particle extinction measurements directly, while the wide-angle part of the image can be used to fit the scattering phase function in the case of horizontally homogeneous layers. These measurements will provide significant new constraints on Mars aerosol particle size distribution and optical properties.

Proposed mission: This instrument has been proposed as part of the Mars Volcanic Emission and Life (MARVEL) Scout. In the MARVEL mission proposal, MICA's visible observations are complemented by additional aerosol composition information from a bore-sighted high-resolution FTIR instrument. These combined observations produce an extremely powerful data set for the study of Mars dust and cloud latitudinal, seasonal and vertical variability and microphysical processes. The addition of a flip mirror gives MICA the capability to observe the surface.

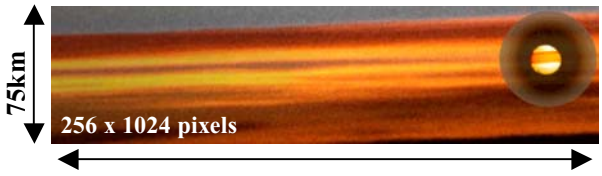

Figure 1: A simulated MICA sunset limb image showing cloud and dust layers. The shadow around the sun is the occulting disk penumbra.

References:
[1] Cantor, B. A. et al (2001) *JGR, 106*
[2] Jaquin et al (1986) *Icarus, 68*

Acknowledgments: This work was supported by the Canadian Space Agency, CREStech and COM DEV LTD.

Further information: Contact Dr. Vicky Hipkin, Dept of Physics, University of Toronto, 60 St. George St, Toronto, Ontario, Canada, M5R 2W3. **Email:** vicky@atmosp.physics.utoronto.ca

MODELING MARTIAN FOG FORMATION IN THE NORTHERN HIGH LATITUDES DURING THE RETREAT OF THE SEASONAL NORTH POLAR CAP. A. Inada, *Max-Planck-Institut für Aeronomie, Katlenburg-Lindau D37191, Germany (inada@linmpi.mpg.de)*, M. I. Richardson, *Division of Geological and Planetary Sciences, California Institute of Technology, Pasadena, CA, USA (mir@gps.caltech.edu)*, A. D. Toigo, *Center for Radiophysics and Space Research, Cornell University, Ithaca, NY, USA (toigo@astro.cornell.edu)*.

Introduction The early stages of spacecraft exploration of Mars showed that dust plays as important a role in the Martian atmosphere as water vapor does for the Earth. Gierasch and Goody (1972) showed that a model including the radiative effects of suspended dust provided a good fit to the atmospheric temperature structure observed by Mariner 9. The effects of water ice particles in the atmosphere and climate is a more recent concern. The vertical distribution of water vapor varies due to the precipitation of cloud particles (*e.g.,* Kahn 1990; Clancy *et al*., 1996; Richardson *et al*., 2002). The radiative effect of cloud particles has been discussed by Colaprete and Toon (2000). Water vapor condenses at high altitudes of about 80 km as a detached haze, at altitudes (depending on the season and latitude) of 10-50 km as clouds, over the polar caps as polar hoods, and near the surface as fogs. The various clouds, hazes, and fogs make up one component of the the water cycle on Mars (Jakosky, 1983; Richardson and Wilson, 2002). For example, as suggested by Kahn (1990) and demonstrated by Richardson *et al*. (2002), clouds in late northern summer are essential for returning water to the surface at a rate consistent with observations. In addition, the condensed phase of atmospheric water may play a significant role in modifying the spatial distribution of dust, through sequestration, as well as affecting surface temperatures and the atmospheric temperature structure.

Ice particle motions and radiative effects depend on particle size. Additionally, the particle size is sensitive to the manner in which the water ice particle was nucleated (homogeneous or heterogeneous nucleation). This important parameter has been estimated using Mie theory to fit observed infrared spectral data (Curran *et al*., 1973), using one-dimensional haze models to fit Viking limb images (Kahn, 1990), and most recently, using multi-angle thermal and visible observations (R. T. Clancy, private communication, 2003).

These data, combined with morphological information from images (Wang and Ingersoll, 2002), provide important constraints on microphysical models, which seek to provide more detailed insight into the dynamic nature of clouds, hazes, and fogs. One of the earliest explicit models of cloud formation was that of Michelangeli *et al*. (1993), who used the method developed by Toon *et al*. (1988) in a one-dimensional Martian climate model. Recently microphysical processes codes have been included in the Geophysical Fluid Dynamics Laboratory (GFDL) Mars General Circulation Model (GCM) (Rodin *et al*., 2001) and the NASA Ames Mars GCM (Colaprete and Haberle, 2001).

Most previous work modeling atmospheric ice aerosols has focused on clouds. Near-surface water ice particles ("fogs") have been less widely discussed. The boundary layer model of Savijärvi (1995) was used to model fog formation. It showed thin fog formation at the Viking Lander 1 site (22.5° N, 48.0° W). Fogs at the Pathfinder landing site (19.2° N, 33.2° W) and in the Memnonia region (15.0° S, 145.0° W) were simulated with microphysical processes by Inada (2002). Both are one-dimensional models and the simulated locations are in the low-middle latitudes. Fogs imaged by the Viking Orbiter, Mars Global Surveyor, and Mars Odyssey cameras have been observed to form in craters and channels, which motivates the simulation of fogs with models that explicitly treat three-dimensional atmospheric flow in response to high-resolution topographic information. Additionally, the abundance of water vapor sublimated from the northern polar cap leads to a large mixing ratio in high latitudes, and indicates that this may be a place of common fog formation. The purpose of this work is to investigate fog formation in the northern high latitudes during the retreating phase of the seasonal cap.

Figure 1: Fog in canyons seen by Viking Orbiter.

Observations It is generally difficult to identify optically thin clouds and fogs in images taken from orbiters; however, some of these images show brightening in craters, channels, and other depressions (Figure 1). This indicates that the bright feature is related to the surface topography, and is most likely ice aerosol formed near the surface, which can be called fogs. The optical depth of a typical crater fog observed in an orbiter images taken near the Viking Lander 1 site measured by Hoekzema (personal communication, 2003) was 0.92 in the red and 0.93 in violet, while that over the clear surface was about 0.55.

The Mars Atmospheric Water Detector (MAWD) on the Viking Orbiters provided a dataset of the column water vapor abundance that was the primary source of information on the water cycle for many years(Farmer *et al*., 1977; Jakosky and Farmer, 1982). Recently, spectra from the Thermal Emission Spectrometer (TES) on Mars Global Surveyor (MGS)

have been used to determine the annual variation of column-integrated water vapor (Smith, 2002). Both observations show the peak of water vapor amount in the northern high latitudes after the seasonal cap retreat. The maximum column density is over the edge of the northern polar cap in early-to-mid-summer and is more than 75 precipitable microns (pr. μm). This water vapor is contributed to a polar atmosphere which is quite cool, and thus the northern summer pole becomes one of the very few places on Mars when the atmosphere is nearly saturated (Richardson *et al*., 2002). The vapor distribution (the mass mixing ratio) is likely to decrease with height from the surface; elsewhere on the planet, it is likely uniformly distributed with height to at least 10 km. The northern polar atmosphere is thus a likely place for water recondense in the atmosphere due to the diurnal temperature cycle.

Model The simulation of fogs in the polar region is implemented with the Mars MM5 described by Toigo and Richardson (2002). This model is based on the Pennsylvania State University (PSU)/National Center for Atmosphere Research (NCAR) Mesoscale Model Version 5 (MM5) (Dudhia, 1993) and converted for use on Mars. It has been developed to research atmospheric dynamics on scales of a few hundreds meters to a few hundreds of kilometers, so that it is the most suitable model to study fog formation. The surface topography is taken from MGS Mars Orbiter Laser Altimeter (MOLA) high-resolution data set. Boundary conditions are provided by the GFDL Mars GCM (Richardson and Wilson, 2002)

For this study, we add the fog model of Inada (2002) to the Mars MM5. This enables the mesoscale atmospheric model to better simulate the water ice cycle. The microphysical processes of nucleation, condensation, sublimation and sedimentation are included. Coagulation due to sedimentation will be added in the future. Brownian coagulation is negligible because it affects only small particles with r less than 0.01 μm, where r is particle radius. The nucleation rate is a function of the radius of nuclei particles, with nucleation on large dust particles being faster than that on small particles. All dust particles are assumed to act as nuclei. Since there are typically many large dust particles near the surface, little nucleation occurs on particles with $r < 1.0$ μm.

Outlook Fog formation in the northern high latitudes is driven by the retreat of the northern seasonal polar cap. We will present the diurnal time sequence of fog formation, the size distribution of fog particles, water ice amount and the optical depth. The radii of formed ice particles depends on the pre-existing dust particles which are active as nuclei. Since water ice particles are segregated to the surface during the formation phase of the seasonal cap, large dust particles which act nucleation cores of water ice particles are removed from the atmosphere. The seasonal variance of dust size distribution is also simulated. Finally we compare the simulated fogs with observations from the Viking Orbiters cameras, the Mars Orbiter Camera (MOC) and TES on MGS, and the Mars Odyssey THEMIS.

References

Colaprete, A., and R. M. Haberle, A comparison of Mars GCM cloud simulations with observations, American Geophysical Union, Fall Meeting 2001, abstract P31A-0534

Curran R. J., B. J. Conrath, R. A. Hanel, V. G. Kunde, and J. C. Pearl, Mars: Mariner 9 spectroscopic evidence for H_2O ice clouds, 1973

Dudhia, J., A nonhydrostatic version of the Penn State-NCAR mesoscale model: Validation tests and simulation of an Atlantic cyclone and cold font, *Mon. Weather Rev.*, 121, 1493–1513, 1993

Farmer, C. B., D. W. Davies, A. L. Holland, D. D. LaPorte, and P. E. Doms, Mars: Water vapor observations from the Viking Orbiters, *J. Geophysics, Res.*, 82, 4225–4248, 1977

Inada, A., Numerical simulations of Martian fog formation and inflight calibration of Mars Imaging Camera on NOZOMI for its future observations, Doctoral Thesis, Kobe Univ., Kobe, 2002

Jakosky, B. M., and C. B. Farmer, The seasonal and global behavior of water vapor in the Mars atmosphere: Complete global results of the Viking atmospheric water detector experiment, *J. Geophys. Res.*, 87, 2999–3019, 1982

Jakosky, B., The role of seasonal reservoirs in the Mars water cycle–II. Coupled models of the regolith, the polar caps, and the atmospheric transport, *Icarus*, 55, 10–39, 1983

Kahn, R., Ice haze, snow, and the Mars water cycle, *J. Geophys. Res.*, 95, 14677–14693, 1990

Michelangeli, D. V., O. B. Toon, R. M. Haberle, and J. B. Pollack, Numerical simulations of the formation and evolution of water ice clouds in the Martian atmosphere, *Icarus*, 100, 261–285, 1993

Richardson, M. I., and R. J. Wilson, Investigation of the nature and stability of the Martian seasonal water cycle with a general circulation model, *J. Geophys. Res.*, 107(E5), doi:10.1029/2001JE001536, 2002

Richardson, M. I., R. J. Wilson, and A. V. Rodin, Water ice clouds in the Martian atmosphere: General Circulation Model experiments with a simple clouds scheme, *J. Geophys. Res.*, 107(E9), doi:10.1029/2001JE001804, 2002

Rodin, A. V., R. J. Wilson, and M. I. Richardson, GCM simulations of the current Martian water cycle: Clouds and dynamical leverage *Bull. Am. Astro. Soc.*, 33(3), abstract 27.04, 2001

Savijärvi, H., Mars boundary layer modeling: Diurnal moisture cycle and soil properties at the Viking Lander 1 Site, *Icarus*, 117, 120–127, 1995

Smith, M. D., The annual cycle of water vapor on Mars as observed by the Thermal Emission Spectrometer, *J. Geophys. Res.*, 107(E11), doi:10.1029/2001JE001522, 2002

Toigo, A. D. and M. I. Richardson, A mesoscale model for the Martian atmosphere, *J. Geophys Res.*, 107(E7), doi:10.1029/2000JE001489, 2002

Toon O. B., R. P. Turco, D. Westphal, R. Malone, and M. S. Liu, A multidimensional model for aerosols: Description of computational analogs, *J. Atmos, Sci.*, 45, 2123–2143, 1988

Wilson, R. J. and K. P. Hamilton, Comprehensive model simulation of thermal tides in the Martian atmosphere, *J. Atmos, Sci.*, 53, 1290–1326, 1996

PROSPECTING FOR MARTIAN ICE FROM ORBIT. L. C. Kanner[1], M. S. Bell[2], and C. C. Allen[3], [1]Carleton College (300 N. College Street, Northfield, MN 55057), [2]Lockheed Martin @ Johnson Space Center (2400 NASA Rd. 1, Mail Code C23, Houston, TX 77058, mary.sue.bell1@jsc.nasa.gov), [3]NASA @ Johnson Space Center (Mail Code ST, Houston, TX 77058)

Introduction: Recent data from the Gamma-Ray Spectrometer (GRS) on Mars Odyssey indicate the presence of a hydrogen-rich layer tens of centimeters thick in high latitudes on Mars [1]. This hydrogen-rich layer correlates to previously determined regions of ice stability. It has been suggested that the subsurface hydrogen is ice and constitutes 35 +/- 15% by weight near the north and south polar regions [2]. This study constrains the location of subsurface ice deposits on the scale of kilometers or smaller by combining GRS data with surface features indicative of subsurface ice.

The most recognizable terrestrial geomorphic indicators of subsurface ice, formed in permafrost and periglacial environments, include thermokarst pits, pingos, pseudocraters and patterned ground. Patterned ground features have geometric forms such as circles, polygons, stripes and nets. This study focuses on the polygonal form of patterned ground, selected for its discernable shape and subsurface implications. Polygonal features are typically demarcated by troughs, beneath which grow vertical ice-wedges. Ice-wedges form in thermal contraction cracks in ice-rich soil and grow with annual freezing and thawing events repeated over tens of years. Ice wedges exist below the depth of seasonal freeze-thaw [3]. Terrestrial ice wedges can be several meters deep and polygons can be tens of meters apart [4, 5, 6], and, on rare occasions, up to 1 km [7]. The crack spacing of terrestrial polygons is typically 3 to 10 times the crack depth [8].

Polygonal terrain is the dominant form of patterned ground seen on Mars [9] and has been recognized in several high resolution Viking Orbiter images [10,11,12,13] and Viking Lander 2 images [14]. High-resolution images from Mars Orbital Camera (MOC) on Mars Global Surveyor reveal Martian surface features in unprecedented detail and meter-sized polygons are more easily discernible and characterized [15]. Martian polygons range in size from 10 m [16] to 10 km [14] or on rare occations up to 20 km [11]. Polygonal terrain is generally grouped based on size and theorized origin into small-scale (~10-250 m) and large-scale (~250 m-20 km) polygons. Small-scale polygons are applicable to this study because it is thought that the origin of small-scale polygons on Mars is the result of permafrost thermal contraction cracking similar to that found on Earth [17,16]. The presence of polygonal ground on the surface generally indicates the presence of ground ice at depths of several meters and can reveal much about the latitudinal distribution of ground ice and ground ice history [17]. Large, multi-kilometer scale polygons likely form by processes unrelated to subsurface ice.

Methods: Using high-resolution narrow-angle MOC images (1.55-12.39 m/pixel), we have noted the presence, absence, and possibility of polygonal terrain around the planet in a latitude band from 30°N to 65°N. Data sets from August 1997-July 2002 were used, less the September 1999-February 2000 set. Polygonal terrain identified in this study can be characterized by the following features: diameter of individual polygons range in size from 25 m - 250 m, polygons are bounded by nearly straight troughs or raised rims and angular joins. Troughs and raised rims frequently show a preferred north-south orientation.

The distribution of polygonal terrain was compared to a mercator projection of GRS relative hydrogen abundance [1,2] as well as a recent geologic map of Mars [18].

Observations: A total of 5,280 images were analyzed and 283 images revealed the presence of polygonal terrain. The distribution of polygonal terrain is scattered throughout the regional band at low elevations (<0m) and nearly all latitudes. The distribution is similar to that found by Seibert and Kargel (2001) [16]. Polygons were identified neither below 35°N nor in the cratered highlands. Particularly high concentrations of polygonal ground are present in the Casius quadrangle between 278°W-258°W and 40°N-50°N. In this region of the Utopia Planitia basin, 74% of the total 132 images analyzed showed the presence of polygonal terrain.

GRS detects hydrogen in high concentrations poleward of 50 +/- 5° [1,2]. The comparision of GRS hydrogen abundance data to the distribution of polygonal terrain shows no correlation (Figure 1). Polygons are present in areas of low concentrations of near subsurface ice as frequently as they are present in areas of high concentrations of near subsurface ice. The high concentration of polygonal ground in western Utopia Planitia correlates to an area of lower concentrations of near subsurface ice.

The majority of polygonal terrain in Utopia Planitia correlates to Hesperian-age units, while there are some occurances to Amazonian-age units [18]. According to Greely and Guest, these units, Hesperian and Ama-

zonian, are of diverse origin – volcanic, tectonic, alluvial, and eolian.

Discussion and Interpretation: What can the anti-correlation between near subsurface ice and presence of polygonal terrain in the Casius quadrangle between 282°W-262°W and 40°N-50°N suggest about the composition of the near and deeper subsurface? One possibility is that the presence of this type of polygonal terrain on Mars is not a response to thermal contraction cracking of ice-rich ground. Ice may be absent at depths of several meters, in turn making the polygonal terrain a response to other contraction processes---desiccation, fracturing of cooling lava, deep-seated horizontal stresses , or stratigraphic control.

On the other hand, ice may exist and do so both as near subsurface ice in the first meter as detected by GRS and as deeper ground ice as seen by the presence of ice-wedging terrain. Data collected in this study suggests the existence of near subsurface and deeper subsurface ice layers which can be explained as a response to climate oscillations. It is likely that hydrogen concentrations in the first meter of the Martian surface are a result of climate conditions at present obliquity. Diurnal termperature occillations affect only the first 2-3 m of the Martian regolith [19]. Ground ice is thought to exist in equatorial regions despite its current instability at the surface [10,20,21]. This conflict can be resolved if deep ground ice is a relic of a colder climate during periods of high obliquity [22]. Theoretical modeling shows that ground ice may have persisted at depths greater than 200 m shortly after the beginning of Mars's geologic history and that ground ice will persist for longer periods of time in regolith of small pore size [23].

If the abundace of Martian small-scale polygons are geomorphically, and structurally similar to terrestrial polygons, their presence should not correlate to hyrdrogen abundance in the first meter for the following reasons: initial propagation of ice wedges occurs below the freeze-thaw layer, or the ice would melt (or sublime), and ice-wedges can extend tens of meters deep. Martian ice-wedge polygons may correlate to thicker layers of ground ice not detected by GRS.

Acknowledgements: We thank William C. Feldman and William V. Boynton for allowing us to use the GRS data and Buck Janes for sending it. Jan Bednarski has provided numerous aerial photos and interpration of Canadian, as well as Martian, permafrost features.

References: [1] Feldman W. C. et al. (2002) *Science., 297,* 75-78. [2] Boynton W. V. et al. (2002) *Science., 297,* 81-85. [3] Williams P. J. and Smith M. W. (1989) *The Frozen Earth: Fundamentals of Geocryology,* p23. [4] Lachenbruch A. H. (1962) *GSA Spec. Pap., 70,* 69p. [5] Kerfoot D. E. (1972) *Arctic, 25,* 142–150. [6] Pewe T. L. (1973) *Geoforum, 15,* 15–26. [7] Pratt W. E. (1958) *AAPG Bulletin, 40,* 2249-2251. [8] Mellon M. T. (1997) *LPS XXVIII,* Abstract #1495. [9] Squyres A. B. et al. (1992) *Mars,* p549. [10] Carr A. B. and Schaber C. D. (1977) *JGR, 82,* 4039–4054. [11] Morris E. C. and Underwood J. R. (1978) *Rep. Planet. Geol. Prog, NASA TM 79729,* 97-99. [12] Evans N. and Rossbacher L. A. (1980) *Rep. Planet. Geol. Prog., NASA TM 82385,* 376-378. [13] Brook G. A. (1982) *Rep. Planet. Geol. Prog., NASA TM 85127,* 265-267. [14] Mutch T. A. et al. (1977) *JGR., 82,* 4452-4467. [15] Malin M. C. et al. (June, July 2003) *Malin Space Center Systems Mars Orbiter Camera Image Gallery* (http://www.msss.com/moc_gallery/). [16] Seibert N. M. and Kargel J. S. (2001) *GRL, 28,* 899-902. [17] Mellon M. T. (1997) *JGR, 102,* 25,617-25,628. [18] Greeley R. and Guest J. E. (1987) *USGS Misc. Inv. Series Map I-1802-B.* [19] Clifford S. M. (2003) *personal contact*. [20] Moughins-Mark P. (1979) *JGR, 84,* 8011-8022. [21] Allen C. C. (1997) *JGR, 84,* 8048-8059. [22] Mellon M. T. and Jackosky B. J. (1993) *JGR, 98,* 3345–3364.

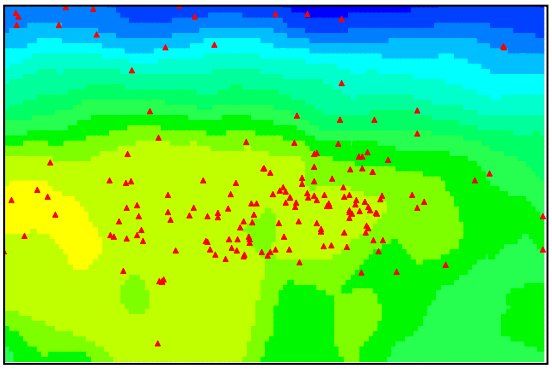

Figure 1. Map of the Casius quadrangle in terms of relative hydrogen abundance (yellow-shaded regions represent areas of low concentrations, blue-shaded regions areas of high) [1,2] and distribution of polygonal terrain marked by the red triangles.

ASTER IMAGERY AND INTERPRETATION OF GLACIERS IN JASPER NATIONAL PARK AND ELSEWHERE IN THE CORDILLERA. J.S. Kargel[1] and B. Molnia[2], [1]U.S. Geological Survey, 2255 N. Gemini Dr., Flagstaff, AZ 86001, U.S.A.; Email: jkargel@usgs.gov; [2]USGS, Reston, Email: bmolnia@usgs.gov.

Fourteen-band ASTER imagery has a spatial resolution of 15 m/pixel in VNIR, one band of which is in stereo; 30 m/pixel in SWIR; and 90 m/pixel in TIR. Variable gain settings selectable for snow and ice targets, high radiometric and geometric fidelity, 60-km scene width, special acquisitions of glacier imagery as a part of the GLIMS project (Global Land Ice Measurements from Space, www.glims.org), and high data downlink rate make ASTER ideal for many glacier studies. Spectacular imagery of glaciers in the Cordillera, including some in Jasper Nat. Park, are being used for detailed assessments of glacier morphology, extent, dynamics, hazards, and value as Mars analogs. A large-format poster will present a sample of ASTER imagery for Jasper Nat. Park and other selected areas of the Cordillera in Alaska and British Columbia.

Fig. 1 (above). Glaciers in South-central Alaska. Portion of ASTER image, VNIR RGB, June 27, 2001.

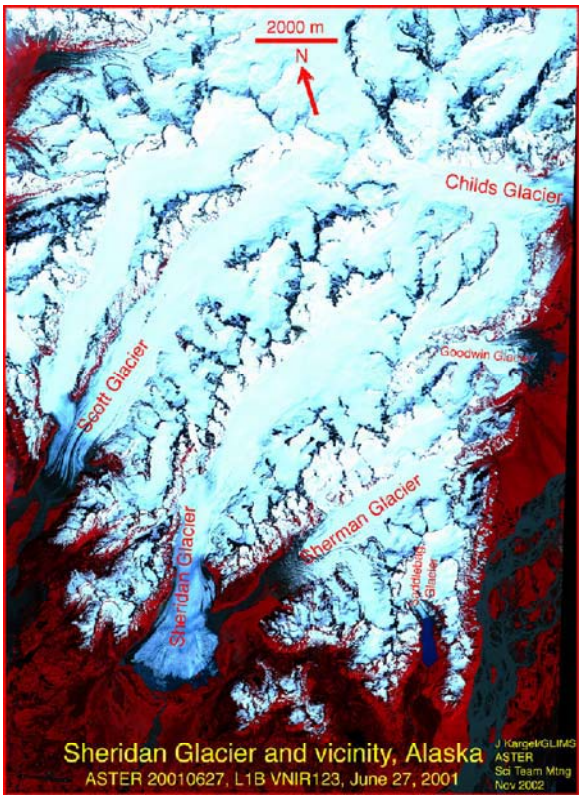

Fig. 3 (next page). Part of the Clemenceau Ice Field, Jasper National Park. Portion of ASTER VNIR R-G-B image July 22, 2002; scene width about 10 km.

Fig. 2. (Below) Sheridan Glacier, SC Alaska, June 27, 2001. Blown up sections of image shown in Fig. 1.

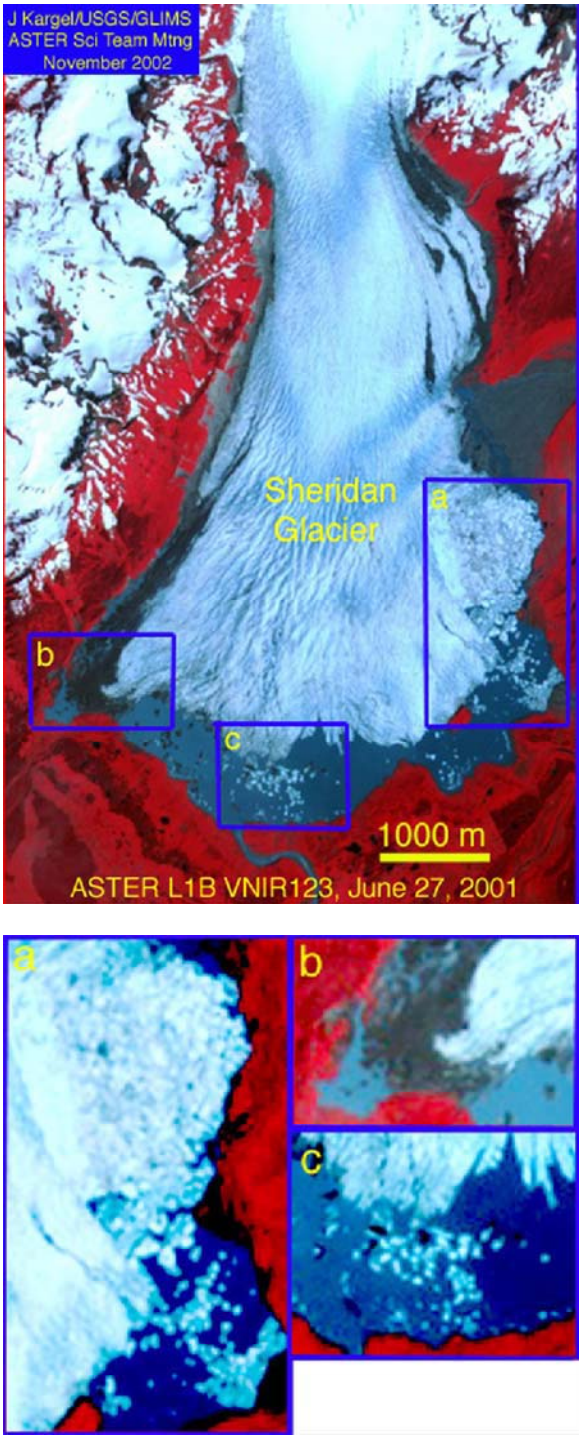

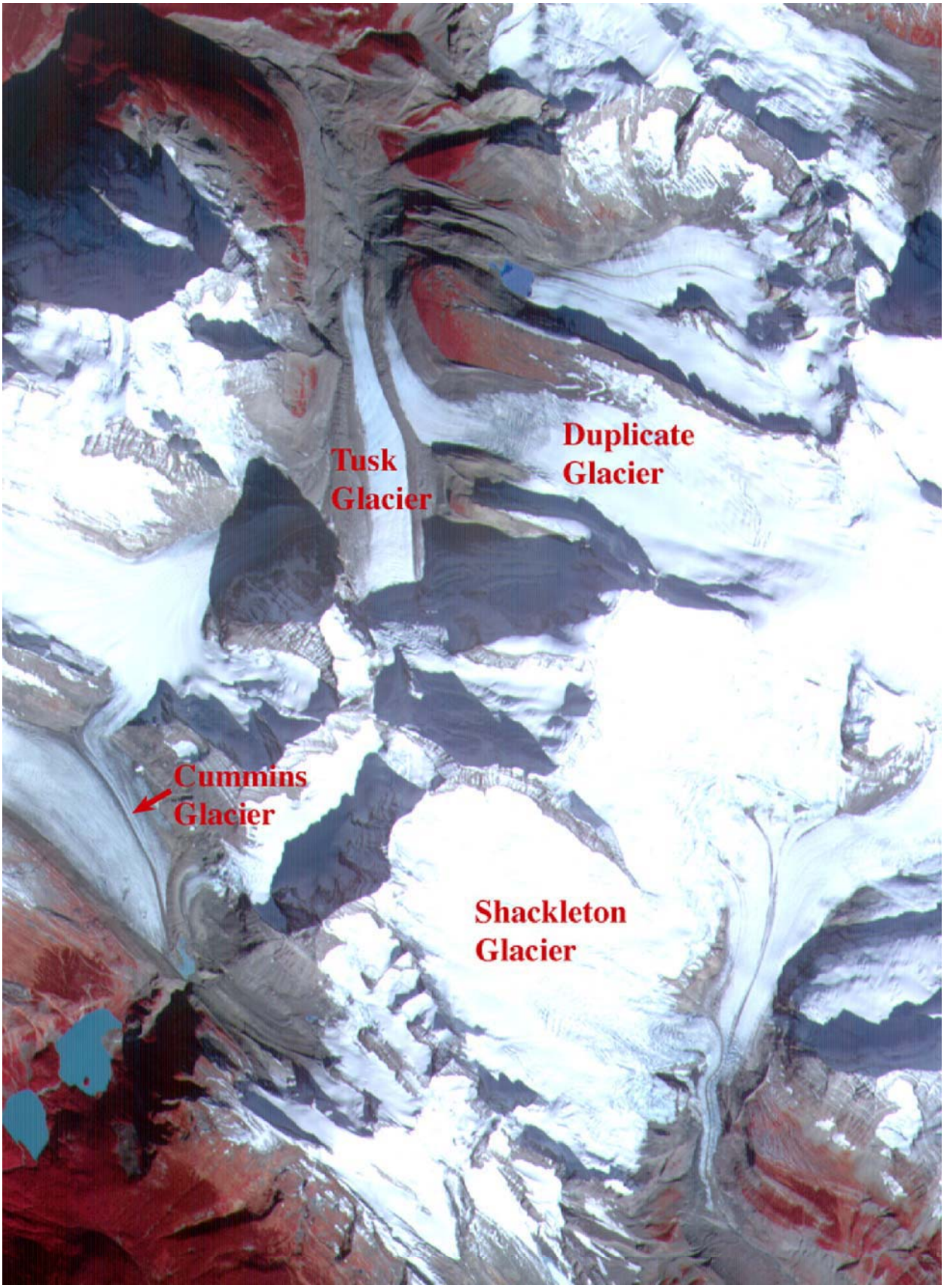
Tusk
Glacier
Duplicate
Glacier
Cummins
Glacier
Shackleton
Glacier

INTERCRYSTALLINE SWELLING OF STRATIFIED SILICATES EXPOSED TO NEGATIVE TEMPERATURES.

I.A. Komarov Department of Geocryology, Faculty of Geology, Moscow State University, Vorob'evy Hills, Moscow, 119899, Russia. ilya_komarov@mail.ru

ABSTRACT: Theoretical calculations based on a thermodynamic model together with experimental results based on differential scanning calorimetry are used to test whether intercrystalline swelling occurs in montmorillonite under negative temperatures.

Introduction

The analysis of adsorption properties of expandable stratified silicates, exposed to positive temperatures, provides the basis of proposing the existence of intercrystalline swelling caused by the interaction of silicates with water or other polarizing liquids. Swelling produces characteristic peaks (figure 1) on curves relating differential heat adsorption Q_v and moisture W when observing isotherms for the sorption of water vapor by montmorillonite and vermiculite clays. In particular, the heat of adsorption Qw for askangel drops as a result of saturation with water. Two maxima on the Q_w =F (W) curve at W≈10 % and W≈23% are associated with the intrusion of water between silicate layers of askangel. Minimums on the Q_w =F (W) curve are associated with loss of heat due to expansion of the mineral skeleton during adsorption [5]. Similar maxima and minima are observing for oglanlin and pigew Na-montmorillonite, kovdor vermiculite, and Ca montmorillonite. It is proposed, therefore, that intercrystalline swelling could also take place at negative temperatures, because of presence of unfrozen water near sediment and rock surfaces. Signs of swelling at negative temperatures should be evident from differential thermal analyses (DTA) of temperature curves and heat capacities because water between silicate layers could liberate heat. I examine this problem theoretically using thermodynamic equations for a range of temperature and moisture conditions.

Oservation

1.1. Thermodynamic model.

Proposed swelling of stratified silicates at negative temperatures is based on the calculations developed from a model of phase and adsorption equilibrium for water in unsalted and salted frost rocks proposed by Komarov (2001). The basis for this model is that pore liquids are part of a multi-component solution. This point of view is obvious for salted rocks. For unsalted rocks H_2O can occur in a solid, liquid or gaseous phase. A wide range of experimental data derived by various authors using various techniques (e.g. nuclear magnetic resonance (NMR), X-ray, calorimetric) show that unfrozen water is structurally and energetically non-homogeneous [2]. It is proposed, therefore, that water act as a binary solution even without presence of soluble ions in the liquid. Furthermore, I propose that individual H_2O molecules do not associate with the surface of rock particles. Instead water molecules next to the rock surface occur as monomers, which are 5^{th}-8^{th} layers of single water molecules with a thickness of 15 - 25 Å. These monomers are the first pseudo-component of Komarov's [3] model. Moving away from the rock surface, the next layer occurs in a field that is influenced by long distance forces associated with the rock surface. As the distance from the rock surface increases rock-induced forces are diminished such that forces associated with interactions between water molecules and structures within associated polymers dominate. This part of pore liquid is the second pseudo-component of the Komarov [3, 4] model.

The thermodynamics of this model requires that the first component of water have strong adsorption that is localized in the surface layer of the rock particles. This will stratify the solution creating a border between the first component and other components further from the rock surface. This border is characterized by a dynamic equilibrium between water monomers and associated polymers. The ice solution in the binary pore solution is representing by two processes, thawing of ice and mixing of the two determinate components of unfrozen water.

The main preconditions for model construction are in the labour [3, 4]. Evaluation of phase equilibrium parameters of water in salted and unsalted rocks follows Komarov [3]:

$$\sum_{i}^{2}[\ln(m_j f_j)_i]_{T=T_f} = \sum_{i}^{2}[-\frac{L\theta_i}{RT_0^2}\sum_{1}^{n}(\frac{\theta_i}{T_0})^{n-1}]+\sum_{i}^{2}[\frac{\alpha_i\theta_i^2}{RT_0^2}\sum_{1}^{n}\frac{n}{n+1}(\frac{\theta_i}{T_0})^{n-1}]+ \sum_{1}^{2}[\frac{\beta_i\theta_i^3}{RT_0^2}\sum_{1}^{n}\frac{n}{n+2}(\frac{\theta_i}{T_0})^{n-1}]+\sum_{i}^{2}[\frac{\gamma_i\theta_i^4}{RT_0^2}\sum_{1}^{n}\frac{n}{n+3}(\frac{\theta_i}{T_0})^{n-1}] +\frac{I}{R}[\frac{(T_v-T_0)+\theta_i}{T_v(T_0-\theta_i)}]\sum_{i}^{2}(H_j^0-H_j)_i,(n=1,2..n) \quad (1)$$

where: m_j , f_j - mole concentration and coefficient of activity; j – component (solution); $\theta = T_f - T_o$ – freezing point temperature (T_f – K degrees); L – molar latent heat of crystallization of water in the volume; R – gas constant; α_i, β_i, γ_i - coefficients determined from the heat capacity of ice and unfrozen water for single temperatures in unsalted rocks and from salt concentrations and compositions for salted rocks; T_v - the temperature of experiment; (H^o_j - H_j) – the difference in enthalpies, which is the value of differential heat of adsorption and moistening with back sign for unsalted rocks, and it is the differential heat of solution for salted rocks; i = 1 for unsalted pore solutions, i = 2 – for pore solutions with soluble ions, n – the number of the member of sum (n=1, 2, … n).

Equation (1) is a generalization of methods obtained by authors [6]. These authors considered single unsalted rocks where unfrozen water occurs in one of the three phases of H_2O and water properties correspond to the properties of deep cool water in freezing volume. This approach is less physically based. In contrast, properties of the solution in the freezing volume in my model are peculiar to the second conditionally determinate component, which is the solvent. Specific interactions between the surface of rock particles and adjacent layers of pore liquid, which do not freeze even under low negative temperatures, is not taking into account in previous approaches. The value for moisture of first component in my current analyzes varies from 0.45 to 0.7 which corresponds to maximum hygroscopic moisture. Transfer to the real surface layers of water is accomplished by adding a coefficient of surface activity for active salt ions.

1.2.The results of simulation.

The temperature curve of unfrozen water for askangel, calculated by equation (1) for unsalted rocks (i=1) and corresponding adsorption data are presented in Figure 1. Parameters used in equation (1) to generate the figure are described by Komarov [4]. Theoretical calculations (Fig. 1) are within 10-15% of experimental results (Figure 2). Data received from labours [2] derived using a variety of methods (e.g. nucleus magnetic resonance (NMR), calorimetry, contact and cryoscopic methods) produce characteristic peaks for calculated curves in temperature ranges of –16 to÷ –18 ^{0}C and - 45 to÷ - 47^{0}C (Figure 2).

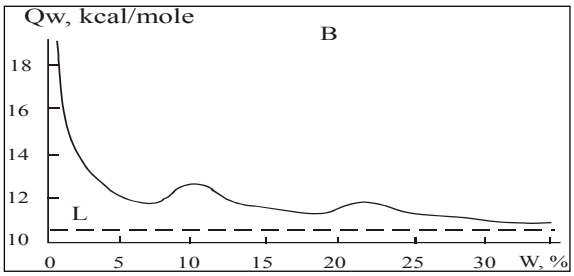

Figure 1. Dependence of differential adsorption heat Q_w on humidity W for the samples of montmorillonite [5].

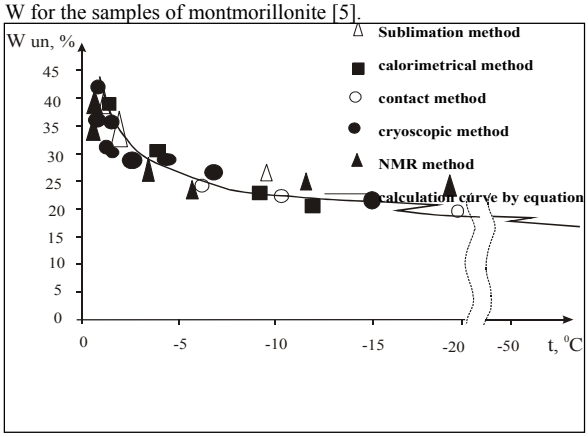

Figure 2. The comparison of calculated curve and experimental (obtained with different methods) data of volume of unfrozen water Wun for the samples of Na – montmorillonite.

These peaks are influenced by the interdependence of Qw = f(W) (Figure 1) and uncertainty that arises when the same value of heat adsorption can result from moisture with three possible phases moisture. Researchers have not previously considered this type of temperature dependence of unfrozen water. In my view this dependence is sensitive to small changes in the quantity of unfrozen water and considerable precision is required when using methods for determining phase consistence. This results in the smoothing of estimated adsorption on the graph. I suspect that this dependence of phase consistence on temperature is related to the intrusion of water between stratified silicate layers and expansion the lattice. Peaks in calculated curves are likely caused by the using of thermodynamic calculations to generate adsorption data. This would require that the surface of the rock not be deformed. However, the results of some work [8, 7] shows that this proposition is not correct even for rocks with inflexible cell structures (e.g. kaolin, talk and pyrophyllite). In particular, parameter B of cell structure changes as water is incorporated. The epitaxial growth of water films creates tension which drives mechanical deformation of particles. As a result, changes in phase consistence are gradual.

1.3. Experimental data.

Thermal capacity and enthalpy was determined by low-temperature differential scanning calorimetry (DSC) (calorimeter "Mettler TA-2000B"). This method is explained at length by Komarov [4]. Hysteresis was fixed for cycles of heating and cooling using the curves of DSC for heat capacity. Shifts in emission peaks varied from 10 to 17 degrees. Circumstantial evidence supporting the existence of crystal swelling in montmorillonite at negative temperatures is obtained by measuring heat capacity, which is a subtle indicator of structure deformations. There are three peaks in the plot of experimental data that relates heat capacity Cp and temperature $C_p = f(t)$ (Figure 3).

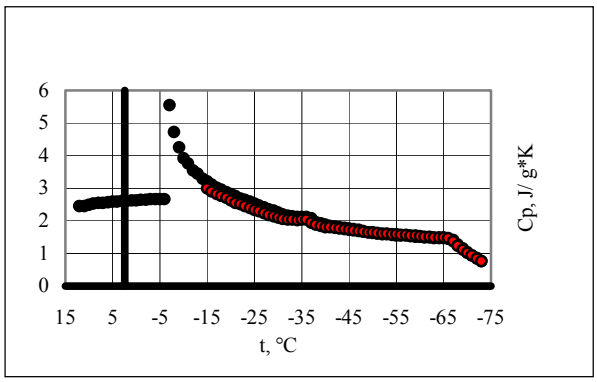

Figure 3. Experimental temperature curves of heat capacity for two samples of Na – montmorillonite (W=15%).

Two of these peaks are likely caused by gradual intrusions of the first and second layers of water between silicate layers in montmorillonite. The range of these peaks corresponds to predicated values that take into consideration shifts in peak caused by changing temperature. These structural reformations cause heating that can be recognized on the DSC curves. In fact, these peaks fix for Li, Na, K, and Ca – montmorillonite [1] .

The origin of these peaks was not explained by the original authors. We present our DSC curve in the labour (Komarov 2001, 2003), that we use to evaluate heat effects Q_{11} of the intrusion of second water layer into silicate structures. However, the sensitivity of calorimeters was insufficient to quantity the effect for first layer. It is Q_{11} = 0.11-0.13 j/g (related on gram of weight of sample of rock). It use calculated curve (Figure 2), which let to evaluate the quantity of unfrozen intruded water, that is necessary for evaluation of Q_{11} meaning on gram of unfrozen water. It is 1.2 ÷ 1.5 %. Then the heat effect for gram of water is Q_{11} = 20÷30 j/g. This meaning is close to experimental data in positive range of temperatures, the valuations of heat of moistening of second water layer, which intrude to inter layer space of Na – montmorillonite and come to Q_{11} =12÷20 J/g [8]. The evaluation is less on order as latent heat, which is emitted during the freezing of water. The fundamental interpretation of this effect with help of modeling, x-ray analyses transgress from borders of this paper and was discussed in the labour [4].

It is reasonably to appoint two ideas as applied to Martian conditions: a) taking into account the discussed phenomena lets to correct in the side of increasing adsorption moisture content in the regions with stratiform silicates in the surface layer; b) As the water evaporation heat could exceed ice sublimation heat in 1,5 times and more under low humidity, so ice existence in the rock leads to ice sublimation or its thawing and next adsorption of formed moisture as these processes are more thermalphysically efficiently.

Reference: 1. Anderson, D. M. and Tace, A. R. (1971). *Soil Science Society of America Proceedings, ,vol.35*, no.1, pp. 47-54

2. Ershov, E. D. et. al. (1979). Phase compound of moisture in frozen rocks. MSU.pp.189

3. Komarov, I. A. (2001), *7-th International Symposium on Thermal Engineering and Sciences for Cold Regions*, Seoul ,Korea.

4. Komarov I.A., (2003), Thermodynamic and heat mass transfer in disperse frozen grounds, Moscow, *Scientific world*, pp.608.

5. Korolev, V. A. (1983), The collection of scientific works. Moscow. *MSU Publishing, Vol. 5.*

6. Low, P. F., Anderson, D. M., Hoekstra P. , (1968), *Water Resources Researchv.4, N 2*, p. 379-394.

7. Osypov, V. I. (1979), The origin of mechanical and deformation properties of clay rocks. Moscow. *Nedra*

8. Tarasevich, J. M. Ovcharenko, F. D. (1975), Kiev. *Scientific thought*, pp.351.

PROPERTIES OF DISPERSE FROST ROCK IN THE RANGE OF LOW NEGATIVE TEMPERATURES.

I.A. Komarov, V.S.Issaev, L. V. Mel'chakova
Geological Department, Moscow State University, Vorob'evy Hill, Moscow, Russia,119899
tpomed@garnet.ru

Abstract: this paper presents experimental data for thermophysical properties of disperse terrestrial soils in the wide range of negative temperatures from 0 to –120 ^{0}C. We represent results of comparision with data of thermal lag of Marthian surface.

Introduction

Frozen soils are multi phases and multi component systems in the thermodynamic sense. As heat capacity is an additive amount, so its value is the sum of the heat capacities of its constituents: minerals of rock skeleton and organic components; pore solutions; pore ice; pore gases. Heat capacity of rocks was studied mainly for a range of positive and comparatively high negative temperatures [2].

Observation

Experimental researches were surveyed on the basis of adiabatic and differential scanning calorimetry. Methods are described in the labours [5].Experiments measuring heat capacity of rocks on using calorimetry were made for quartz sand, loam-sand and clays: kaolin, hydromicaceous. The samples were dried at a temperature of 105 ^{0}C.

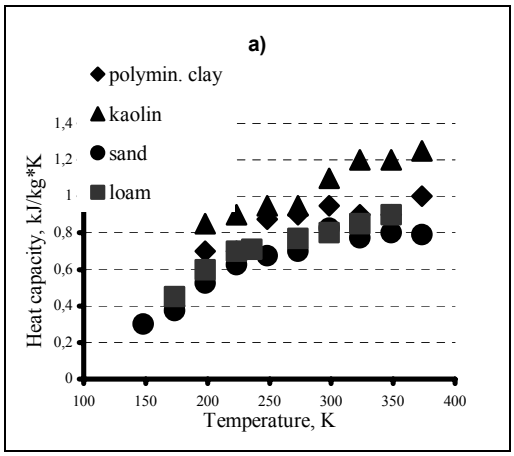

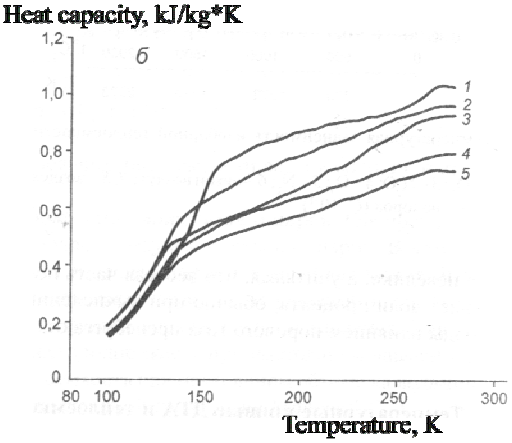

Figure 1. Dependence of heat capacity of skeleton mineral material of various grain size and mineral composition on temperature: a – the data has received with adiabatic calorimeter, b – the data has received with differential scanning calorimeter "Mettler TA-2000B".

In accordance with Figure 1-a specific heat of the skeleton mineral material C_{sk} of soils varies with temperature: it changes little in the range of temperatures from –25 to 100 ^{0}C; C_{sk} falls with temperature decrease to –100 ^{0}C (30% for hydromicaceous clay). Satisfactory agreement (less 5-10% difference) is observed with similar data from [4] for calorimetric experiments in the range of temperature from 223 to 318 K with temperature steps of 15º and data of [7], who did experiments using a massive calorimeter. It is necessary to consider temperature dependence of heat capacity of skeleton minerals for a wider range of negative temperatures. The influence of mineral grain size in the range of temperatures from 100K to 140K correlates to notions about behavior of the heat capacity of minerals.

Results of experimental investigation of temperature dependence of heat conductivity coefficient of clay loam and quartz sand with fractions of 0.1 -0.25 mm under different values of moisture are given in Figure 2 a,b.

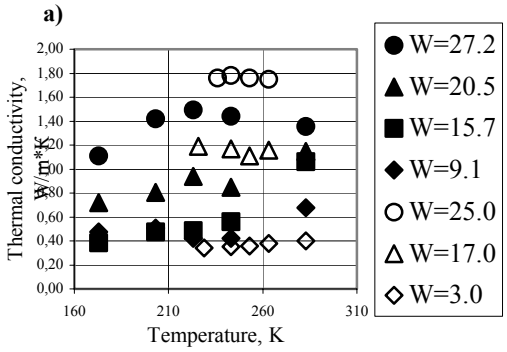

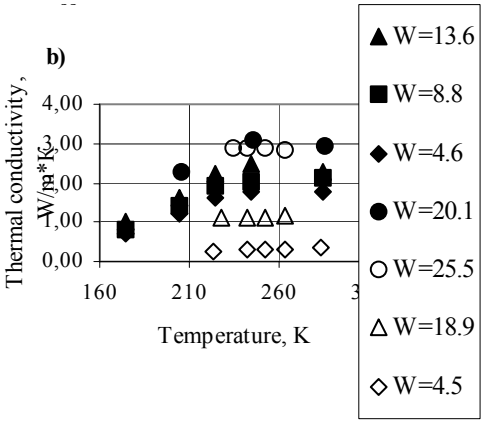

Figure 2. Dependence of thermal conductivity on temperature of various moisture contents: a - of quartz sand (fr.0.1-0.25); b - of clay loam. Unfilled badges are experimental results, filled budges are data from [4].

The coefficient of heat conductivity has inconsiderable dependence on temperature for the air-dry rocks in the light of represent dependencies. These data are comparable with data from [4] for the samples of soils with different dispersion in a more narrow range of temperature about -50^{0}C (Figure 2 a, b). The sum of heat conductivity of soil in an air-dry state has to increase with decreasing temperature, as a result of increasing of heat conductivity of the mineral skeleton.

There is temperature dependence of coefficient of heat conductivity λ of quarts sand of two fractions (0.1 -0.25 mm and 0.25- 0.5 mm) form moisture on the Fig. 2 a. We observe considerable decreasing of λ value under temperature decreasing from -30 to -100 ^{0}C, that has confirmed with data for more narrow interval of temperature (to -50^0 C) [4]. It conflict with assumption that summary coefficient of heat conductivity λ of ice-saturated rocks have to increase with decreasing of temperature. This assumption is based on the character of temperature dependence of thermal conductivity of separate rock's components. λ value of ice increase twice in the temperature range from 0 to –110^{0}C. λ value of organic-mineral rock's skeleton in the same temperature range is not changed. λ value of loamy rocks in air-dry state also isn't related to the same temperature change. We supposes that the causes of λ decreasing are 1) micro-cracks formations in the pore ice (for temperature below –12 ^{o}C); 2) micro-cracks formations on the pore ice - rock particle's boarder contact as the cause α values differences of phases; 3) micro-cracks formations in the organic-mineral skeleton of rock as the cause α values differences of minerals. Structure's formation leads on decreasing of λ as the cause of increasing of pore gas contents. Comparison of calculation and experimental data with data of distance probe and of morphometric analyses of Martian surface. Data of thermophysical properties for surface layer of Mars could be received from the values of thermal lag I. These values are transmitted from landing space modules. The value $I = (\lambda C\rho)^{1/2}$ equals to 0.004÷0.017 cal/cm sec$^{1/2}$ K, and rock's density ρ is from 1 to 1.6 g/cm^3 [6]. λ value changes from 0.2 to 0.12 W/m K for C = 0.42 kJ/kg K. λ values for sandy rocks are in this range. It received from calculation of experimental data for terrestrial atmosphere's conditions with correction to the value of Martian atmosphere's pressure on the surface (6 mm of mercury) Figure 5. It is based on the method [1] for conditions of gaseous phase flowing $22 \geq Kn \geq 0.1$, where Kn is Knudsen's criterion. Accommodation coefficient is chosen for CO_2-quarts system.I value changes from 0.004 to 0.006 cal/cm sec$^{1/2}$(Kuzmin, 1983)· K. It corresponds to λ values from 0.05 ÷ 0.12 W/m K. This range for Martian atmosphere corresponds to thermal conductivity of dusty particles.

The reason for non increase of heat conductivity of mineral skeleton is heterogeneity of mineral composition and differences in coefficient of linear growth which leads to formation of micro cracking in organic mineral skeleton of rocks. The summary effect of these processes could be dominant and could lead to a decrease in the value of heat conductivity. The reason of this is increasing of gaseous phase content. Micro cracking process was proved by micro photograph researches, which were done on the basis of the replica method [5]. These effects are more clearly revealed in the analyses of the behavior of heat conductivity of wet soils (Figure 2 a, b). As the temperature dependence of the coefficient of heat conductivity of air-dry soil sand of ice shows by its behavior (abruptly increase of coefficient of heat conductivity with decreasing of temperature about 50 K, so it is reasonable to propose that the sum effect of heat conductivity will increase with fall of temperature for wet rocks. It confirms by experimental data of linear expansion α received on the basis of laboratory work with Japanese dilatometer "Sinky-Rico" model DL-150LS [3].

Nevertheless experimental data does not prove this suggestion. Heat conductivity of kaolin changes inconsiderable with temperature decreases under moisture content of 20%. Heat conductivity firstly decreases and later inconsiderably increases for rocks with moisture content of less than 20%. Heat conductivity falls under temperature decreases from –30 to-100^{0}C for sand samples, which have some individual differences for each sand fraction.

The reasons, which are determined experimentally for decreasing of the value of coefficient of heat conductivity under decreasing of temperature, are the following: formation of micro cracks inside pore ice; formation of micro cracks on the particle – ice interface; existence of micro cracking in organic mineral skeleton. The sum effect of these processes became dominant and leads to decreasing of value of coefficient of wet rock heat conductivity.

References

1. Dulnev, G.N. & Zarychnyak, Y.P. (1974). Leningrad, *Energy*, p. 264

2. Ershow, E. D. (1996). Moscow: *MSU*. p. 397.

3. Ershow, E.D., Komarov, I. A., Brushkow A.V., Hors M.N., (2001), *Proceeding of 2 conference of Russian geocryologists, . V.1*, pp 81-88.

4. Haynes, F. D., Carbu, D. L. & Van Pett D.J.(1991). *United State army. Corps of engineers. Cold regions research and engineering laboratory. Hanover*, New Hampshire, USA, Ser Crel.

5. Komarov, I.A. (2003). Thermodynamics и thermomasse transfer and frozen disperse rocks. *Scientific world*, Moscow.pp608

6. Kuzmin, R. O. , (1983), Moscow, *Science Press*. 144 p.

7. Shusherina, E. P. (1973), *Proceeding of 1 All union symposium of rheology of rocks*: 282-292. Erevan: Erevan University.

SEASONAL MELTING OF SURFACE WATER ICE CONDENSING IN MARTIAN GULLIES.. K. J. Kossacki, *Institute of Geophysics, Warsaw University, Pasteura 7, 02-093 Warsaw, Poland, (kjkossac@fuw.edu.pl)*, W. J. Markiewicz, *Max-Planck-Institute for Aeronomy, Max-Planck-Str. 2, 37191 Katlenburg-Lindau, Germany*.

Abstract

In this work we consider when and how much liquid water during present climate is possible within the gullies observed on the surface of Mars. We analyze the conditions for melting of H_2O ice, which seasonally condenses within the troughs of the gullies. The model includes both an approximate topography of the gullies as well as the inclination of the slope where the gullies appear. We have found, that water ice condensed in winter on the walls of gully-like troughs can undergo transition to the liquid phase after complete sublimation of CO_2 ice. The amount of liquid water obtained in this way, depends on several parameters but is most likely to be very small.

Introduction

The gullies are one of the most intriguing features discovered with the recent high resolution orbiter imaging of the surface of Mars. They are mostly found on slopes of craters but also on sides of isolated knobs. The gullies are believed to indicate recent surface flows, presumably of liquid water. To date, the details of the formation process of the gullies are not known. Several authors considered creation of gullies by seasonal melting of ice condensing on the surface ((2), (7), (1), (3)). However, these authors assumed flat surface, or at best smooth crater slope without local topography. According to (3) the conditions for melting of water ice can be satisfied on preferentially insolated slopes almost everywhere on Mars, but only at the surface. On the other hand, (1) has shown possibility of water ice melting to a depth of some meters below the appropriately inclined slopes, but not at the present obliquity.

In this paper we address the problem of the role of the shape of the gullies in the diurnal and seasonal cycles of the surface temperature in the present Mars climate conditions. The local topography needs consideration, because the exact slope of the local surface is of key importance for the energy balance and hence for quantifying the conditions for the possible condensation and melting of water ice. We try to answer the question, when and how much liquid water is it possible to form within the gullies on poleward directed slopes. The first condition for this is that the surface has to be above the melting temperature of water ice. At current obliquity, even at high latitudes Martian surface can warm up to temperatures allowing melting of water ice, but only in a very thin surface layer. The second condition is that the atmospheric pressure is above the triple point of water which is 6.1 mbar. In the north hemisphere pressure is high enough for this even at high latitudes, but in the south only at low and regionally middle latitudes.

Model

We analyze heat transport and evolution of ice distribution in the near surface layer of the regolith, in the vicinity of the north-south oriented trough located on a slope, as are most of the the gullies in the south hemisphere (1). The model includes diurnal and seasonal variations of the position of the Sun as well as seasonal variations of atmospheric pressure and composition. Surface condensation and sublimation is calculated for CO_2 and H_2O, on all facets of the troughs. Condensation and sublimation of H_2O is calculated accounting for the temperature dependence of the sublimation/condensation coefficient correcting Hertz-Knudsen equation (5). The model used in this work is based on that presented in (6). The current version differs from the previous one by allowing local inclination of the surface, accounting for the condensation of atmospheric water and including a more consistent way of treating the scattering of light in the atmosphere toward the surface (4).

Results and conclusions

We present the results obtained for two example locations at middle latitude in both hemispheres. They are 50°S, 50°E and the region of Viking 2 landing site at 48°N, 134°E. The surface density of the condensed water ice strongly depends on the atmospheric conditions, in particular strength of the local eddy diffusion which in turn can be parameterized in terms of the speed of the surface wind. For the volcano slopes (8) predict wind speeds reaching 40 m/s. We performed simulations with wind speed 5 m/s and 30 m/s. Toward the end of winter, more and more of the interior facets of the trough become exposed to the direct light. However, the walls receive significant flux of energy only when they are insolated at small angle to the local normal, in the morning at about 6:00 and in the afternoon about 18:00 LST. Thus, seasonal CO_2 ice remains on the walls for some time after the end of winter. When the trough is located on a slope at 50°S, 50°E the middle parts of the walls remain covered by CO_2 ice until $L_s \sim 250^\circ$. Rapid warming of the surface free of CO_2 ice leads to an almost immediate melting of H_2O ice. In the trough located at 48°N, 134°E melting process starts several sols after the complete sublimation of CO_2 ice, when the layer of H_2O ice is thin enough to have no significant influence on the albedo. Fig.1 displays model results for the Viking 2 landing site at 48°N, 134°E. The gully is assumed to be on a slope inclined by 30°. The curves show the evolution of the diurnal maximum of amount of water ice and liquid water on the middle of the west wall of the trough. Thus, the vertical distance to the surface of the slope from this point is 1m. In this place the surface density of ice reaches the maximum value of about $0.7\ kg\,m^{-2}$, at $L_s \sim 69^\circ$. After this date diurnal maximums of surface

water ice decreases with the rate depending on the chosen form of the sublimation/condensation coefficient α. When $\alpha = 1$ (classical approach), water ice disappears within one sol. When α is a function of temperature (5), water ice persists until $L_s \sim 73$. The amounts of liquid water, which may appear,

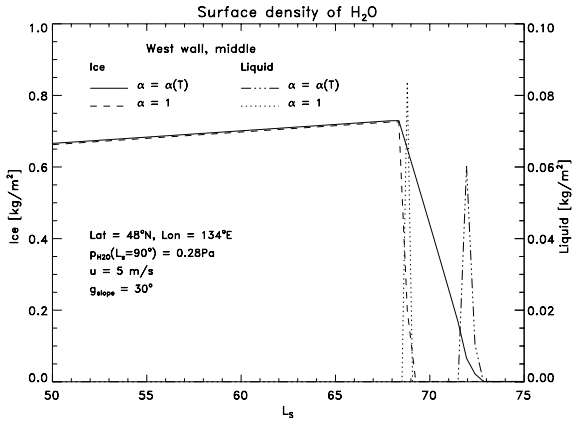

Figure 1: Daily maximum of the surface density of water ice and liquid water, on the middle part of the west wall of the gully-like trough at 48°N, 134°E. The seasonal maximum of vapour pressure is 0.28Pa. The curves are for the sublimation coefficient $\alpha = 1$, and for $\alpha = \alpha(T)$.

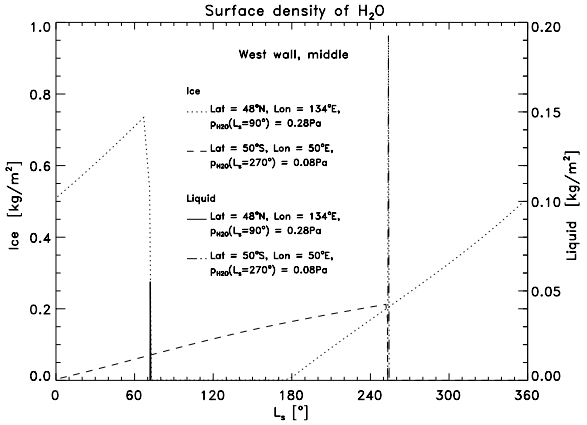

Figure 2: As Figure 1 but for both areographic locations: 48°N, 134°E and 50°S, 50°E, and for a whole Martian year with $\alpha = \alpha(T)$.

are shown as dotted and dashed-dotted lines. The curves are for the diurnal maximum of the surface density of liquid water, again for both forms of the coefficient α. In both cases amount of liquid is less then 0.1 $kg\,m^{-2}$, significantly smaller than the seasonal maximum of the accumulated amount of ice. This is because the surface covered by thick layer of ice has high enough albedo for the water ice to absorb enough energy to significantly sublime but not to melt. Ice can start melting only when the amount of surface ice is so small, that it does not affect the optical properties of the surface (in our model 100μm). For the trough located in the southern hemisphere, at 50°S, 50°E the spring time insolation is higher and the albedo enhanced due to presence of ice does not prohibit warming of the surface to the melting temperature. This results in the surface density of liquid water being comparable to that of the accumulated water ice, Fig. 2. During the day when the liquid appears in a given place, maximum local temperature greatly exceeds boiling point under low pressure of the Martian atmosphere. Thus, no moisture is likely to remain on the surface until next day. The maximum surface density of liquid water for this location is 0.2 $kg\,m^{-2}$.

We analyzed the seasonal cycle of condensation and sublimation of CO_2 and H_2O in the gully like troughs, about ten meters wide. Our simulations show that the H_2O ice deposited in seasonal (winter) cycle on the walls can undergo transition to the liquid phase in spring. When the trough is on the slope at 50°S, 50°E and inclined by 30°, the amount of moisture resulting from our simulations is only about 0.2 $kg\,m^{-2}$ and can appear in a given place during one day only. The rate of condensation is proportional to the wind speed so that simulations with winds of 30 m/s result in about 1 $kg\,m^{-2}$ of liquid water. This amount is probably still not enough to cause surface flow.

References

[1] Costard, F.,F. Forget, N. Mangold and J. P. Peulvast, Formation of Recent Martian Debris Flows by Melting of Near-Surface Ground Ice at High Obliquity, *Science*, *295*, 110–113, 2002.

[2] Haberle, R. M., C. P. McKay, J. Schaeffer, N. A. cabrol, E. A. Grin, A. P. Zent, and R. Quinn, On the possibility of liquid water on present-day Mars, *J. Geophys. Res*, *106*, 23,317–23,326, 2001.

[3] Hecht, M., Metastability of liquid water on Mars, *Icarus*, *156*, 373–386, 2002.

[4] Kieffer, H. H., T. N. Titus, and K. F. Mullins, Mars south polar spring and summer behavior observed by TES: Seasonal cap evolution controlled by frost grain size., *J. Geophys. Res*, *105*, 9653–9699, 2000.

[5] Kossacki, K. J., W. J. Markiewicz, Y. Skorov, and N. I. Kömle, Sublimation coefficient of water ice under simulated cometary-like conditions, *Planet. Space Sci.*, *47*, 1521–1530, 1999.

[6] Kossacki, K. J., and W. J. Markiewicz, Surface temperature of Martian regolith with polygonal features: influence of the subsurface water ice., *Planet. Space Sci.*, *51*, 569–580, 2003.

[7] Mellon, M. T., and R. J. Philips, Recent gullies on Mars and the source of liquid water., *J. Geophys. Res*, *106*, 23,165–23,180, 2001.

[8] Rafkin, S. C. R. and Sta. Maria, M. R. V. and T.I. Michaels, Simulation of the atmospheric thermal circulation of a martian volcano using a mesoscale numerical model., *Nature*, *419*, 697-699, 2002.

SURFACE FEATURES OF THE SOUTH POLAR LAYERED DEPOSITS OF MARS AND POSSIBLE TERRESTRIAL ANALOGUES M. R. Koutnik[1], S. Byrne[2], and B. C. Murray[2], [1]University of Washington (Box 351310, Seattle, WA 98195, mkoutnik@geophys.washington.edu), [2]California Institute of Technology (shane@gps.caltech.edu, bcm@gps.caltech.edu).

Introduction: Data from the Mars Orbiter Camera (MOC) and the Mars Orbiter Laser Altimeter (MOLA) aboard the Mars Global Surveyor (MGS) mission have provided important new clues to the past history of the South Polar Layered Deposits (SPLD). There are distinct features presented here that have been observed almost exclusively with these data sets and are unique to the south polar region of Mars. Although we do not conclusively know the origin of these features and don't rule out other interpretations, we consider here the possiblity that relatively recent subglacial volcanism and possibly the influence of ice flow may have been active in their formation.

Regional Description: We focus primarily on one region of the SPLD, approximately 190° - 230° W, 85° - 87°S (no MGS coverage south of 87°), where nearly all the features discussed here are found. Most extensive in this area are enigmatic large-scale grooves, termed here the "Wire Brush" terrain. Coverage of the Wire Brush terrain in the MOLA shaded relief map are showin in Figure 1. This region can be identified in Viking coverage of this area and shows that the grooves possibly have a connection with the current residual cap. Poleward of Chasma Australe and possibly one area off the cap are the only other locations where we see this grooved pattern at the south pole.

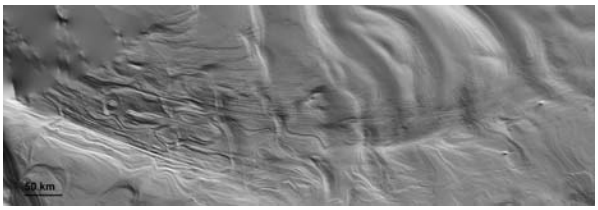

Figure 1. MOLA shaded relief map of the full extent of the Wire Brush Region, 190° - 230° W, 85° - 87°S.

The overall grooved pattern of the Wire Brush region is continuous for more than 300 km, though tracing of individual grooves is difficult to do with certainty for more than about 50 km. The grooves do continue linearly across local topography and are several hundreds of meters across with vertical relief of only a few tens of meters. The slope over the extent of the wire brush terrain is very slight and the grooves to do not seem to be influenced by any larger scale topography.

Near to the Wire Brush terrain there are numerous other unique features that may provide clues to the origin and timing of formation of the large-scale grooves.

Sinuous Ridges and Enclosed Chasma: There are sinuous ridges cross-cutting the Wire Brush which we have termed "Snakes". The Snakes are up to 2 km in width and tens of km long, although they are only a few tens of meters high. The presence of such vertical features is unusual. It could imply an episode of deformation or fracturing that has been filled subsequently with more resistant material than the surrounding layered deposits. The Snakes are found primarily within the Wire Brush but do extend out from this region as well. At least one Snake extends into an adjacent elongated depression and can be seen to interact with layering in this chasma. The enclosed chasma, shown in Figure 2, is a significant feature in association with the Wire Brush terrain. Unlike Chasma Australe, this chasma does not cut all the way through the layered terrains to the underlying basement rock and does not have an outlet. Given the positions of these two chasmas, on both sides of the Wire Brush Terrain, it is possible that all of these features may be related.

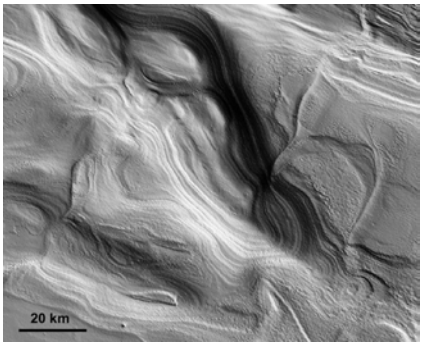

Figure 2. Enclosed depression adjacent to the Wire Brush region (seen in upper right). The Snake features can be seen cutting into the chasma from the right of the image.

Polar Potholes: Another interesting component of the Wire Brush and surrounding region is the presence of small, circular pits. They are found distinctly in the regions 190° - 230° W, 85° - 87° S (within the Wire Brush terrain) and 135°-175° W, 85°-87° S and can be roughly distinguished by orientation and morphology within these two regions. All of the individual polar potholes in both regions are approximately 50-100 m

in diameter. The potholes found within the Wire Brush region are circular, distinct forms. An interesting grouping of potholes is shown in Figure 3 where they are clustered in local circular depressions. The entire population of potholes is found only on the south polar layered deposits and these clustered forms are only in the Wire Brush region.

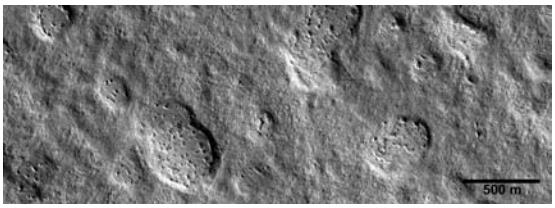

Figure 3. MOC NA m1102900 showing a distribution of potholes in the Wire Brush terrain that are grouped in larger circular depressions.

Mounds: North along the direction which the grooves trend in the Wire Brush terrain, there is a clustering of distinctive mounds, shown in Figure 4 and can also be seen in the far right of Figure 1. The mounds are few km in diameter and all have similar topographic features as observed from MOLA. The occurrence of these mounds in this location (and nowhere else we have found) and that they share a similar shape leads us to believe they could have a volcanic origin.

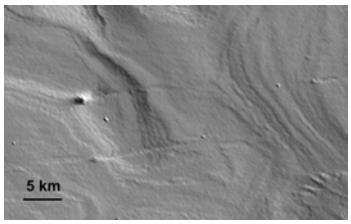

Figure 4. Two of the mound features associated with the Wire Brush region. They appear to act as obstructions, as evidenced by the linear "tail".

Interpretations: The Wire Brush region and associated features could conceivably be the signature of unusual past winds, ancient ice sheet motion, or episodes of catastrophic flooding originating from beneath earlier residual caps. We have explored these interpretations [1] and now look for a mechanism or combination of mechanisms that can best explain all the features we have presented here near to the Wire Brush terrain. Assuming the features we see in this localized region of the SPLD originate from the same or a similar event in south polar history, the interpretation of subglacial volcanism is favored here. As the clustered mounds, enclosed chasma, and sinuous ridges are especially supportive evidence for volcanism. As well, elsewhere in the south polar region, Ghatan and Head [2] have proposed a past episode of subglacial volcanism of Hesperian age. We do not attempt to explain why there would be a period of increased heat flux in this region but acknowledge that an event like this cannot be completely ruled out.

We will also assess the possiblity of ice sheet motion driven by basal melting from changes in cap configuration, not from increased heat flux, active at the south pole in the Martian past. Basal melting beneath the Martian polar caps has been considered possible but is highly sensitive to surface temperature, cap thickness, thermal conductivity, and heat flux [3, 4]. With a heat flux one-third to one-half the terrestrial value [3] basal melting can most easily occur when the ice cap is thick and the conductivity is low, assuming negligible heat production from internal deformation [4]. If basal melting or meltwater generation occurred in the past without increased heat flux, it is assumed that the south polar cap was more extensive or there was a warmer climate. We look at the cap configurations and timing necessary to produce meltwater at the base for the south polar cap.

If the base was lubricated (by cap configuration or increased heat flux) it could be possible to produce large grooved features in the layered terrain by ice flow, analogous to terrestrial ice streams. We also consider the possiblity of a large outburst flood occurring, as seen in Icelandic jokulhlaups. It has been proposed that Chasma Australe was formed by a large outburst flood [5] and, given the possible relation of these features to the Chasma, these same arguments could apply for the Wire Brush region.

We consider the processes of subglacial volcanism and ice sheet motion to be possibly active in forming the enigmatic surface features seen in this region of the Martian south pole. The unique location of all these features is evidence of a significant event in the Martian past that had a considerable influence on the SPLD.

References: [1] Koutnik, M., et al. (2003) 6th Internation Mars Conference. [2] Ghatan, G. and J. Head (2002) *J. Geophys. Res.* 107, E7, 2002. [3] Clifford, S. (1987) *J. Geophys. Res.* 92, B9, 9135-9152. [4] Larsen and Dahl-Jensen (2000) *Icarus* 144, 456-462 [5] Aquita, F. et al. (2000*) Icarus* 144, 302-312.

POLAR WANDER IN THE GEOLOGICAL HISTORY OF MARS: CONSTRAINTS FROM TOPOGRAPHY STATISTICS. ***M. A. Kreslavsky***[1,2] and ***J. W. Head***[1], [1]Dept. Geological Sci., Brown University, Providence, RI 02912-1846, USA; misha@mare.geo.brown.edu, [2]Astronomical Institute, Kharkov National University, Ukraine.

Introduction: True polar wander (that is change of position of the spin axis of a planet relative to the crust) has been hypothesized for Mars long ago (see [1] for review). The general idea is the formation of Tharsis rise should shift any initial spin axis position so that the rise is centered at the equator.

P. Schultz and A. Lutz [2,3] presented two principally different lines of observational evidence for true polar wander in the past. First, they found [2] a significant excess of large impact craters made by grazing impacts, and attributed them to impacts of tidally decelerated former satellites of Mars, which dynamically could only orbit Mars close to its equatorial plane; location and orientation of such craters suggested a position of the equator very different form that of the present-day. Second [3], Schultz and Lutz found concentration of specific deposits in Arabia Terra and on the opposite side of the planet (Medusae Fossae Formation) which they interpreted as remnants of former layered terrain similar to the present-day polar caps.

Recently, analysis of strong magnetic anomalies in the southern highlands of Mars provided some new evidence for the polar wander in the past. J. Arkani-Hamed [4] showed that if one suggests that the crustal magnetization reflects the extinct planetary dipole magnetic field at some moment in the past, then inferred positions of the magnetic dipole axes are clustered in a 30° wide area around 130°W 25°N. Since the deflection of the magnetic dipole axis from the spin axis is not high (at least for the same mechanism of magnetic field generation as on the Earth), the inferred pole position in the Early Noachian is close to this point. This point does not coincide with, but is rather close to, the former pole location proposed in [3].

Analysis of the current topography and rotation state of Mars led B. G. Bills and T. S. James [5] to the conclusion that the present-day rotation of Mars is secularly unstable. If the data used for the inference are accurate, than the spin axis can wander at a rate defined by the characteristic time scale of relaxation of elastic stresses in the lithosphere.

Our recent studies showed pronounced latitudinal zonality of the statistical characteristics of the kilometer-scale topography of Mars [6-8]. Here we analyze constraints that our findings put on the hypotheses of past true polar wander.

Observations: Statistical analysis of martian topography along topographic profiles obtained with MOLA altimeter [9] onboard MGS showed [6] that the circumpolar regions (above 60° latitude) are consistently smoother at kilometer and subkilometer scales than the equatorial zone (below 30° latitude) with a gradual transition with some statistical peculiarities [7] between them. Recently we found [8] that the latitudinal trend of roughness is accompanied by even more pronounced latitudinal trend of steep slope occurrence. **Fig. 1** shows the relative frequency of slopes steeper than 20° as a function of latitude for typical southern highlands in Terra Cimmeria. It is seen that the steep slopes practically disappear above 50° latitude. **Fig. 2** shows locations of the steepest slopes on Mars. The paucity of extremely steep slopes at high latitudes is obvious. (Detailed analysis of the steepest slope occurrence will be published elsewhere).

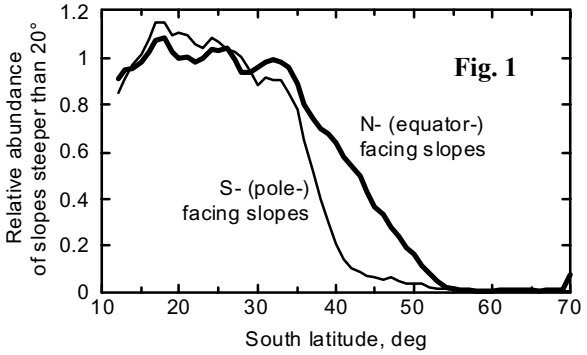

When we move from the equator to the poles, the abundance of steep slopes drops down sooner for the pole-facing slopes and later for the equator-facing slopes (Fig. 1). This produces a strong asymmetry in steep slope abundance at 40-50°S.

Fig. 3 shows the map of normalized median differential slope at 0.3 km baseline inferred from along-profile statistics. This parameter is a characteristic of the north - south slope asymmetry (see [8] for details). Fig. 3 shows two distinctive belts around 45° latitude in both hemispheres with the opposite sign of the asymmetry parameter, which shows that the equator-facing slopes in both bands are systematically steeper than pole-facing slopes. Note that the map in Fig. 3 reflects the behavior of typical (a few degree steep) slopes, while Fig. 1 and 2 are related to the steepest slopes on the planet. (For discussion of other features seen in Fig. 3 see [8].)

Both belts of slope asymmetry (Fig. 3) show a small deflection from ~45° parallel to the south in the western hemisphere and to the north in the eastern one. The

bands are well approximated by minor circles with 45° radii and the centers shifted ~5° from the poles toward 60-90°W in the northern hemisphere and to the opposite direction in the southern hemisphere.

Interpretation: The approximate symmetry relative to the equator strongly suggests that the role of insolation was important in the formation of the observed trend and the anomalous belts. F. Costard and co-authors [9] have pointed to the possibility of melting of thick layers of ground ice at higher obliquity. Their calculations showed that starting at ~35° obliquity, the summertime day-average surface temperature reaches 0°C at high (>~60°) latitudes; for higher obliquity the zero summer isotherm shifts toward the equator. The day-average temperature can exceed the ice melting point down to ~40° latitude at 45° obliquity, but only on steep pole-facing slopes.

We suggest that transient melting of ground ice in summer during periods of high obliquity promotes downslope movement of material and lowers steep slopes. Over geological time scales, this process removed almost all steep slopes above 50° latitude. At 40-50° latitude, the summertime melting and related movement can occur only on pole-facing slopes, making these slopes less steep. The equator-facing slopes in this zone remain intact. This produces the observed latitudinal trend and strong asymmetry of the steepest slopes.

Implications for past polar wander. Well preserved steep slopes in the equatorial highlands are mostly related to impact craters. If our interpretation of the latitudinal trend of the steep slope occurrence and the slope asymmetry bands is correct, the preservation of steep slopes in the equatorial highlands means that the day-average temperature have never exceed 0°C in these regions. Hence, these regions have never been at high latitudes during the time comparable to the highland crater population age. This constrains the true pole position during the whole Amazonian (and probably the Hesperian; more detailed analysis is necessary) to the vicinity of the present poles.

The deflection of the belts from 45° latitude might be related to effects of persistent atmospheric circulation or albedo patterns during the high obliquity epochs. We believe that it is more plausible that the current pole position is shifted ~5° from a formerly stable or long-term-average position. The direction of this shift is neither similar nor opposite to the shift of the geometric centers of the present-day polar layered deposits [10]. The same is true for the platy unit, a geologically older layer of the northern polar deposits [11]. Thus, we see not too strong, but positive evidence for polar wander of ~5° amplitude around its average position, which is determined by the centers of the slope asymmetry belts. The dynamic plausibility of such a process is the subject of a separate study.

Thus, we conclude that planetary-scale polar wander has not occurred since the Hesperian. The topographic information about the Noachian is more obscured, because of the large number of steep slopes produced by cratering and tectonics since that time. However, some information could survive in the topographic record of the Noachian-age highlands. We are presently analyzing this information to test the hypothesis of a different location of the spin axis in the Noachian.

References: [1] Ward, W. R. (1992) In *Mars*, Univ. Arizona Press, 298-320. [2] Schultz, P., and Lutz-Garihan A. B (1982) *Proc. LPSC XIII*, A84-A96. [3] Schultz, P., and Lutz A. B. (1988) *Icarus 73*, 91-141. [4] Arkani-Hamed, J. (2001) *GRL 28*, 3409-3412. [5] Bills, B. G., and T. S. James (1999) *JGR 104*, 9081-9096. [6] Kreslavsky, M. A. and J. W. Head (2000) *JGR 105*, 26695-26712. [7] Kreslavsky, M. A. and J. W. Head (2002) *JGL 29*, 1719, 10.1029/2002GL015392. [8] Kreslavsky, M. A. and J. W. Head (2003) *JGL 30*, 10.1029/2003GL017795 [9] Costard, F. et al. (2002) *Science 295*, 110-113. [10] Fishbaugh, K. E., and J. W. Head (2001) *Icarus 154*, 145-161. [11] Byrne, S. and B. C. Murray (2002) *JGR 107*, 10.1029/2001JE001615.

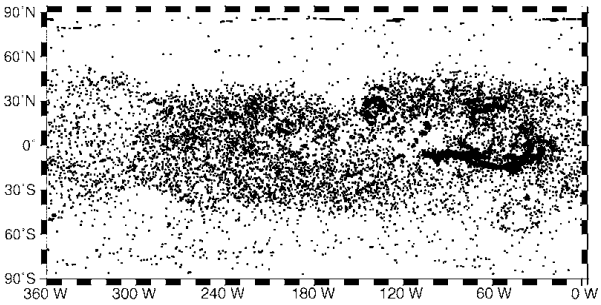

Fig. 2. Distribution of the steepest slopes on Mars. Each dot denotes a 300 m long segment of MOLA profile with slope steeper than 30°. In high-concentration areas the dots strongly overlap.

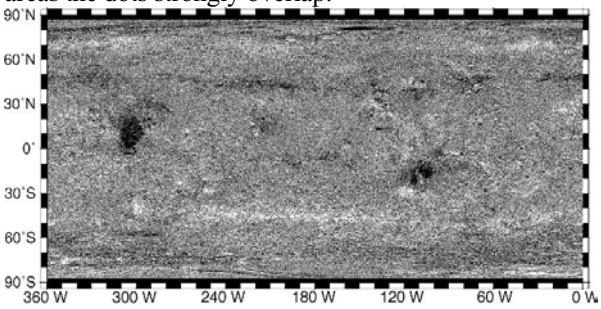

Fig. 3. Distribution of slope asymmetry parameter. Brighter (darker) shades mean that north- (south-) facing slopes are steeper.

DETERMINING STRUCTURAL AND MECHANICAL PROPERTIES OF SNOW WITH A HIGH-RESOLUTION PENETROMETER. K. Kronholm[1] , J. B. Johnson[2] and M. Schneebeli[1], [1]WSL Swiss Federal Institute for Snow and Avalanche Research SLF, Flüelastrasse 11, CH-7260 Davos Dorf, Switzerland, kronholm@slf.ch, [2]Cold Regions Research and Engineering Laboratory CRREL, Fairbanks, Alaska.

Introduction: On Earth, and possibly in extraterrestrial environments, the snow cover consists of individual snow layers that metamorphose over time. The stratigraphic record of snow layers is the result of erosional and depositional events. Adjacent layers differ in terms of their structural and mechanical properties. The structural properties of the upper snow layers are important for the chemical exchange between the atmosphere and the snow cover, snow hydrology, and the spectral properties of the snow cover. The mechanical properties are relevant for over-snow trafficability of vehicles and animals, and for avalanche release. Traditionally, snow is characterized by subjective measures of grain shape and size, and hardness [1]. Until recently, no fully automatic and objective methods to describe snow microstructure were available. The recent development of a snow micropenetrometer (SMP) now provides an objective way to measure the structural and mechanical properties of snow layers at different spatial scales [2, 3]. The SMP interpretation methods used for snow have also been used to objectively characterize soil [4].

Methods: With the SMP, we measured the penetration resistance of a seasonal snow cover. The force-distance signal had a sampling interval of 4 μm. The microstructural properties (microstructural element length and mean grain size) were derived from the signal by relating each force spike to a fracture of a microstructural element. The distance between fractures is directly related to the size of the microstructural elements [5]. Mechanical properties (compressive strength and elastic modulus) were derived using a mechanical theory developed for cohesive granular materials [5]. For comparison, a traditional stratigraphic profile with grain shape, size and hand hardness was done in addition to the SMP measurements. Snow samples were taken from individual layers. The spatial variation of structural and mechanical properties was analyzed for individual layers using geostatistics.

Results: The microstructural element length and the mean grain size derived from the penetrometer signal corresponded well with the results from the traditional methods. The derived compressive strength was within the previously reported ranges [Fig. 1]. The derived elastic modulus was a factor two lower than previously reported values. The mechanical properties of individual layers showed a large spatial variation on a single slope. The spatial variation in microstructure was not as large. Large spatial variation in structural and mechanical properties of individual layers was mainly found in layers deposited during windy conditions.

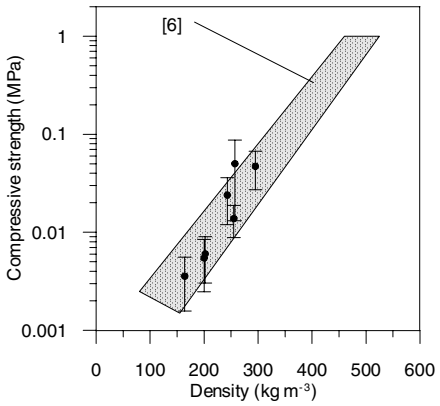

Fig. 1. Compressive strength of snow layers as a function of bulk density. Previously reported values are indicated by the grey area.

Discussion: The large spatial variation found in a terrestrial snow cover emphasizes the need to carry out multiple measurements to accurately characterize the three-dimensional variations of the snow cover properties. The representativity of a single measurement depends on the influence of wind in the snow stratigraphy. On Earth, a single measurement is usually not representative for a large area. The SMP can be used to derive important structural and mechanical properties of individual snow layers in a natural setting. An accurate description of the structural and mechanical properties of the upper snow layers and low density layered deposits on the polar areas of Mars could be obtained with a micropenetrometer mounted on a rover. Measurements could be done at certain intervals as the rover explores the Martian surface.

References: [1] Colbeck S. C. et al. (1990) *IAHS-ICSI Publ.* [2] Johnson, J. B. and Schneebeli M. (1998). Snow strength penetrometer, United States Patent 5,831,161, U. S. Patent Office. [3] Schneebeli M. and Johnson J. B. (1998) *Ann. Glaciol. 26*, 107-111. [4] Johnson, J. B. (2000). *Transportation Research Record, 1714*, 83-88. [5] Johnson J. B. and Schneebeli M. (1999) *Cold Reg. Sci. Technol. 30*, 91-100. [6] Mellor M. (1975) *IAHS Publ. 114*, 251-291.

PRELIMINARY CHARACTERIZATION OF A MICROBIAL COMMUNITY OF ROCK VARNISH FROM DEATH VALLEY, CALIFORNIA. K. R. Kuhlman[1], M. T. La Duc[1], G. M. Kuhlman[1], R. C. Anderson[1], D. A. Newcombe[1,2], W. Fusco[2], T. Steucker[2], L. Allenbach[2], C. Ball[2], and R. L. Crawford[2], [1]Jet Propulsion Laboratory, California Institute of Technology, 4800 Oak Grove Dr., Pasadena, CA 91109, kkuhlman@jpl.nasa.gov; [2]Environmental Research Institute, University of Idaho, Moscow, ID 83844, crawford@uidaho.edu.

Introduction: Rock varnish (also referred to as desert varnish in the literature because it is particularly noticeable in desert environments) is a dark, thin (typically 50-500µm thick), layered veneer composed of clay minerals cemented together by oxides and hydroxides of manganese and iron [1-4]. Some scientists suggest that varnish may provide a historical record of environmental processes such as global warming and long-term climate change. However, despite more than 30 years of study using modern microanalytical and microbial culturing techniques, the nucleation and growth mechanisms of rock varnish remain a mystery [4,5].

Rock varnish is of interest to the Mars science community because a varnish-like sheen has been reported on the rocks at the Viking Lander sites [6,7]. It therefore important for us to understand the formation mechanisms of terrestrial varnish – abiotic, biotic, or a combination of the two -- as this understanding may give us clues concerning the chemical and physical processes occurring on the surface of Mars. It is strongly believed by some in the biogeochemistry community that microbes have a role in forming rock varnish, and iron- and manganese-oxidation by microbes isolated from varnish has been extensively investigated [815-16]. Only two of these studies have investigated the microbial genetics of varnish [16,16]. These studies examined the morphological, physiological and molecular characteristics of microbes that had previously been cultured from various rock varnishes and identified the cultivars using 16S rDNA sequencing techniques. However, it is well known that most of organisms existing in nature are refractory to cultivation [17-20], so many important organisms would have been missed.

The currently described work investigates the genetics of rock varnish microbial community from a site in the Whipple Mtns., south of Death Valley, CA, near Parker, Arizona (Figure 1). We employed both cultural and molecular techniques to characterize the microorganisms found within the varnish and surrounding soil with the objectives of (a) identifying microorganisms potentially involved in varnish formation, and (b) discovering microorganisms that simply use the varnish as an extreme habitat.

Varnish collection: Since we are investigating the biocomplexity of the microbial communities of rock varnishes, it was critical that the samples be collected aseptically as possible. The samples were approached from the downwind direction, photographed *in situ*, picked up at arm's length using sterile gloves, placed within sterile Whirl-paks™ and sealed. Loose dirt on the undersides of the varnished rocks has proven to be a contamination problem during storage and harvesting of the varnish in the laboratory. The samples were then wrapped in protective material to prevent damage. In future collections, glass containers will be used to prevent the deposition of polymers from the Whirl-paks™ on the surface of the varnish, thus contaminating the surface for microanalytical work [21].

The varnish was harvested from the host rock in a laminar flow bench. A Dremel tool with a coarse bit that had been flame sterilized was used to grind the varnish off the host rock and into a sterile container [22]. For use as controls we also collected soil samples adjacent to some of the varnished clasts.

Figure 1. Macro photograph of a varnished clast used in our study. The underlying grid has 10 divisions per inch.

Microbial Enumerations: Powdered rock varnish (0.1 gram) was added to 1 milliliter of sterile double-distilled H_20. The samples were then stained with a stock DAPI (or Acridine Orange) (50mg/mL) solution. Samples were filtered onto 25mm Millipore Isopore 22µm pore size black polycarbonate filters with Whatman 25mm GF/F filters used for support. Fluorescing cells were counted on a Zeiss Research epifluorescence microscope equipped with an Osram

Xenon short arc photo optic lamp XBO 75W, and Chroma #31000 filter set for DAPI/Hoechst/AMCA.

The mean field (n) counted per sample was 57.16. The field standard deviation per sample was 7.48. The rock varnish had an average DAPI direct count of $9.0x10^7$ cells $gram^{-1}$ (standard deviation = 1.2E+07). There was no determinable difference between DAPI and Acridine Orange direct counts.

Cultivable UV-resistant microorganisms: Five distinct colony types were purified from TSA plates after exposure to the UV irradiation treatment. These strains were examined microscopically using both a standard light and a transmission electron microscope (TEM). The 16S rDNA gene of each isolated was amplified by PCR, cloned and sequenced for comparison to the RDP phylogenetic database.

We examined each cultivated strain for its resistance to UV(C) irradiation. The strains were quite resistant, and still showed growth on TSA plates after exposure for five minutes at UV(C) intensities that readily killed E. coli. Affiliations were estimated for three of the strains to genus level only using a similarity level of >98%.

Strain RV1 (white colony). Multiple *Arthrobacter* strains were found in a white colony (*A. polychromogenes, A. ramosus, A. oxidans, A. globifromis, and* unspeciated *A. spp.* show 99% sequence similarity with this isolate). Eppard, et al. (1996) reported the culturing of three strains highly related to *Arthobacter agilis* from rock varnish in the Mojave desert, but did not report UV resistance. [13].

Strain RV2 (orange colony). Various strains of *Curtobacterium flaccumfaciens* (e.g., AY273208.1) and an unidentified glacial ice bacterium (AF479342.1) show 98% sequence similarity to this isolate. Thus, this strain could be a candidate for survival in conditions such as those found in the polar regions of Mars.

Strain RV4 (black colony). This strain shows 16S rDNA sequence similarities of 98% (forward primers) and 99% (reverse primers) to a *Geodermatophilus obscura* originally isolated from soil samples from the Amargosa Desert of Nevada by Luedemann (1968) [20] and found in Negev desert soil and monuments by Eppard, et al., (1996) [13]. The strain's morphological and growth characteristics fit the description of *Geodermatophilus obscura* cluster I as described by Eppard, et al. (1996).

The uncultivable microbial community: We generated three rDNA libraries from the Death Valley rock varnish community DNA and two control libraries from soil adjacent to the varnished rock and lacking varnish. Varnish 16S rDNA libraries were prepared for Eubacteria and Archaea, and an 18S rDNA library for Eukarya. The control soil libraries were prepared for Eubacteria and Archaea. An 18S rDNA control library for Eukarya was not obtained for the soil despite six attempts. Between 100-200 clones were prepared for each library.

The clones within each library have been arranged into related subgroups through examination of their RFLP patterns, and 16S rDNA PCR products of representative members of each subgroup were sequenced.

Acknowledgements: This work was sponsored by the Jet Propulsion Laboratory (JPL) Director's Research and Development Fund and carried out at JPL, California Institute of Technology, under a contract with the National Aeronautics and Space Administration.

References: [1] Potter, R.M. and G.R. Rossman (1977) *Science*, 196(4297), 1446-1448. [2] Potter, R.M. and G.R. Rossman (1979) Chemical Geology, **25,** 79-94. [3] Perry, R.S. and J.B. Adams (1978) *Nature*, **276**(5687) 489-491. [4] Broecker, W.S. and T.Z. Liu (2001) *Geology Today*, **11**(8) 4-10. [5] Dorn, R.I. (1998) *Rock Coatings. Developments in Earth Surface Processes*. Vol. 6, Amsterdam: Elsevier. [6] Guinness, E.A., R.E. Arvidson, et al. (1997) *Journal of Geophysical Research-Planets*, **102**(E12) 28687-28703. [7] Israel, E.J., R.E. Arvidson, et al. (1997) *Journal of Geophysical Research-Planets*, **102**(E12) 28705-28716. [8] Dorn, R.I. and T.M. Oberlander (1981) *Science*, **213**(4513) 1245-1247. [9] Krumbein, W.E. and K. Jens (1981) *Oecologia*, **50**(1) 25-38. [10] Staley, J.T., M.J. Jackson, et al. (1983) *Bmr Journal of Australian Geology & Geophysics*, **8**(1) 83-87. [11] Taylor-george, S., F. Palmer, et al. (1983) *Microbial Ecology*, **9**(3) 227-245. [12] Palmer, F.E., J.T. Staley, et al. (1986) *Geomicrobiology Journal*, **4**(4) 343-360. [13] Hungate, B., A. Danin, et al. (1987) *Canadian Journal of Microbiology*, **33**(10) 939-943. [14] Grote, G. and W.E. Krumbein (1992) *Geomicrobiology Journal*, **10**(1) 49-57. [15] Eppard, M., W.E. Krumbein, et al. (1996) *Archives of Microbiology*, **166**(1) 12-22. [16] Perry, R.S., J. Dodsworth, et al. (2003) *NASA Astrobiology Institute Annual Meeting*, NASA Ames Research Center, Moffet Field, CA. [17] Amann, R.I., W. Ludwig, and K.H. Schleifer (1995) *Microbiological Reviews*, **59**(1) 143-169. [18] Barns, S.M., R.E. Fundyga, et al. (1994) *Proceedings of the National Academy of Sciences of the United States of America*, **91**(5) 1609-1613. [19] Ward, D.M., R. Weller, and M.M. Bateson (1990) *Nature*, **345**(6270) 63-65. [20] Torsvik, V., J. Goksoyr, and F.L. Daae (1990) *Applied and Environmental Microbiology*, **56**(3) 782-787. [21] Perry, R.S., (2002) Personal communication. [22] Luedemann (1968) Journal of Bacteriology, 96(5), 1848-1858.